



**HAL**  
open science

# Massive matter and the double copy : bootstrapping amplitudes in gauge and gravity theories

Ingrid A. Vazquez-Holm

► **To cite this version:**

Ingrid A. Vazquez-Holm. Massive matter and the double copy : bootstrapping amplitudes in gauge and gravity theories. High Energy Physics - Theory [hep-th]. Université Paris-Saclay, 2021. English. NNT : 2021UPASP066 . tel-03522506

**HAL Id: tel-03522506**

**<https://theses.hal.science/tel-03522506>**

Submitted on 12 Jan 2022

**HAL** is a multi-disciplinary open access archive for the deposit and dissemination of scientific research documents, whether they are published or not. The documents may come from teaching and research institutions in France or abroad, or from public or private research centers.

L'archive ouverte pluridisciplinaire **HAL**, est destinée au dépôt et à la diffusion de documents scientifiques de niveau recherche, publiés ou non, émanant des établissements d'enseignement et de recherche français ou étrangers, des laboratoires publics ou privés.

Massive matter and the double copy:  
Bootstrapping amplitudes in gauge and  
gravity theories

*La matière massive et la double copie:  
Bootstrap des amplitudes dans les théories de  
jauge et de gravité*

Thèse de doctorat de l'université Paris-Saclay

École doctorale n°564 : physique de l'Île-de-France (PIF)

Spécialité de doctorat: Physique

Unité de recherche : Université Paris-Saclay, CEA, Institut de physique théorique, 91191,  
Gif-sur-Yvette, France

Référent : Faculté des sciences d'Orsay

Thèse présentée et soutenue à Paris-Saclay,  
le 06/09/2021, par

**Ingrid A. VAZQUEZ-HOLM**

**Composition du Jury**

**Poul Henrik DAMGAARD**

Professeur, Niels Bohr Institute

Président et Rapporteur

**Zvi BERN**

Professeur, UCLA

Rapporteur et Examineur

**Pierre VANHOVE**

Directeur de recherche, IPhT

Examineur

**Andrea PUHM**

Chargée de recherche, CNRS, Ecole  
Polytechnique, 91128 Palaiseau  
cedex, France

Examinatrice

**Radu ROIBAN**

Professeur, The Pennsylvania State  
University

Examineur

**Direction de la thèse**

**John Joseph CARRASCO**

Professeur, Northwestern University

Directeur de thèse

**David KOSOWER**

Directeur de recherche, IPhT

Co-Directeur de thèse

*“Det er like vanskelig å lære å svømme på det dype som på det grunne.”*

**Hans Petter Langtangen**

UNIVERSITE PARIS-SACLAY

## *Abstract*

The LHC and the advent of gravitational wave observation have motivated tremendous progress in developing approaches to precision predictions in fundamental gauge theories and classical general relativity, and the two can be intimately connected. The color-kinematics duality of Bern, Carrasco, and Johansson (BCJ) for gauge theories is a duality where in amplitudes, graph-by-graph, kinematic weights obey the same general algebraic constraints as color weights. When arranged in such a representation the color-weights can be replaced by another copy of kinematic weights, generating diffeomorphic invariant scattering amplitudes for gravitational theories in a procedure known as double-copy construction. These gravitational amplitudes can then in turn be applied to predicting classical observables.

The color-dual form for gauge theory predictions means we only need to fix the physical information in a small number of basis graphs, and algebraic relations propagate this to the full prediction—both at tree-level and importantly at loop-level for the integrand description. This thesis develops a BCJ duality satisfying representation of tree- and loop-level amplitudes in massive scalar coupled QCD. The double-copy amplitudes are then relevant to non-rotating black hole scattering. We use the BCJ duality to reduce the set of graphs of amplitudes up to one-loop five-point to a smaller set of basis graphs, to which we give ansätze that are constrained by unitarity cuts and color-kinematics relations.

Our color-dual representations have an important feature. The same kinematic weights, graph by graph, are applicable to scalars regardless of whether they are charged in the fundamental or the adjoint. Indeed one can use adjoint-type ordered cuts to constrain these kinematic weights to be used for predictions in a multitude of theories, depending on which graphs you allow to contribute and how you weight their color.

The double copy construction maps from the scattering of gluons to the scattering of gravitons in  $N = 0$  supergravity, with additional massless states beyond the graviton coupling to the massive scalars. At tree- and loop-level we show that a projective double copy, combining naive double-copy with an application of the method of maximal cuts, can be easily exploited to project out non-gravitational states from the naive double copy, bootstrapping the predictions associated with pure-gravitational interactions between massive scalars.

We expect that the integrands found in this thesis can be used to find one-loop five-point predictions towards radiative corrections to classical observables. With that in mind, we warm up by using the amplitudes found in this thesis to reproduce known results for the color-impulse at leading and next-to-leading order, and radiation at leading order.



## *Résumé*

Le LHC et l'avènement de l'observation des ondes gravitationnelles ont motivé des progrès considérables dans le développement d'approches des prédictions de précision dans les théories de jauge fondamentales et la relativité générale classique, et les deux peuvent être intimement liés. La dualité couleur-cinématique de Bern, Carrasco et Johansson (BCJ) pour les théories de jauge est une dualité où en amplitudes, graphique par graphique, les poids cinématiques obéissent aux mêmes contraintes algébriques générales que les poids de couleur. Lorsqu'ils sont disposés dans une telle représentation, les poids de couleur peuvent être remplacés par une autre copie des poids cinématiques, générant des amplitudes de diffusion invariantes difféomorphes pour les théories gravitationnelles dans une procédure connue sous le nom de construction en double copie. Ces amplitudes gravitationnelles peuvent à leur tour être appliquées à la prédiction d'observables classiques.

La forme bicolore pour les prédictions de la théorie de jauge signifie que nous n'avons besoin de fixer les informations physiques que dans un petit nombre de graphes de base, et les relations algébriques propagent cela à la prédiction complète, à la fois au niveau de l'arbre et surtout au niveau de la boucle pour l'intégrande la description. Cette thèse développe une dualité BCJ satisfaisant la représentation des amplitudes au niveau de l'arbre et de la boucle dans la QCD massive couplée scalaire. Les amplitudes en double copie sont alors pertinentes pour la diffusion des trous noirs non rotatifs. Nous utilisons la dualité BCJ pour réduire l'ensemble de graphes d'amplitudes jusqu'à une boucle à cinq points à un ensemble plus petit de graphes de base, auxquels nous donnons des ansätze qui sont contraints par des coupes unitaires et des relations couleur-cinématique.

Nos représentations à double couleur ont une caractéristique importante. Les mêmes poids cinématiques, graphe par graphe, sont applicables aux scalaires qu'ils soient chargés dans le fondamental ou dans l'adjoint. En effet, on peut utiliser des coupes ordonnées de type adjoint pour contraindre ces poids cinématiques à utiliser pour les prédictions dans une multitude de théories, en fonction des graphiques que vous autorisez à contribuer et de la façon dont vous pondérez leur couleur.

La construction en double copie va de la diffusion des gluons à la diffusion des gravitons en supergravité  $N = 0$ , avec des états sans masse supplémentaires au-delà du couplage du graviton aux scalaires massifs. Au niveau de l'arbre et de la boucle, nous montrons qu'une double copie projective, combinant une double copie naïve avec une application de la méthode des coupes maximales, peut être facilement exploitée pour projeter des états non gravitationnels à partir de la double copie naïve, en amorçant les prédictions associée à des interactions gravitationnelles pures entre scalaires massifs. Nous nous attendons à ce que les intégrandes trouvés dans cette thèse puissent être utilisés pour trouver des prédictions à une boucle en cinq points vers des corrections radiatives aux observables classiques. Dans cet esprit, nous nous réchauffons en utilisant les amplitudes trouvées dans cette thèse pour reproduire les résultats connus pour l'impulsion de couleur à l'ordre dominant et sub-dominant, et le rayonnement à l'ordre dominant.



## *Acknowledgements*

First and foremost I would like to thank my thesis advisor John Joseph for all the guidance, support and friendship throughout my PhD. It has been a pleasure to work and discuss physics with you, whether it was in front of a blackboard, over countless hours of Zoom, or over a crêpe and a glass of cider. Learning from someone with so much love for their field has been an inspiration and an honor, and I can only hope to keep some of that enthusiasm with me as I go out into the world – proudly a graph-based person.

Being a PhD student navigating through the French system and additional SAGEx work would not have been possible without my colleagues and friends Sebastian, Maxence, Linnea and Sarah. It has been great to have someone to share the PhD experience with, everything from the travelling all over the world to complaining over a cup of coffee in the break room.

I also want to thank the people who have made lunch at work worth coming out from Paris: Jonathan, Niall, Thiago, Federico, Anurag, Elba and Ben. I feel very lucky to have been at IPhT at the same time as you – I think our (at times) weekly beers saved me many times.

I would like to thank everyone at Université Paris-Sud and at École Doctorale en Ile-de-France as well as all of the administrative staff at IPhT, ENS and CEA, in particular Laure Sauboy, Sylvie Zaffanella, Loic Bervas and Emmanuelle de Laborderie.

My time in Paris has been made absolutely wonderful by the people I met here – my dear friends Fernanda, Clement, Solveig and Camila. When I came to Paris and accidentally joined a choir for pensioners, I had no idea this was where I would meet two of my best friends and favorite people – Amelie and Perrin. There is no work crisis or otherwise that you have not been able to make me laugh away over a rosé piscine, meeting you has been one of my favourite things about Paris (and that is saying something) and I appreciate you and your friendship enormously.

An important reason for pursuing my PhD was the lovely time I had during my Bachelor and Master's degree at the University of Oslo. I would therefore like to give a big thank you to the theory group in Oslo, in particular Are, Anders, Jeriek and Eli, and of course my good friend, office mate and partner in crime August. I would also like to thank my wonderful group of incredibly cool, strong and independent physics girls, faministene: Pernille, Vilde, Mari, Helene, Elisabeth, there is no way I would be where I am had it not been for you.

I owe a big thank you to my family, mom, dad and Georg, for their love, good humor, numerous trips to wherever I go, and for always picking up the phone when I go to the supermarket. Your love and support has given me the safety to move around in the world and continue my 'Ingrid does things she cannot do' project. Thank you also to my grandmother, who was the first person to think it absolutely obvious that I should pursue a PhD. And Markus – no acknowledgement section is big enough. Thank you for believing more in me than I do myself, and for following me wherever academia takes us. You are my rock, and I cannot wait to continue this adventure together.



Finally, I am privileged to have been a part of the SAGEX network. I met so many great people with whom I got to travel and enjoy Europe, Kays, Andrea, Stefano, Manuel, Luke, Canxin, Anne, Lorenzo, Nikolai, Gabriele, Davide and Marco. My PhD experience was tremendously enhanced by the many opportunities made possible by SAGEX, from workshops, PhD schools, conferences, outreach, secondments, and meeting innumerable fellow physicists. This project has received funding from the European Union's Horizon 2020 research and innovation programme under the Marie Skłodowska-Curie grant agreement No. 764850 "SAGEX".

# Contents

<b>Acknowledgements</b>	<b>vii</b>
<b>1 Introduction</b>	<b>7</b>
<b>2 Amplitudes in gauge and gravity theories</b>	<b>9</b>
2.1 Color factors .....	9
2.2 The duality between color and kinematics .....	11
2.3 Unitarity methods .....	12
2.4 Graph representation .....	13
Ordered graphs .....	14
Unordered Graphs .....	14
2.5 Unitarity cuts with graphs .....	16
2.6 Representing kinematics .....	18
2.6.1 Kinematics in four dimensions: The spinor helicity formalism .	18
2.6.2 Kinematics in $D$ dimensions.....	21
<b>3 Loop-Level Double-Copy for Massive Quantum Particles</b>	<b>23</b>
3.1 Introduction.....	23
3.2 Bootstrapping Tree Amplitudes .....	25
3.2.1 Three-point trees.....	27
3.2.2 Four-point trees .....	27
Two massive scalars .....	28
Bootstrapping the two pairs of massive scalars four-point am- plitude.....	28
One massive scalar .....	30
3.2.3 Five-point trees .....	31
Two massive scalars .....	31
One massive scalar .....	33
3.3 Bootstrapping One-loop Integrands .....	34
3.3.1 Loops (just like trees!) .....	34
3.3.2 Four-point one-loop construction .....	34
3.3.3 Five-point one-loop construction.....	37
3.3.4 Verification.....	41
3.4 Conclusion.....	42
3.4.1 Kinematic Jacobi-like relations at one-loop four-point.....	44
<b>4 Extracting Einstein from the Loop-Level Double-Copy</b>	<b>45</b>
4.1 Introduction.....	45
4.2 Review of the method of maximal cuts .....	47
4.3 Projective double-copy .....	48
4.4 Extracting Einstein-Hilbert at Tree and Loop Level .....	49
4.4.1 Tree-level.....	50
4.4.2 Loop Level.....	54

	Four-point one-loop .....	55
	Five-point one-loop .....	61
4.5	Conclusion .....	61
<b>5</b>	<b>Classical limits</b> .....	<b>67</b>
5.1	Introduction .....	67
5.1.1	Restoring $\mathfrak{n}$ and classical point particles .....	68
5.1.2	Color Impulse .....	69
5.1.3	Color Radiation.....	70
5.2	Reproducing the classical impulse and radiation .....	71
5.2.1	Leading order impulse calculation .....	72
5.2.2	Next-to-leading order impulse calculation.....	73
	The cut box.....	78
	Combining terms .....	79
5.2.3	Leading order radiation calculation .....	80
5.3	Conclusion .....	83

*Dedicated to all the people I would have loved to celebrate with*

*Farfar  
Abuela  
T'io Mario  
T'ia Cata  
Hans Petter  
Vero*

*And to my eternal support group  
Markus, Mamma, Pappa and Georg*



# Resumé

L'avènement de l'observation des ondes gravitationnelles au LIGO et à VIRGO [1] et les expériences de haute précision pour les théories de jauge fondamentales au LHC sont une forte motivation pour repousser les limites des calculs analytiques. Dans les théories de jauge non abéliennes et la gravité, les amplitudes de diffusion ont toujours été difficiles à calculer car le nombre de graphes de Feynman contributeurs augmente de façon exponentielle avec la multiplicité et le niveau de boucle, et les expressions intermédiaires deviennent grandes et lourdes. En particulier, parce que la gravité a des termes de contact à toutes les multiplicités, écrire les graphes de Feynman d'une amplitude peut rapidement devenir une tâche impossible. Au cours des dernières décennies, le domaine des amplitudes de diffusion a évolué pour décrire la physique des hautes énergies d'une manière moins dépendante des choix temporaires effectués en cours de route dans les calculs, tels que la dépendance de jauge - en exploitant et parfois en découvrant de nouvelles symétries des quantités observables de la nature. Un certain nombre de techniques puissantes ont été développées, telles que les méthodes récursives pour les amplitudes au niveau de l'arbre [2, 3], les méthodes d'unitarité généralisée [4–6] et la dualité Bern-Carrasco-Johansson (BCJ) entre couleur et cinématique [7] et sa construction en double copie associée pour les amplitudes gravitationnelles [8].

La dualité Bern-Carrasco-Johansson (BCJ) entre la couleur et les ingrédients cinématiques des amplitudes est un bel aperçu de la structure des amplitudes de la théorie de jauge. Dans une théorie de jauge où cette dualité est manifeste, les amplitudes peuvent être agencées de telle sorte que les poids de couleur et les poids cinématiques des diagrammes contributeurs obéissent aux mêmes identités algébriques. Pour le cas des scalaires massifs couplés à la théorie de jauge, ces identités sont représentées sur la Figure 5.3. Cela signifie que les numérateurs cinématiques des graphiques d'amplitude ne sont pas indépendants, mais peuvent en fait être exprimés en termes d'un plus petit ensemble de numérateurs de base. Cela nous permet de recycler les informations entre les diagrammes et en pratique réduit considérablement le nombre de calculs nécessaires pour une amplitude à  $n$ -points.

Une avancée cruciale dans les prévisions de jauge et de gravité est d'inclure les effets des particules avec une masse intrinsèque. Cependant, l'introduction de masses pour les amplitudes au niveau de la boucle apporte une complexité plus élevée. On peut comparer, par exemple, l'amplitude à une boucle dans  $N = 4$  sYM, où les coefficients des intégrales de triangle et de bulle disparaissent, avec l'amplitude à une boucle pour les quarks massifs en QCD, où il faut prendre en compte non seulement les triangles et les bulles, mais inclure des diagrammes de têtards massifs dont l'accessibilité via les méthodes d'unitarité est subtile. La dualité entre la couleur et la cinématique a ici un réel potentiel : propager les informations de coupe à partir de graphiques maîtres accessibles vers des contributions plus délicates.

Dans cette thèse, je développe une représentation graphique des amplitudes au niveau des arbres et des boucles avec des scalaires massifs couplés à des bosons de Yang-Mills qui obéissent à la dualité BCJ. Les diagrammes relatifs à une amplitude sont générés simultanément avec les relations BCJ entre eux, ce qui nous permet de

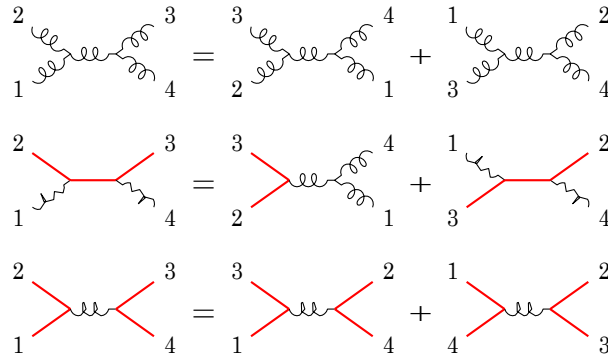


Figure 1: Représentation schématique des relations possibles entre les poids de couleurs et les poids cinématiques des diagrammes. Les lignes pleines (rouges) représentent des particules scalaires de même masse.

réduire les numérateurs de diagrammes cinématiques à des ensembles de diagrammes de base plus petits. Je choisis des ansätze pour les fonctions du numérateur des diagrammes de base dont les coefficients sont fixés par les relations BCJ entre les diagrammes, les propriétés de symétrie et les coupes unitaires généralisées. Par exemple, l'amplitude à quatre points au niveau de l'arbre avec un scalaire massif a deux topologies de diagrammes cubiques qui reçoivent des fonctions de numérateur distinctes

$$\begin{array}{c} c \\ \diagup \\ \text{---} M \text{---} \\ \diagdown \\ b \end{array} \begin{array}{c} d \\ \diagdown \\ \text{---} \\ \diagup \\ a \end{array} = n_{4,1}^M(a, b, c, d), \quad \begin{array}{c} d \\ \diagdown \\ \text{---} \overline{M} \text{---} \\ \diagup \\ c \end{array} \begin{array}{c} a \\ \diagdown \\ \text{---} \\ \diagup \\ b \end{array} = n_{4,1}^{\overline{M}}(a, b, c, d), \quad (1)$$

où les fonctions du numérateur sont liées par la relation BCJ suivante

$$n_{4,1}^{\overline{M}}(a, b, c, d) = n_{4,1}^M(a, b, c, d) - n_{4,1}^M(b, a, c, d). \quad (2)$$

Un ansatz cinématique est donc donné au diagramme de base  $n_{4,1}^M$  et est complètement déterminée par les propriétés de symétrie et de factorisation des diagrammes individuels et des amplitudes ordonnées. Au niveau de la boucle, les coefficients sont déterminés en se fixant sur des coupes unitaires généralisées.

Nous constatons que des représentations satisfaisantes BCJ existent à la fois au niveau de l'arbre et de la boucle, et les numérateurs cinématiques résultants ont une caractéristique intéressante : ils peuvent être utilisés pour décrire des scalaires massifs à la fois dans la représentation fondamentale et adjointe du groupe de jauge. Nous trouvons des représentations satisfaisantes BCJ pour les amplitudes au niveau de l'arbre à quatre et cinq points avec un et deux scalaires massifs respectivement. Nous trouvons également des représentations pour l'amplitude à quatre points à une boucle avec deux scalaires massifs, qui a six topologies cubiques distinctes<sup>1</sup>. Les coefficients physiquement pertinents de cette amplitude sont fixés sur trois coupes unitaires. Nous trouvons également une représentation satisfaisante BCJ pour l'amplitude à cinq points à une boucle avec deux scalaires massifs et un gluon externe, qui a 33

<sup>1</sup>Ne pas inclure les topologies de têtards.

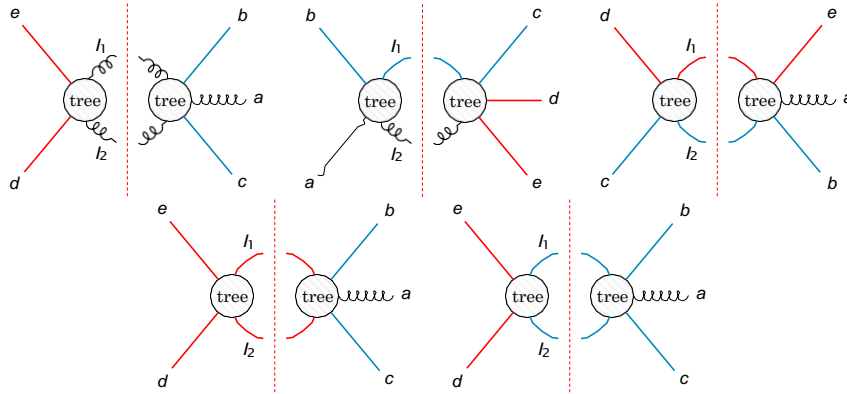


Figure 2: Coupes unitaires généralisées pour l’amplitude à une boucle à cinq points avec deux scalaires massifs de masse distincte.

topologies cubiques distinctes, et est fixée sur les cinq coupes unitaires illustrées à la Figure 5.4.

Les numérateurs cinématiques qui obéissent aux relations BCJ manifestent également un autre ensemble de relations profondes liant les théories physiques et qui doivent encore être complètement comprises : la structure en double copie des prédictions. Pour les numérateurs BCJ, nous pouvons, graphique par graphique, échanger les facteurs de couleur par un autre ensemble de numérateurs cinématiques, ce qui donne l’amplitude correspondante dans une théorie gravitationnelle. La construction en double copie a remplacé l’énorme complexité des calculs gravitationnels par la relative simplicité des prédictions de la théorie de jauge. Cela a été important pour les explorations formelles des propriétés UV des théories de la supergravité, et a maintenant un réel impact phénoménologique à l’ère de l’observation précise des ondes gravitationnelles. Dans cette thèse, la double copie de scalaires massifs couplée à la théorie de Yang-Mills donne la théorie des scalaires massifs en supergravité  $N = 0$ .

Comme les numérateurs cinématiques que nous générons obéissent aux relations BCJ par construction, nous pouvons facilement prendre la double copie pour obtenir les amplitudes de supergravité  $N = 0$ . Cependant, les amplitudes de cette théorie ont - en plus des gravitons souhaités - d’autres particules sans masse qui circulent comme états internes. Nous présentons donc une approche basée sur des diagrammes, que nous appelons double copie projective, qui combine des idées de la méthode des coupes maximales [9] et de la construction en double copie pour obtenir des numérateurs de gravité d’Einstein-Hilbert. Premièrement, les numérateurs  $N = 0$  sont trouvés en mettant au carré les numérateurs de la théorie de jauge. Ceux-ci sont ensuite modifiés en effectuant les coupes maximales de toutes les topologies pertinentes, et en les comparant avec les expressions obtenues avec un projecteur d’état physique qui permet uniquement aux gravitons de traverser la coupe. Tout écart entre les deux est ensuite attribué à des états supplémentaires, puis soustrait des numérateurs. Ensuite, une procédure similaire est effectuée pour les coupes presque-maximales, les coupes presque-presque-maximales, et ainsi de suite, jusqu’à ce qu’aucune autre condition de coupe ne puisse être retirée. À titre d’exemple, considérons l’amplitude d’une boucle à quatre points avec deux scalaires massifs. Le numérateur de supergravité  $N = 0$  de la topologie boîte est le carré du numérateur QCD, et avec des conditions de coupe maximale imposées, nous trouvons

$$M_4^{1\text{-loop}\uparrow\text{cut}}_{\text{MC1}} = n_{N=0} \left( \begin{array}{c} 2 \\ \text{---} \\ 1 \end{array} \begin{array}{c} 3 \\ \text{---} \\ 4 \end{array} \right) \uparrow_{\text{MC1}}^{\text{cut}} = (k_1 \cdot k_4)^4. \quad (3)$$



Nous comparons cela avec la somme des états du projecteur d'états physiques sur le produit des amplitudes de l'arbre à trois points,

$$\begin{aligned}
\mathcal{M}_{MC1}^{\text{trees}^1} &= \mathcal{M}_{\text{states}}^{\text{tree}}(k_3^{m_1}, l_1^{m_1}, l_1^{s_3}) \mathcal{M}_3^{\text{tree}}(-l_3^{m_1}, k_1^{m_1}, l_2^{s_2}) \\
&\quad \times \mathcal{M}_3^{\text{tree}}(-l_2^{s_2}, k_3^{m_2}, -l_4^{m_2}) \mathcal{M}_3^{\text{tree}}(l_4^{m_2}, k_4^{m_2}, -l_3^{s_3}) \\
&= \frac{m_1^2 m_2^2}{D_s - 2} - (k_1 \cdot k_4)^2.
\end{aligned} \tag{4}$$

La contribution des états non gravitationnels est alors donnée par la différence entre l'expression complète de la supergravité  $N = 0$  et l'expression médiée par le graviton

$$\begin{aligned}
\Delta_{MC1} &= \mathcal{M}_4^{\text{loop cut}} - \mathcal{M}_{MC1}^{\text{trees}^1} \\
&= 2 \frac{(k_1 \cdot k_4)^2}{m_1 m_2} - \frac{(m_1^2 m_2^2)^2}{(D_s - 2)^2},
\end{aligned} \tag{5}$$

et la contribution d'Einstein-Hilbert est alors obtenue en soustrayant le terme d'états supplémentaires du numérateur  $N = 0$ . Nous continuons ainsi, en corrigeant les numérateurs à l'aide des coupes proches du maximum *etc.* La procédure projective de double copie est complètement systématique, et nous trouvons un ensemble de numérateurs de gravité d'Einstein-Hilbert pour des amplitudes au niveau de l'arbre à quatre et cinq points avec un et deux scalaires massifs, et pour des intégrandes d'amplitude à une boucle à quatre et cinq- points avec deux scalaires massifs.

Les avantages du calcul des amplitudes de diffusion ont incité les physiciens à utiliser les connaissances obtenues des théories quantiques dans la recherche d'observables en physique classique (voir *eg* [10–54]). Les modèles d'ondes gravitationnelles qui peuvent être comparés aux données d'expériences nécessitent que nous combinions la relativité numérique avec une entrée analytique. Cela peut être sous la forme d'hamiltoniens gravitationnels et des équations de mouvement ultérieures, ou directement sous forme d'observables, tels que le changement d'impulsion de deux corps gravitationnels en collision. Il y a déjà eu d'énormes progrès dans ce domaine – le potentiel du problème binaire du trou noir a été déterminé jusqu'au troisième et quatrième ordre dans l'expansion post-minkowskienne [51, 55], ainsi que le rayonnement effets de réaction [49, 52, 54]. Une méthode d'extraction directe d'observables classiques à partir d'amplitudes de diffusion, le formalisme de Kosower-Maybee-O'Connell (KMOC), a été introduite dans [36] où le changement d'impulsion et de rayonnement dans la limite classique de l'électrodynamique quantique est donné. De manière analogue, le formalisme KMOC a été utilisé pour trouver l'impulsion de couleur et la couleur totale rayonnée dans la limite classique de QCD [56], et nous constatons que les numérateurs développés dans cette thèse reproduisent avec succès certains des résultats de cet article.

Nous reproduisons l'impulsion de couleur à l'ordre dominant (au niveau de l'arbre) et à l'ordre sub-dominant (au niveau d'une boucle), qui est décrit dans [56] et donné par

$$\Delta c_1^a \rightarrow \Delta c_1^a = i \int d^4 \hat{q} \delta(2m_2 t \hat{q}) \delta(2p_2 \cdot \hat{q}) e^{-ib \cdot q} \mathcal{G}, \tag{6}$$

où le noyau de couleur  $G$  est défini comme

$$\begin{aligned}
 G^a &= n^2 [C^a, C(D)] A_D(p_1, p_2 \rightarrow p_1 + q, p_2 - q) \\
 &- in^4 \prod_{i=1,2}^D \int \tilde{d}^4 \bar{\omega}_i \delta(2p_1 \cdot \bar{\omega}_i + n\bar{\omega}_i^2) \delta^{(4)}(\bar{\omega}_1 + \bar{\omega}_2 - \bar{r}_X) C(D)^\dagger [C^a, C(D)] \\
 &\times A_{D^\dagger}^*(p_1 + q, p_2 - q \rightarrow p_1 + \omega_1, p_2 + \omega_2, r_X) A_D(p_1, p_2 \rightarrow p_1 + \omega_1, p_2 - \omega_2, r_X). \quad (7)
 \end{aligned}$$

Le calcul de l'impulsion de couleur d'ordre suivant dans la représentation BCJ des amplitudes développée dans cette thèse diffère de l'article original car toutes les topologies sont cubiques

$$\begin{aligned}
 A^{(1)} &= C \left[ \begin{array}{c} \square b \\ \square a \end{array} \right] \left[ \begin{array}{c} \square c \\ \square d \end{array} \right] I_{b1}^{(1)} + C \left[ \begin{array}{c} \square a \\ \square b \end{array} \right] \left[ \begin{array}{c} \square c \\ \square d \end{array} \right] I_{b2}^{(1)} + C \left[ \begin{array}{c} \square b \\ \square a \end{array} \right] \left[ \begin{array}{c} \square c \\ \square d \end{array} \right] I_{t1}^{(1)} \\
 &+ C \left[ \begin{array}{c} \square b \\ \square a \end{array} \right] \left[ \begin{array}{c} \square c \\ \square d \end{array} \right] I_{t2}^{(1)} + C \left[ \begin{array}{c} \square b \\ \square a \end{array} \right] \left[ \begin{array}{c} \square c \\ \square d \end{array} \right] I_{f1}^{(1)} + C \left[ \begin{array}{c} \square b \\ \square a \end{array} \right] \left[ \begin{array}{c} \square c \\ \square d \end{array} \right] I_{f2}^{(1)} \\
 &+ C \left[ \begin{array}{c} \square b \\ \square a \end{array} \right] \left[ \begin{array}{c} \square c \\ \square d \end{array} \right] I_o^{(1)} + C \left[ \begin{array}{c} \square b \\ \square a \end{array} \right] \left[ \begin{array}{c} \square c \\ \square d \end{array} \right] I_{\delta 1}^{(1)} + C \left[ \begin{array}{c} \square b \\ \square a \end{array} \right] \left[ \begin{array}{c} \square c \\ \square d \end{array} \right] I_{\delta 2}^{(1)} \\
 &+ C \left[ \begin{array}{c} \square b \\ \square a \end{array} \right] \left[ \begin{array}{c} \square c \\ \square d \end{array} \right] I_{s1}^{(1)} + C \left[ \begin{array}{c} \square b \\ \square a \end{array} \right] \left[ \begin{array}{c} \square c \\ \square d \end{array} \right] I_{s2}^{(1)} + C \left[ \begin{array}{c} \square b \\ \square a \end{array} \right] \left[ \begin{array}{c} \square c \\ \square d \end{array} \right] I_{s3}^{(1)} \\
 &+ C \left[ \begin{array}{c} \square b \\ \square a \end{array} \right] \left[ \begin{array}{c} \square c \\ \square d \end{array} \right] I_{s4}^{(1)}. \quad (8)
 \end{aligned}$$

Dans le formalisme présenté dans [56] les facteurs de couleur avec des constantes de structure,  $f^{abc}$ , obtiennent une puissance supplémentaire de  $n$  par rapport aux générateurs,  $T_{ij}^a$ , supprimant ainsi ces termes dans la limite classique. On retrouve donc une base de couleur cubique qui privilégie les topologies avec des sommets composés uniquement de gluons, qui diffère de la base présentée dans l'article

$$C \left[ \begin{array}{c} \square b \\ \square a \end{array} \right] \left[ \begin{array}{c} \square c \\ \square d \end{array} \right] I_{s1}^{(1)}, C \left[ \begin{array}{c} \square a \\ \square b \end{array} \right] \left[ \begin{array}{c} \square c \\ \square d \end{array} \right] I_{s2}^{(1)}, C \left[ \begin{array}{c} \square b \\ \square a \end{array} \right] \left[ \begin{array}{c} \square c \\ \square d \end{array} \right] I_{s3}^{(1)}, C \left[ \begin{array}{c} \square b \\ \square a \end{array} \right] \left[ \begin{array}{c} \square c \\ \square d \end{array} \right] I_{s4}^{(1)}. \quad (9)$$

L'impulsion de couleur calculée à l'aide des représentations satisfaisantes BCJ à l'ordre dominant et à l'ordre sub-dominant correspond aux résultats dans [56], tout comme le rayonnement de couleur à l'ordre dominant.



## Chapter 1

# Introduction

The advent of gravitational wave observation at LIGO and VIRGO [1] and high precision experiments for fundamental gauge theories at the LHC are a strong motivation to push the boundaries of analytic calculations. In non-Abelian gauge theories and gravity, scattering amplitudes have historically been difficult to calculate because the number of contributing Feynman graphs increases exponentially with multiplicity and loop-level, and intermediate expressions grow large and unwieldy. In particular, because gravity has contact terms at all multiplicities writing down the Feynman graphs of an amplitude can quickly turn into an impossible task. Over the last decades the field of scattering amplitudes has evolved to describe high energy physics in a way that is less dependent on the temporary choices made along the way in calculations, such as gauge dependence – exploiting and occasionally discovering new symmetries of nature’s observable quantities. A number of powerful techniques have been developed, such as recursive methods for tree-level amplitudes [2, 3], generalized unitarity methods [4–6] and the Bern-Carrasco-Johansson (BCJ) duality between color and kinematics [7] and its associated double-copy construction for gravitational amplitudes [8].

Recursive methods have allowed for the calculation of tree-level amplitudes of increasing multiplicity by using on-shell data from lower-level trees. Similarly, unitarity methods – pioneered in the 90s by Bern, Dixon, and Kosower and generalized to involve three-point trees in the 2000s by Britto, Cachazo, and Feng – allow for complicated loop-level predictions to be constructed systematically using compact on-shell tree-level data.

A beautiful insight into the structure of gauge theory amplitudes is the Bern-Carrasco-Johansson (BCJ) duality between the color and kinematic ingredients of the amplitudes. In a gauge theory where this duality is manifest, amplitudes can be arranged in such a way that the color weights and kinematic weights of the contributing graphs obey the same algebraic identities. This means that the kinematic numerators of the amplitude graphs are not unrelated, but can in fact be expressed in terms of a smaller set of basis numerators. This allows us to recycle information between graphs and in practice reduces the number of necessary computations for an  $n$ -point amplitude considerably.

Kinematic numerators that obey the BCJ relations also manifest another set of deep relationships between physical theories which are still to be completely understood: the double-copy structure of predictions. For BCJ numerators we can, graph-by-graph, exchange the color factors by another set of kinematic numerators, and this yields the corresponding amplitude in a gravitational theory. For example, the case most relevant to this thesis is that the double copy of massive scalars coupled to Yang-Mills theory yields the theory of massive scalars in  $N = 0$  supergravity. The double copy construction has replaced the tremendous complexity of gravitational calculations with the relative simplicity of gauge theory predictions. This has

been important for formal explorations of the UV properties of supergravity theories, and now has real phenomenological impact in the era of precision gravitational wave observation.

A crucial advance in both gauge and gravity predictions is to include the effects of particles with intrinsic mass. However introducing masses for amplitudes at loop-level brings higher complexity. We can compare, for example, the one-loop amplitude in  $N = 4$  sYM, where the coefficients of triangle and bubble integrals disappear, with the one-loop amplitude for massive quarks in QCD, where we have to take into account not only triangles and bubbles, but include massive tadpole diagrams whose accessibility via unitarity methods is subtle. The duality between color and kinematics has a real potential upside here—propagating cut information from accessible master-graphs to more delicate contributions.

In this thesis we develop a graph representation of tree- and loop-level amplitudes with massive scalars coupled to Yang-Mills that obey the BCJ duality. The graphs pertaining to an amplitude are generated simultaneously as the BCJ relations between them, which allows us to reduce the kinematic graph numerators to smaller sets of basis graphs. We find that these representations exist both at tree- and loop-level.

As the kinematic numerators we generate obey the BCJ relations by construction, we can easily take the double copy to obtain the  $N = 0$  supergravity amplitudes. However, the amplitudes in this theory have – in addition to the desired gravitons – other massless particles running around as internal states. We therefore present a graph-based approach, which we call projective double copy, that combines ideas from the method of maximal cuts [9] and double-copy construction to obtain pure Einstein-Hilbert gravity numerators.

The computational advantages of scattering amplitudes have inspired physicists to use quantum insights in the search for classical physics observables (see *e.g.* [10–54]). Gravitational wave templates that can be compared with data from experiments require that we combine numerical relativity with analytic input. This can be in the form of gravitational Hamiltonians and the subsequent equations of motion, or directly as observables, such as the change in impulse from two colliding gravitational bodies. There has already been tremendous progress in this field – the potential of the binary black-hole problem has been determined up to third and fourth order in the post Minkowskian expansion [51, 55], as well as radiation reaction effects [49, 52, 54]. A method for directly extracting classical observables from scattering amplitudes, the Kosower-Maybee-O’Connell (KMOC) formalism, was introduced in [36] where the classical QED change in impulse and radiation are given. Analogously, the KMOC formalism was used to find the classical color impulse and total radiated color found in [56], and we find that the numerators developed in this thesis successfully reproduce some the results in this paper.

The first chapter of this thesis will give an overview of methods and advances in the field of scattering amplitudes relevant to this thesis, and introduce graph representation. In the second chapter we develop a BCJ duality satisfying representation for massive amplitudes at one-loop level, based on the publication [57]. In the third chapter we use projective double copy to determine tree-level amplitudes, and one-loop integrands in Einstein-Hilbert gravity from gauge theory amplitudes. The fourth chapter demonstrates how the amplitudes developed in the previous chapters can be used to find classical observables in Yang-Mills theory using the KMOC formalism.

## Chapter 2

# Amplitudes in gauge and gravity theories

In this chapter I review some relevant concepts in the field of scattering amplitudes. I give a brief introduction to color factors and color-ordered amplitudes for massive and massless particles. The BCJ duality between color and kinematics is introduced, with the subsequent double-copy construction to obtain gravity amplitudes. I also introduce unitarity methods and graph representation for amplitudes, and how to perform unitarity cuts using graphs. Finally I give a review on representing kinematics, in particular how we represent four-dimensional kinematics using the spinor helicity formalism.

The general form of a  $m$ -point  $L$ -loop gauge theory amplitude  $A_m^{(L)}$  in  $D$  space-time dimensions with gluons and massive particles can be written as

$$A_m^{(L)} = i g^{L m - 2 + 2L} \sum_{i \in \Gamma} \int \prod_{l=1}^L \frac{d^D p_l}{(2\pi)^D} \frac{n_i C_i}{(p_{\alpha_i}^2 - m_{\alpha_i}^2)}, \quad (2.1)$$

where  $g$  is the gauge coupling constant, and  $m_{\alpha_i}^2$  is the on-shell mass of the particle with momentum  $p_{\alpha_i}$ . The sum runs over the complete set  $\Gamma$  of  $m$ -point  $L$ -loop graphs with only cubic vertices, including all possible permutations of external legs. The integrations are over the independent loop momenta  $p_l$ , and each graph is dressed with a kinematic numerator  $n_i$  unique to the graph topology, a color factor  $C_i$  and the propagator structure of the graph. The kinematic numerators  $n_i$  are in general not gauge invariant objects. We take the convention of all external kinematics outgoing. At tree level *color ordered amplitudes* can be constructed from purely kinematic contributions (numerators over propagators) for graphs with the same external leg ordering<sup>1</sup>. Indeed these gauge-invariant expressions emerge naturally when expressing the color-weights in terms of a basis of color-factors in full tree-level amplitudes. The kinematic coefficient of each basis color-weight will be a color-ordered amplitude.

## 2.1 Color factors

The color factors are constructed from two types of terms: structure constants  $f^{abc}$  from purely gluonic vertices, and generators  $T_{ij}^a$  from vertices with two massive scalar lines and a gluon (cf. Figure 2.1). As mentioned above, we only concern ourselves with cubic graphs as we find that quartic vertices, or *contact terms*, can be expanded in terms of cubic expressions. For example, the Feynman rule for the four-gluon

<sup>1</sup>And therefore the same color factor.

Figure 2.1: Color-weights of cubic vertices. The solid (red) lines represent massive scalars charged under the fundamental representation of the group.

vertex can be written as

$$\begin{aligned}
 & \sim f^{abg}f^{gcd}n_s + f^{acg}f^{gbd}n_u + f^{adg}f^{gbc}n_t \\
 & = f^{abg}f^{gcd}n_s \left(\frac{s}{s}\right) + f^{acg}f^{gbd}n_u \left(\frac{u}{u}\right) + f^{adg}f^{gbc}n_t \left(\frac{\hat{t}}{\hat{t}}\right) \quad (2.2) \\
 & \sim \begin{array}{c} b \\ \text{---} \\ \text{---} \\ a \end{array} \begin{array}{c} c \\ \text{---} \\ \text{---} \\ d \end{array} + \begin{array}{c} c \\ \text{---} \\ \text{---} \\ a \end{array} \begin{array}{c} b \\ \text{---} \\ \text{---} \\ d \end{array} + \begin{array}{c} d \\ \text{---} \\ \text{---} \\ a \end{array} \begin{array}{c} b \\ \text{---} \\ \text{---} \\ c \end{array},
 \end{aligned}$$

where  $s = (a + b)^2$ ,  $u = (a + c)^2$  and  $t = (a + d)^2$  are the Mandelstam invariants and  $n_i$  is the kinematic part of the Feynman rule. We see that we can multiply in factors of  $(k_i + k_j)^2 / (k_i + k_j)^2$  to distribute the contribution from the contact term amongst graphs where the quartic term has been expanded in the propagator  $(k_i + k_j)^2$ .

The structure constants are completely antisymmetric, and therefore the color-weights of adjoint vertices obey a flipping symmetry where exchanging the order of two of the legs in a vertex introduces a relative minus sign. As noted in [58], a convenient antisymmetry for the fundamental generators similar to the structure constants can also be realized,

$$f^{abc} = -f^{bac} \quad \text{and} \quad T_{ij}^a = -T_{ji}^a. \quad (2.3)$$

From the structure of the group, the color factors obey Jacobi and analogous commutation relations associated with four-point subgraphs entirely in the adjoint, and in mixed adjoint-fundamental given by

$$\begin{aligned}
 f^{dac}f^{bce} - f^{lbc}f^{cae} &= f^{abc}f^{lce}, \\
 T_{ij}^a T_{jk}^b - T_{ij}^b T_{jk}^a &= f^{abc}T_{ik}^c.
 \end{aligned} \quad (2.4)$$

We will introduce an additional type of three-term color identity, corresponding to a four-point sub-graph with all same-mass scalars. One can generalize the  $SU(N)$  Fierz identity to optionally require

$$T_{ij}^a T_{kl}^a = T_{ik}^b T_{jl}^b + T_{li}^c T_{jk}^c. \quad (2.5)$$

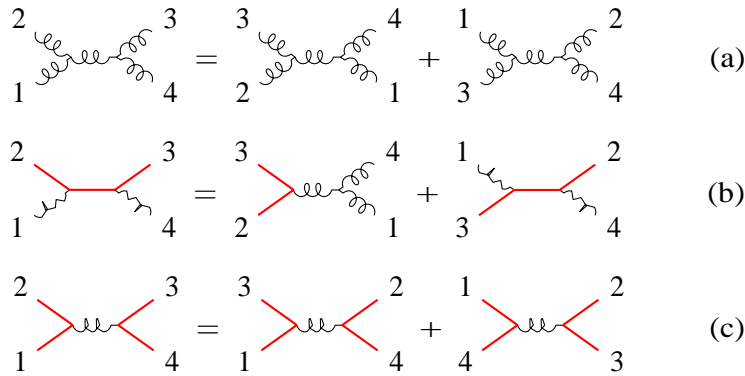


Figure 2.2: Pictorial representation of the relations between color weights and potentially kinematic weights of graphs. The solid (red) lines represent same-mass scalar particles.

This allows us the freedom to construct either adjoint scalar amplitudes or fundamental scalar amplitudes at our discretion<sup>2</sup>. We will refer to the set of these three-term identities as Jacobi-like relations.

These relations are illustrated graphically in Figure 2.2 for gluons and massive scalar lines, and also represent the subsequent Jacobi-like and antisymmetry relations between color factors

$$c_i - c_j = c_k, \quad c_i \rightarrow -c_i. \quad (2.6)$$

The relationship shown in Figure 2.2 applies to the four-point tree sub-graphs shown, but also to any set of three graphs that only differ by one internal leg with the three connectivities, where all other legs are held fixed.

## 2.2 The duality between color and kinematics

In general, due to the cubic-assignment ambiguity of the four-point gluonic contact-term – as illustrated in Equation (2.2) – there is some degree of gauge freedom when choosing the kinematic and color numerator basis. The gauge invariance of an amplitude under different kinematic numerator choices is called *generalized gauge freedom*. A fortuitous choice is a representation that obeys *color kinematics duality*. This means choosing a representation where the kinematic numerators obey the same Jacobi-like relations and flipping symmetry as the color factors

$$\begin{aligned} n_i - n_j = n_k & \Leftrightarrow c_i - c_j = c_k, \\ n_i \rightarrow -n_i & \Leftrightarrow c_i \rightarrow -c_i \end{aligned} \quad (2.7)$$

in analogy to Equation (2.6). These relations are known to hold up to all multiplicities at tree-level and conjectured to hold off-shell to all multiloop levels.

Once we have found a representation of kinematic numerators that satisfy these

<sup>2</sup>The kinematic weights of individual graphs will be applicable to either.



relations, we can exchange the color factors in Equation (2.1) for another set of color-dual kinematic numerators

$$M_m = i \binom{(L)}{L+1} \binom{\kappa}{2}^{m-2+2L} \prod_{i \in \Gamma} \int_{l=1}^L \frac{d^D p_l}{(2\pi)^D} \frac{1}{S_l} \frac{n_i \tilde{n}_i}{(p_{\alpha_i}^2 - m^2)^{\alpha_i}}, \quad (2.8)$$

where the tilde on  $\tilde{n}$  signifies that there can be two distinct gauge theories. Indeed, only one of the numerator sets needs to manifest the color kinematics duality. The expression obtained in Equation (2.8) is now a gravitational amplitude, and we call this relationship the *double copy construction* of gravitational amplitudes. There are many possible combinations of kinematic numerators from different gauge theories, with varying degrees of supersymmetry, which lead to amplitudes in different gravitational theories. However, in this thesis I will focus on the double copy construction of scalar QCD theory.

### 2.3 Unitarity methods

One of the main focuses of the field of scattering amplitudes is to write amplitudes in terms of fewer and simpler expressions, by for example relating the kinematics of graphs using the BCJ duality. As we move upwards in loop-level, writing amplitudes in terms of simpler components becomes a necessity. Luckily, the unitarity properties of amplitudes allow us to partially write loop amplitudes as products of tree amplitudes, by using what we call *unitarity methods* [4]. Recall that we can write an  $L$ -loop amplitude as

$$A_n^{L\text{-loop}} = i \int_j^L \prod_{k=1}^L \frac{d^D l_k}{(2\pi)^D} \frac{1}{S_j} \frac{n_j c_j}{p_{\alpha_j}^2}.$$

To understand how to extract data from integrals of this form, we examine the unitarity property of the  $S$ -matrix,  $SS^\dagger = 1$ . We can write  $S = 1 + iT$ , which requires that the discontinuity across a branch cut is  $\text{Disc } T = -i(T - T^\dagger) = TT^\dagger$ . This constraint implies that the imaginary part of  $T$  is a product of lower-order results. For example, we can write the four- and five-gluon scattering amplitudes in QCD perturbatively as

$$T_4 = g^2 T_4^{(0)} + g^4 T_4^{(1)} + g^6 T_4^{(2)} + \dots, \quad (2.9)$$

$$T_5 = g^3 T_5^{(0)} + g^5 T_5^{(1)} + g^7 T_5^{(2)} + \dots, \quad (2.10)$$

where  $g$  is the coupling, and  $T_n^{(L)}$  is the  $L$ -loop  $n$ -gluon amplitude. The discontinuities of the 4-gluon amplitude can now be written in terms of these expansions [59]

$$\text{Disc } T_4^{(0)} = 0, \quad (2.11)$$

$$\text{Disc } T_4^{(1)} = T_4^{(0)\dagger} T_4^{(0)}, \quad (2.12)$$

$$\text{Disc } T_4^{(2)} = T_4^{(0)\dagger} T_4^{(1)} + T_4^{(1)\dagger} T_4^{(0)} + T_5^{(0)\dagger} T_5^{(0)}, \quad (2.13)$$

where there is an implied sum over the types and helicities of the intermediate states. The second equation, Equation (2.12), states that we can write the discontinuity of the one-loop amplitude as a product of tree amplitudes, and similarly the third equation states that we can write the two-loop discontinuity as a product of a one-loop and a tree amplitude, and of two four-point tree amplitudes. We can think of

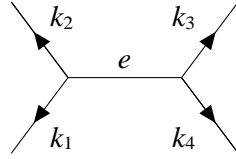


Figure 2.3: Four-point ordered graph with external momenta  $k_1, k_2, k_3, k_4$ .

the trees on the left sides of these equations as particular values of the loop momenta – namely their on-shell values  $k_i^2 = m_i^2$ . We refer to this procedure of putting internal edges on-shell as *unitarity cuts*, and I will review these in Section 2.5.

One approach of unitarity methods is to compare the information from the generalized unitarity cuts with cuts of this linear function of integrals, in order to determine such coefficients [60, 61]. This works particularly well when there is a known basis of relevant loop integrals like at one loop. Another application is known as cut construction [5, 9, 62, 63]. A sufficient condition for loop integrands organized graphically is that they satisfy all physical unitarity cuts. This leads to a constructive approach called the method of maximal cuts which I will describe in detail in Chapter 4 after reviewing graphical methods in the rest of this chapter.

## 2.4 Graph representation

An important step in determining an amplitude is to identify the graphs that contribute. The graph representation of an amplitude is not unique – as alluded to earlier, we can for example choose whether or not to include quartic graphs in our representation. The methods presented in this thesis will take advantage of the relationship between cubic graph topologies. I therefore give a brief introduction to the representation and features of graphs.

Computationally, a graph can be represented in several ways, including in the *node representation* and in the *edge representation*. The former is useful for preserving the order of a graph and is easily mapped to the edge representation, which is useful for plotting and finding isomorphisms. In the node representation a graph is represented as a list of nodes, which we call a *necklace*. A node represents a trivalent vertex, and so has three legs. Incoming legs get a minus sign. As an example, the graph in Figure 2.3 would be represented as

$$\{(k_1, k_2, e), (-e, k_3, k_4)\},$$

where  $e$  is the internal edge momenta. Similarly, we can find a node representation of more complicated graphs by enumerating the internal edges. The two-loop four point diagram in Figure 2.4a can be expressed as the necklace of nodes

$$\{(k_1, -e_1, -e_6), (k_2, -e_2, e_1), (e_2, e_3, e_7), (-e_3, k_3, e_4), (-e_5, -e_4, k_4), (e_6, -e_7, e_5)\}.$$

To get the ordering of the external momenta one simply collapses the nodes with matching in- and outgoing edges

$$\{(k_1, k_2, e), (-e, k_3, k_4)\} \rightarrow \{(k_1, k_2, k_3, k_4)\}.$$

The translation from node representation to edge representation is straightforward, and necessary to visualize graphs in Mathematica. Every vertex is labelled

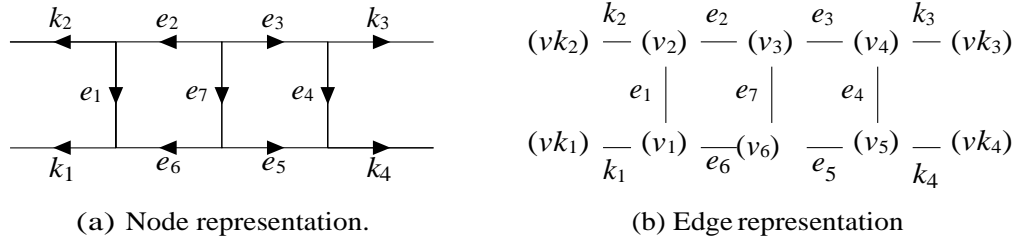


Figure 2.4: Four-point two-loop ordered graph with external momenta  $k_1, k_2, k_3$  and  $k_4$ .

$v_i$ , where  $i \in 1, \dots, m$  and  $m$  is the number of internal vertices. Drawing graphs in Mathematica requires that external edges are also specified, so these are labelled  $vk_j$  where  $j \in 1, \dots, n$  for an  $n$ -point graph. Every edge is then specified as the connection between two vertices. As an example, an edge in Figure 2.4a could be represented as

$$e_1 : v_2 \overset{\leftarrow}{f} v_1.$$

The full graph representation (vertices and edges) of the graph in Figure 2.4a is shown in Figure 2.4b.

### Ordered graphs

Given an amplitude of multiplicity  $n$  with color-ordering  $k_1, k_2, k_3, \dots, k_n$ , we can generate all contributing tree graphs using a relatively simple algorithm. Consider a 3-point amplitude given by graphs in the node representation

$$(k_1, k_2, k_3).$$

There is only one graph with the correct ordering. To find the next multiplicity graphs, *i.e.* the four-particle graphs, we must add the fourth leg to the *right* of  $k_3$  and to the *left* of  $k_1$ . This can be done in two ways

$$\left\{ (k_1, k_2, e), (-e, k_3, k_4) \right\}, \left\{ (k_4, k_1, e), (-e, k_2, k_3) \right\},$$

so there are two graphs that contribute to this color ordering. We can continue in this way for five-point, where we find there are five distinct graphs, by always adding the new leg to an internal propagator or external leg to the right of the last leg, and to the left of the first leg.

### Unordered Graphs

We can go about finding all graphs that contribute to an unordered amplitude in a few different ways. I will here go through the method that will later allow us to generate all the unique *graph topologies* that contribute to a given amplitude. Let us take the four-point amplitude as an example. In the previous section we saw that we can generate one of the four-point graphs by simply adding the fourth leg to a three-point amplitude. By considering the internal edge of the four-point graph as a Mandelstam  $s$ -channel (where  $s = (a + b)^2$ ), we can define operators  $\hat{u}$  and  $\hat{t}$  that

change the graph connectivity from an  $s$ -channel to a  $u$ - and  $t$ -channel, respectively,

Diagram (2.14) illustrates the transformation of a four-point graph. On the left, a central horizontal edge connects two vertices. From the left vertex, two edges labeled  $b$  and  $d$  extend outwards. From the right vertex, two edges labeled  $c$  and  $a$  extend outwards. Two arrows originate from this graph: an upper arrow labeled  $\hat{u}$  and a lower arrow labeled  $\hat{t}$ . The upper arrow points to a graph where the central edge is now horizontal and connects vertices  $a$  and  $d$ . Edges  $b$  and  $c$  are now connected to  $a$  and  $d$  respectively, crossing each other. The lower arrow points to a graph where the central edge is now vertical and connects vertices  $b$  and  $c$ . Edges  $a$  and  $d$  are now connected to  $b$  and  $c$  respectively.

We now have three graphs in stead of one. Now, we apply the  $\hat{t}$  and  $\hat{u}$  operators on one of the new graphs, thereby generating new graphs. The algorithm continues in this fashion until no new graphs are generated.

We can do the same thing for amplitudes with massive particles. Consider the four-point amplitude with one massive particle, and one massless particle. As shown in Figure 2.1 we allow three-point interactions between the massless particles, and two-massive-one-massless interactions. That is, we do *not* allow massive contact terms<sup>3</sup>. We consider one of the four-point graphs for this amplitude, and use the  $\hat{u}$  and  $\hat{t}$  operators to generate the new graphs

Diagram (2.15) illustrates the transformation of a four-point graph with massive particles. On the left, a central horizontal edge connects two vertices. From the left vertex, two edges labeled  $b$  and  $a$  extend outwards, colored red. From the right vertex, two edges labeled  $c$  and  $d$  extend outwards, colored grey. Two arrows originate from this graph: an upper arrow labeled  $\hat{u}$  and a lower arrow labeled  $\hat{t}$ . The upper arrow points to a graph where the central edge is now horizontal and connects vertices  $a$  and  $d$ . Edges  $b$  and  $c$  are now connected to  $a$  and  $d$  respectively, crossing each other. The lower arrow points to a graph where the central edge is now vertical and connects vertices  $b$  and  $c$ . Edges  $a$  and  $d$  are now connected to  $b$  and  $c$  respectively.

Note that the internal edges of the graphs generated by the  $\hat{t}$  and  $\hat{u}$  operators are now *massive*. When using these operators on graphs with massive particles, we must take into account the allowed vertices, and allow the massive lines to flow through the graphs in a consistent way. Take as an example the massive four-point tree with two massive particles of distinct mass<sup>4</sup>. Using the  $\hat{t}$  and  $\hat{u}$  operators in this case yields

<sup>3</sup>This could of course be changed to consider a different theory, which would admit other graphs.  
<sup>4</sup>Or graphs that are distinguished by some other quantum number.

graphs that require vertices which we do not permit

$$(2.16)$$

Therefore, there is only one graph that contributes to the unordered amplitude for two massive scalars at tree-level.

The method described above can be used to find something even more useful than the graphs of an unordered amplitude – we can use it to find all the *unique topologies*. Consider the two graphs generated on the right-hand side of Equation (2.15). These are in fact two versions of the same type of graph, or topology, with differently labelled legs

$$(2.17)$$

To this unique topology we can assign a kinematic numerator  $n_1$ , which goes into Equation (2.1) and is a function of the external legs of the graph. In the above case we would then have  $n_1(a, b, c, d)$  and  $n_1(b, a, c, d)$ . We can now go about finding all unique topologies in a similar way as graphs – by using the  $\hat{u}$ - and  $\hat{t}$ -operators to generate new graphs until *no new topologies* show up. This might seem trivial, and at four-point and five-point it can in fact be done as a quick back-of-envelope calculation, but as we move to higher multiplicity and loop-level it might be less apparent whether two graphs are equivalent. For this purpose we must find all *graph isomorphisms*.

If two graphs are isomorphic, there exists a map between their vertices that can transform one graph into the other. Consider again the example in Equation (2.17), these two graphs are isomorphic because we can use the map

$$\{a \rightarrow b, b \rightarrow a\} \quad (2.18)$$

to transform one graph into the other. In contrast, there is no relabeling of vertices that can transform the graph on the left-hand side of Equation (2.15) into either graph in Equation (2.17).

## 2.5 Unitarity cuts with graphs

Now that we have established tools for representing graphs and introduced unitarity methods, we can look at unitarity cuts in terms of graphs. We consider as an example an ordered two-particle cut of a one-loop five-point amplitude, with two massive particles of different masses  $m_1$  and  $m_2$ , and an emitted massless particle. For this cut we put the two internal massive propagators on-shell, which means the integrand

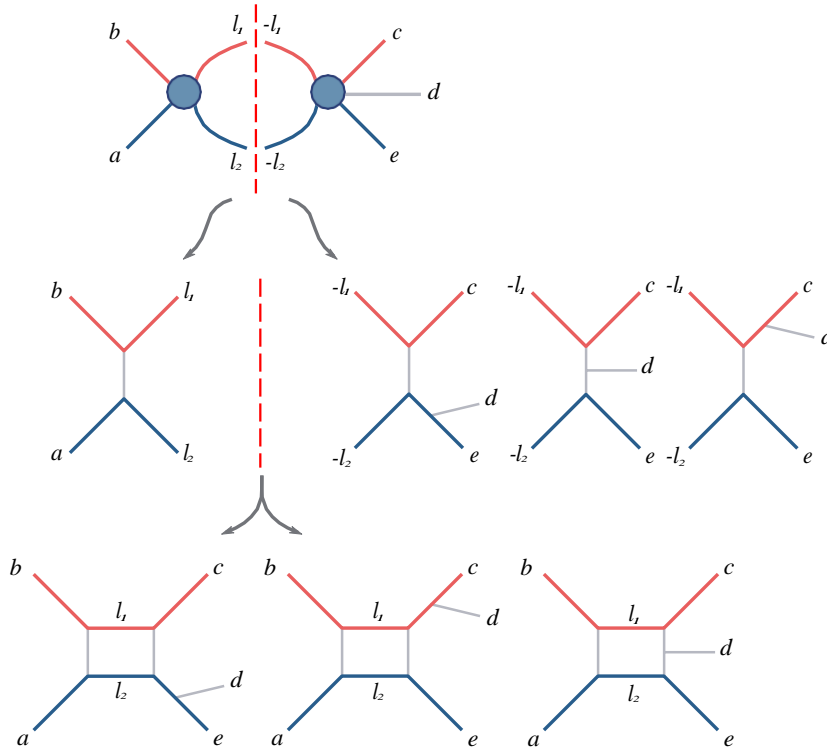


Figure 2.5: Graph representation of a unitarity cut of the one-loop five-point amplitude.

factorizes into the following product of tree amplitudes

$$A_5^{1\text{-loop}}(a^{m_2}, b^{m_1}, c^{m_1}, d, e^{m_2})|_{\text{cut}} = \sum_{s_1, s_2} A_4^{\text{tree}}(a^{m_2}, b^{m_1}, l_1^{s_1}, l_2^{s_2}) \times A_5^{\text{tree}}(-l_1^{s_2}, -l_1^{s_1}, c^{m_1}, d^{m_2}, e), \quad (2.19)$$

where the sum is over the possible states  $s_i$  of the loop momenta  $l_i$ . For this particular cut there is only one possibility for the crossing states, as these have to be scalars<sup>5</sup> of a certain mass, so the sum is trivial

$$A_5^{1\text{-loop}}(a^{m_2}, b^{m_1}, c^{m_1}, d, e^{m_2})|_{\text{cut}} = A_4^{\text{tree}}(a^{m_2}, b^{m_1}, l_1^{m_1}, l_2^{m_2}) \times A_5^{\text{tree}}(-l_2^{m_2}, -l_1^{m_1}, c^{m_1}, d, e^{m_2}). \quad (2.20)$$

This cut is illustrated in terms of graphs in the first line of Figure 2.5.

The right-hand side of Equation (2.20) is simply the product of two on-shell tree-level amplitudes. In general we want to use this product to extract information about the integrand  $A_5^{1\text{-loop}}$ . We can find the right hand side of Equation (2.20) by writing down the full integrand, and then imposing the cut conditions  $l_1^2 = m_1^2$  and  $l_2^2 = m_2^2$ . However, it is often the case that the right-hand side is not known, and we want to attribute the information of the trees to the loop integrand. We can do this in an effective way using the graphs that contribute to the tree amplitudes. The ordered four-point amplitude in Equation (2.20) has a single contributing graph, while the five-point amplitude has three contributing graphs. These are shown on the second line of Figure 2.5, separated by a dashed cutting line. By sewing together the cut legs

<sup>5</sup>So there are no helicities to sum over.

of the four-point graph with the three possible five-point graphs, we obtain the three one-loop graphs that contribute to this cut, shown on the third line of Figure 2.5. We can now write Equation (2.20) as a sum over these graphs, with cut conditions imposed

$$\begin{aligned}
 A_5^{1\text{-loop}(a, b, c, d, e)} \Big|_{\text{cut}} = & \frac{\text{Diagram 1}}{(b+l_1)^2(c+d-l_2-l_1)^2(c+d)^2} + \frac{\text{Diagram 2}}{(b+l_1)^2(c-l_1)^2(d+e)^2} \\
 & + \frac{\text{Diagram 3}}{(b+l_1)^2(c-l_1)^2(c+d-l_1)^2}, \quad (2.21)
 \end{aligned}$$

where mass superscripts have been suppressed, and the loop graphs are dressed with kinematic numerators and the uncut propagators. This way we can probe and determine the one-loop graphs by using on-shell tree amplitudes, which will be central to the methods presented in this thesis.

## 2.6 Representing kinematics

We have so far focused on the gauge structure and graph composition of the general amplitudes described in Equation (2.1) and the double copied amplitudes in Equation (2.8). Finding the color factors of an amplitude and its contributing graphs are usually not the most difficult parts of expressing an amplitude: most of the work is put into finding the kinematic graph numerators, to which the main body of this thesis is dedicated. These kinematic expressions can be described in various forms depending on the dimension  $D$  in which they are given, and the two most relevant cases are the four-dimensional and the general  $D$ -dimensional forms.

### 2.6.1 Kinematics in four dimensions: The spinor helicity formalism

In four dimensions we use a clever formalism called the *spinor helicity formalism*, which is convenient for many purposes. As almost all fermions are ultra-relativistic in high-energy collider experiments, they behave as massless particles. Helicity is thus conserved for particles interacting under a gauge group. Vector particle helicity is not conserved, but most helicity violating processes turn out to be zero at tree level.

To exploit the massless helicity states, we use the two-dimensional Weyl spinors to represent kinematic variables. The traditional four-momentum  $k^\mu$  is now represented by two spinors,  $u_+(k_i)$  and  $u_-(k_i)$ . The spinors are right- and left-handed, respectively. The massless spinors can be chosen in the following way

$$\begin{aligned}
 u_+(k) = v_-(k) = \frac{1}{\sqrt{2}} \begin{pmatrix} \sqrt{k^+} \\ \sqrt{k^-} e^{i\phi_k} \end{pmatrix}, \quad u_-(k) = v_+(k) = \frac{1}{\sqrt{2}} \begin{pmatrix} \sqrt{k^-} e^{-i\phi_k} \\ \sqrt{k^+} \end{pmatrix},
 \end{aligned}$$

where

$$e^{\pm i\phi_k} \equiv \frac{k^1 \pm ik^2}{(k^1)^2 + (k^2)^2}, \quad k^\pm = k^0 \pm \vec{k}.$$

For simplicity we use a bracket representation for the spinors, where

$$u_+(k_i) = v_-(k_i) = |i\rangle, \quad u_-(k_i) = v_+(k_i) = |i], \quad (2.22)$$

$$\bar{u}_+(k_i) = \bar{v}_-(k_i) = [i|, \quad \bar{u}_-(k_i) = \bar{v}_+(k_i) = i|, \quad (2.23)$$

where the  $v_\pm(k_i)$ 's are the negative energy solutions, which are indistinct from  $u_\mp(k_i)$  for  $k_i^2 = 0$ . The spinors solve the massless Dirac equation

$$\mathcal{K}_i u_\pm(k_i) = \mathcal{K}_i |i^\pm = 0, \quad (2.24)$$

and we can use them to build the Lorentz invariants

$$ij \equiv \bar{u}_-(k_i) u_+(k_j), \quad (2.25)$$

$$[ij] \equiv \bar{u}_+(k_i) u_-(k_j), \quad (2.26)$$

which we can think of as the square roots of the momentum invariants, up to a phase

$$ij [ij] = (k_i + k_j)^2 = s_{ij}. \quad (2.27)$$

We also have the following relations between spinors

$$\text{anti-symmetry} \quad : \quad [ij] = -[ji], \quad ij = -ji, \quad (2.28)$$

$$\text{four-momenta} \quad : \quad i|\gamma^\mu|i = 2k_i^\mu, \quad (2.29)$$

$$\text{momentum conservation} \quad : \quad \sum_{j=1}^n ij [ji] = 0, \quad (2.30)$$

$$\text{Schouten identity} \quad : \quad ij kl - ik jl = il kj, \quad (2.31)$$

and the projection operators

$$|p\rangle\langle p| = \frac{1}{2}(1 + \gamma^5)\not{p}, \quad (2.32)$$

$$|p\rangle\langle p| = \frac{1}{2}(1 - \gamma^5)\not{p}. \quad (2.33)$$

### Massless gauge bosons

The spinor helicity formalism also provides a simple way of representing the polarization vectors of massless spin-1 particles, such as gluons. The polarization vectors are represented by the four-momentum of the boson,  $k^\mu$ , and a reference momentum,  $p^\mu$ , that factors out of the final amplitude. The polarization vectors for positive and negative helicity gluons are

$$E_-(k^\mu; q^\mu) = i \frac{k|\gamma^\mu|q]}{2[qk]}, \quad E_+(k^\mu; q^\mu) = i \frac{q|\gamma^\mu k]}{2qk}. \quad (2.34)$$

This representation allows us to simply express amplitudes with external gluons, which could otherwise be a tedious (and at times impossible) task.



### Maximally helicity violating amplitudes

As an example of an amplitude with external gluons, consider the four-gluon tree level amplitude

$$A(1^{v_1} 2^{v_2} 3^{v_3} 4^{v_4}),$$

where  $v_i$  indicates the helicity of the gluon with momentum  $k_i$ . Investigating the different helicity combinations we find that the only non-vanishing amplitude has two positive and two negative helicity gluons [59]

$$\begin{aligned} A^{\text{tree}}(1^+2^+3^+4^+) &= 0, \\ A^{\text{tree}}(1^-2^+3^+4^+) &= 0, \\ A^{\text{tree}}(1^-2^-3^+4^+) &\neq 0. \end{aligned}$$

Gluon amplitudes with two negative helicity gluons are called *maximally helicity violating* (MHV) amplitudes, and can be written in a surprisingly simple form using spinor helicity

$$A^{\text{tree}}(1^-2^-3^+4^+) = \frac{12}{12 \ 23 \ 34 \ 41}.$$

The MHV amplitudes are also called *Parke-Taylor amplitudes*, and the general form for a color-ordered  $n$ -gluon MHV amplitude is

$$A^{\text{tree}}(1^+, \dots, i^-, \dots, j^-, \dots, m^-) = \frac{[ij]^4}{12 \ 23 \dots m-1, m, m, 1}. \quad (2.35)$$

Amplitudes with exactly two positive helicity gluons have a similar form, and are called the anti-MHV amplitudes ( $\overline{\text{MHV}}$ ). They are expressed using square brackets defined in Equation 2.26

$$A^{\text{tree}}(1^-, \dots, i^+, \dots, j^+, \dots, m^+) = \frac{[ij]^4}{[12][23] \dots [m-1, m][m, 1]}. \quad (2.36)$$

Note that for the 4-point case, the MHV and the anti-MHV are the same.

Amplitudes with more than two negative helicity gluons are named according to their ‘proximity’ to the MHV amplitudes. For example, the amplitude with three negative helicity gluons is called the *next-to-MHV amplitude*, and denoted NMHV. Similarly, the amplitude with  $k+2$  negative helicity gluons is the  $N^k$ MHV amplitude.

### Massive states

The spinor helicity formalism can also be used to describe massive states. The description given here, in particular of massive *scalars*, will follow [64] closely, although a more general formulation can be found in [65]. Amplitudes with massive scalars are related to amplitudes with massless scalars in  $D$  dimensions. The massless condition,  $P_D^2 = 0$ , gives the four-dimensional mass-shell equation  $P_4^2 = m^2$ , where  $m^2$  comes from the  $D - 4$  extra dimensions of momenta.

We will build amplitudes involving gluons and massive scalars from the three-point vertices using on-shell recursion<sup>6</sup>. The all-gluon three-point on-shell vertices

<sup>6</sup>Recursion is not described here, but several good descriptions can be found, e.g. in [66].

can have helicity configurations  $(- - +)$ (MHV) or  $(+ + -)$ ( $\overline{\text{MHV}}$ ), and are given by

$$A_3^{\text{tree}}(1^-, 2^-, 3^+) = \frac{12^3}{2331}, \quad A_3^{\text{tree}}(1^+, 2^+, 3^-) = \frac{[12]^3}{[23][31]}, \quad (2.37)$$

assuming complex momenta  $k_i$ .

To find the three-point amplitudes involving scalars, such as  $A_3^{\text{tree}}(1^s, 2^\pm, 2^s)$ , we begin with the vertex rule for a gluon, a scalar and an anti-scalar

$$V(p_1, k^\mu, p_2) = \sqrt{2}(l_1^\mu - l_2^\mu), \quad (2.38)$$

where  $p_1^s$  and  $p_2^{\bar{s}}$  are the momenta of the scalar and anti-scalar, respectively, and  $k^\mu$  is the momentum of the gluon. To get the three point amplitudes we contract the vertex rule with the gluon polarization vector given in Equation 2.34,

$$A_3^{\text{tree}}(1^s, 2^+, 3^s) = \frac{q |p_1| 2]}{q^2},$$

$$A_3^{\text{tree}}(1^s, 2^-, 3^s) = -\frac{2 |p_1| q]}{[q^2]},$$

where  $q$  is the reference momentum of the gluon. Note that the amplitude is still gauge invariant, in spite of the appearance of  $q$  in the expression. We can see this by exchanging the polarization vector with the momentum  $\varepsilon^\mu(p_2, q) \rightarrow p_2^\mu$  and imposing conservation of momenta  $(p_2 + p_1)^2 = p^2 \rightarrow p_1 \cdot p_2 = 0$ . Using the three-point amplitudes and recursion relations we also get the four-point amplitudes for two gluons and two massive scalars [64]

$$A_4^{\text{tree}}(1^s, 2^+, 3^+, 4^s) = i \frac{m^2[23]}{23 t_{12}}, \quad (2.39)$$

$$A_4^{\text{tree}}(1^s, 2^+, 3^-, 4^s) = i \frac{3 |1| 2]^2}{t_{23} t_{12}}, \quad (2.40)$$

where  $t_{ij} = 2p_i \cdot p_j$  and  $p | P|q] = P_\mu p | \gamma^\mu |q]$ .

### 2.6.2 Kinematics in $D$ dimensions

When calculating kinematics in amplitudes in  $D$  dimensions we resort to Lorentz products. All amplitudes are expressed in terms of  $D$ -dimensional momenta  $p^\mu$  and external polarization vectors  $\varepsilon$

$$p_i \cdot p_j, \quad p_i \cdot \varepsilon_j, \quad \varepsilon_i \cdot \varepsilon_j, \quad (2.41)$$

where  $\varepsilon_i = \varepsilon(p_i)$  is the polarization vector of the particle with momenta  $p_i$ .

The spinor helicity formalism is very useful for representing complicated kinematics in four dimensions, but when we extract information about loop amplitudes from unitarity cuts some information is lost if we only consider the results in four dimensions. This thesis will be focused on amplitudes where at least some of the external particles are massive. However, even in physical processes where external particles are massless, we cannot ignore massive contributions that could for example appear in loops at energies close to the mass threshold. We can find the massive loop contributions using unitarity cuts as described above, up to rational terms that

do not appear on any four-dimensional cuts. These rational terms can still be determined by knowing the form of the integrals that contribute to the amplitude, as described in [61]. Recall that in one-loop integrals we use dimensional regularization to get rid of divergences. That is, we integrate over  $D = 4 - 2\epsilon$  dimensions, where  $\epsilon$  is a small perturbation. In massive theories, this means we can have polynomial ambiguities proportional to factors of the form  $(K^2)^{-\epsilon}$ , where  $K^2$  is some kinematic variable. For massive particles these terms become proportional to  $m^{-2\epsilon}$ , which can soak up dimensions and become terms that are not visible on any four-dimensional cuts. When dealing with massive loop amplitudes it is therefore especially useful to have the  $D$ -dimensional form of the kinematics.

## Chapter 3

# Loop-Level Double-Copy for Massive Quantum Particles

We find that scattering amplitudes in massive scalar QCD can manifest the duality between color and kinematics at loop-level. Specifically we construct the one-loop integrands for four-point scattering between two distinct massive scalars, and the five-point process encoding the first correction to massive scalar scattering with gluonic radiation. We find that factorization and the color-kinematics duality are sufficient principles to entirely bootstrap these calculations, allowing us to construct all contributions ultimately from the three-point tree-level amplitudes which are themselves entirely constrained by symmetry. Double-copy construction immediately provides the associated predictions for massive scalars scattering in the so called  $N = 0$  supergravity theory.

### 3.1 Introduction

Traditional methods of calculating quantum gravitational scattering amplitudes using Feynman rules quickly run into difficulties. There are two aspects to Feynman rule gravitational calculation that conspire to cause trouble. First, off-shell Feynman rules for gravitation are large and unwieldy, and have contact terms for every multiplicity of interaction. Second, the scattering amplitudes involve a factorially growing number of local graphs – either as multiplicity or loop level increases. The former trouble can be alleviated by using unitarity methods – the idea that one should only ever write down on-shell physical expressions when constructing predictions. The latter can be mitigated by exploiting the double-copy structure to consider smaller building-blocks of physical predictions relevant to gravity, which are easier to calculate in gauge theories. We will take advantage of both of these approaches to calculate  $D$ -dimensional scattering amplitudes in the  $N = 0$  supergravity theory through the integrand of one-loop five-point scattering between two distinct massive scalars with emitted gravitational radiation. In the classical limit this will describe the gravitationally radiative correction to the scattering of scalar black holes. We will do this by bootstrapping  $D$ -dimensional predictions in massive scalar Quantum Chromodynamics (QCD).

Unitarity cuts [4] allow for the integrands of incredibly complicated loop-level predictions to be verified systematically and invariantly with compact on-shell tree-level data. Better yet, they allow for a principled fusing [60, 61] of tree-level data into multi-loop integrands. This is true independent of presence or absence of supersymmetry, independent of number and representation of colors, or flavors, and independent of number or type of massive particles. Ref. [9] inverted the verification of generalized unitarity cuts [5, 62, 63] towards a constructive approach that was ansatz free (cf. [67]), an approach called the *method of maximal cuts*. This does not

mitigate the factorial explosion in graphs, but it means every stage of construction need only deal with a subset of graphs, and only their compact on-shell expressions.

Double-copy structure is more subtle, but may ultimately prove just as useful for higher order corrections to phenomenological gravitational scattering. We have known since the 1980s, from string theory limits, that color-stripped gauge theory semi-classical (tree-level) amplitudes encode gravitational amplitudes [68, 69]. This realization is often informally referred to as the idea that “Gravity is the square of Yang-Mills.” Bern, Carrasco and Johansson, discovered a local graphical story (BCJ) relating these predictions [7], called double-copy construction, one that generalizes straightforwardly to quantum (multi-loop) corrections [8] at the integrand level.

The key idea behind double-copy construction is that for gauge theory predictions (by definition containing both color and kinematic components), one can find representations where term by term kinematic weights obey the same algebraic relations as generic color weights. Such kinematic weights are said to be color-dual. This makes dynamics and charges interchangeable and indeed realizes graviton (spin-2) scattering, in asymptotically flat space, as gluonic (spin-1) predictions whose charges are the kinematics of gluons (spin-1). This offers a profound calculational advantage even for gauge theories. Because of the rigid algebraic rules locking the kinematic weights of each graph, only a small fraction of the graphs need to be dressed functionally, and all other local graphs inherit that dressing. Color-dual loop-level construction has largely occurred only in massless theories (or those where mass can be clearly associated with the dimensional reduction of a massless higher-dimensional theory). Here we make the novel demonstration that loop-level massive integrands in scalar-QCD admit color-dual descriptions. This is a non-trivial step towards color-dual loop-level massive quark amplitudes.

In four dimensions there are two physical states for every gluon, so one should expect four physical states in the double-copy (the outer product of gluonic states). As (in four dimensions) gravitons also have two physical states, this means the natural double-copy in four-dimensions accounts for additional states beyond gravitons. In  $D$  dimensions the double copy of gluonic states means tracking  $(D - 2)^2$  states (see discussions in [70] and references therein). Indeed, besides a graviton ( $(D(D - 3)/2)$  states), naive double-copy amplitudes generically will have a dilaton (1 state) as well as anti-symmetric tensors  $((D - 2)(D - 3)/2)$  states) contributing to loop-predictions for massless external states. In gravitational double-copy amplitudes for massive external states, even at tree level, one can generically expect the contributions of dilatons [71]. This state counting and attribution naturally fits in with the states that contribute to supergravity theories, which is why the naive double-copy of pure Yang-Mills is often called  $N = 0$  supergravity. This theory involves Einstein gravity coupled to a scalar field (known as the dilaton) as well as a two-form (often called the Kalb-Ramond field)—understandable as an axion in four dimensions. Indeed the amplitudes presented in this chapter double-copy to massive scalars coupled to the  $N = 0$  supergravity theory. Although it does not concern us for the purposes of this chapter, it is worth pointing out that for pure gravities with less than half-maximal supersymmetry, including pure Einstein-Hilbert gravity, there are various strategies for projecting out such extra-gravitational double-copy states (see eg. [39, 72, 73] and references therein).

Besides inviting a calculational virtuosity in gauge theories, there have been many motivations for studying quantum gravitational scattering amplitudes. One recent driver of the field has been to understand the ultraviolet behavior of supergravity theories. This question is indeed responsible for the discovery of the duality between color and kinematics, as well as the associated double-copy construction, and has

benefitted from it in return — see e.g. [8, 74–84]. Even pure gravity manifests many unexpected cancellations beyond naive powercounting [85], suggesting that only a little help in the ultraviolet may be sufficient for perturbative finiteness. The advent of precision gravitational wave observation has provided a new urgency to discovering whether or not the simplicity in quantum gravitational gauge-invariant observable calculation can be applied to classical gravitational observables (see e.g. refs. [10–47]). Recent work has shown that multi-loop scattering amplitudes encode higher-order corrections to classical observables. Indeed the highest order correction in the gravitational coupling,  $G_N$ , (often called post-Minkowskian [PM]) to conservative Black Hole binding energy (3 PM) was only made within the past couple of years and centered amplitudes insights (see [38, 39] and references therein). This calculation required the classical remnant of the two-loop four-point scattering amplitude between two massive scalars.

Optimizing for the classical result, refs. [38, 39] exploit double-copy construction at tree-level, building the classically relevant gravitational integrand using unitarity methods from double-copied gravitational trees. The approach we present here is complementary. All unitarity construction occurs for the gauge theory only. The subsequent gravitational loop-level integrand arises from double-copy directly. In conjunction with an appropriate classicalization procedure, this approach offers interesting possibilities. By lining up simultaneous classical Yang-Mills and Gravitational gauge-invariant observables where the duality between color and kinematics is manifest, one may hope to resolve ambiguities around applying double-copy directly in classical construction. We leave associated extraction of classical predictions from the quantum integrands presented here to future consideration.

We will begin our bootstrap at tree-level in Section 3.2 where we will find symmetry considerations alone completely fix the three-point amplitude, and higher multiplicity are entirely constrained by factorization and the color-kinematics duality. Similarly we will only need to exploit these principles to construct our loop level results at four-point one-loop in Section 3.3.2 and five-point one-loop in Section 3.3.3. We conclude and present next steps in Section 4.5.

## 3.2 Bootstrapping Tree Amplitudes

The calculational setup for arriving at the tree level amplitudes in scalar QCD will be a bootstrapping method that takes advantage of factorization as well as the color-kinematics duality relations to fix kinematic ansatzes for the graphs that contribute to a given amplitude. Let us sketch in general how such a calculation proceeds, then consider specific calculation of relevant tree-level amplitudes needed to constrain via factorization the loop-level amplitudes we will eventually construct.

In general there will be some set of graphs  $\Gamma$  contributing to a tree-level amplitude of a given multiplicity with particular external legs. The graphs and color-kinematic relations between the numerators can be generated simultaneously. As is standard in massless theories in the adjoint, one can introduce an operator that takes an edge of a graph, and returns a different graph which is identical to the first graph except for the rearranged connectivity about the originally specified edge, as illustrated in Figure 3.1. Briefly summarized, a  $\hat{t}$ -operation takes an internal edge in a trivalent graph as a Mandelstam  $s$ -channel subgraph, and rearranges the connectivity to a Mandelstam  $t$ -channel subgraph, while holding all other legs fixed. Similarly, the  $\hat{u}$ -operator rearranges an  $s$ -channel to a  $u$ -channel subgraph. So given an edge of one graph, one can understand the potential three-term identities it contributes to by

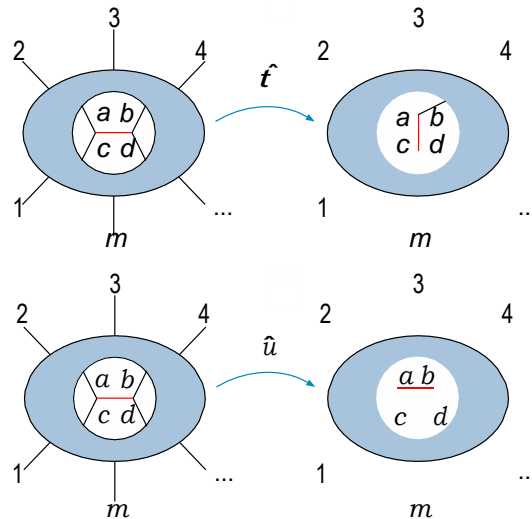


Figure 3.1: Graph manipulation operators that rearrange one internal edge's connectivity. This is useful for specifying Jacobi-like relations, e.g.  $c(g) = c(\hat{t}g) + c(\hat{u}g)$ .

simply considering for each edge:  $n(g) = n(\hat{t} \circ g) + n(\hat{u} \circ g)$ . By tracking any novel topologies introduced into a graph set by these operators, one can start with one tree-graph and generate all cubic graphs relevant to that amplitude simultaneously with all requisite color-dual kinematic constraints by operating on every edge of every graph until closure.

Once all the graphs of an amplitude are determined, the set of graphs can be arranged into a number of distinct topologies with different labelings. Each topology is assigned with a numerator function  $n_i(k_1, \dots, k_m)$ , which encodes all the kinematics of that specific topology, and is fully determined by the order of the  $m$  external legs  $(k_1, \dots, k_m)$ . The generated color-dual kinematic relations then become a system of equations between the numerator functions, which we can solve for in terms of the kinematic weights of *basis graph* topologies. All numerator functions can then be expressed as linear combinations of the basis graphs relabeled with different arguments. The kinematic weight of every basis graph topology is given an ansatz consisting of kinematic products of momenta and polarization vectors, depending on the amplitude in question. For example, consider the purely gluonic amplitude. For such an amplitude there is only one such basis graph at every multiplicity at tree-level, the so-called "half-ladder" or multi-peripheral graph. All other topologies follow from  $\hat{t}$  operations (the color-order preserving whitehead move) away from the half-ladder. The  $\hat{u}$  operator on a half-ladder simply takes one to a half-ladder with permuted leg-label arguments. This means for each multiplicity at tree-level for purely gluonic amplitudes, one need only supply an ansatz to a single topology. We will see in various cases how this may change when we allow a combination of external massive scalars as well as glue.

To constrain the coefficients of the ansatz given to the basis graphs, we consider the relabeling symmetries – or *isomorphisms* – of each topology. The set of all symmetries of all graphs, along with the kinematic duality relations which are not trivial after solving for the basis graphs, constrain the ansatz coefficients. One should note critically – these are operations simply between functional numerators, not the factorial expanse of entire amplitudes nor even the relative exponential expanse of ordered



amplitudes. Any remaining parameters for this theory can be entirely constrained by factorization by considering all cuts of any single-propagator from all of the graph-topologies. This color-kinematic bootstrap begins at the three-point tree-level. For scalar QCD amplitudes, these are entirely-fixed up to the coupling constant by mass dimension and anti-symmetry. It should be noted, this means that for Yang-Mills amplitudes: factorization with color-dual kinematics encodes gauge-invariance.

### 3.2.1 Three-point trees

Let us consider first the purely-gluonic three-point amplitude. If it has a chance of being gauge invariant, every external polarization must appear in each term once and only once. As all external legs are on-shell, conservation of momentum means any inner product between any two external momenta must vanish. The Yang-Mills mass dimension allows us only three potential monomials in our basis:

$$n_3(k_1, k_2, k_3) = \alpha_1(k_3 \cdot E_1)(\varepsilon_2 \cdot \varepsilon_3) + \alpha_2(k_3 \cdot \varepsilon_2)(\varepsilon_1 \cdot \varepsilon_3) + \alpha_3(k_2 \cdot \varepsilon_3)(\varepsilon_1 \cdot \varepsilon_2). \quad (3.1)$$

Antisymmetry immediately constrains our ansatz via:  $\alpha_2 \rightarrow -\alpha_3$ , and  $\alpha_1 \rightarrow \alpha_3$ . We are left with only one free parameter  $\alpha_3$  which can be taken to be the gluonic coupling  $g$  appropriately scaled, fixed to canonical normalization by comparing with Feynman rules in a particular gauge (c.f. Feynman rules in e.g. refs. [58, 87]), or set to unity, absorbing coupling constants in the definition of full amplitudes, and a phase in the definition of ordered amplitudes. We choose the latter to minimize the complexity of kinematic numerator weights.

Next, to complete the three-point amplitudes for scalar QCD we need only consider the three-point amplitude with one external gluon and two external same-mass scalars. Again we are not allowed any inner-products between external momenta, and we only have one polarization. The mass-dimension means we can only write down a single inner-product, fortunately it itself is anti-symmetric via conservation of momenta:  $k_1 \cdot \varepsilon_3 = -k_2 \cdot \varepsilon_3$  as  $k_3 \cdot \varepsilon_3 = 0$ , yielding:

$$n_{3,2}(k_1^m, k_2^m, k_3) = \alpha_1(k_1 \cdot \varepsilon_3). \quad (3.2)$$

Here, once again, we can take  $\alpha_1$  to be the coupling constant suitably normalized, or as is our convention we will set  $\alpha_1 = -1$ , having pulled the coupling constant into the definition of the full amplitude. We have written down all three-point amplitudes purely by considering mass-dimension and anti-symmetry up to normalization convention. Everything else will follow through loop-level by simply considering factorization and the duality between color and kinematics.

### 3.2.2 Four-point trees

At four-point tree level in scalar QCD there are three distinct amplitudes. The two distinct amplitudes that involve external masses: one with one pair and one with two pairs of massive scalars respectively, are illustrated in Figure 3.2. The third amplitude, the purely gluonic amplitude, is not required for our one-loop construction so we do not report on it here, but it follows by the same bootstrap method we apply to these massive scalar amplitudes.



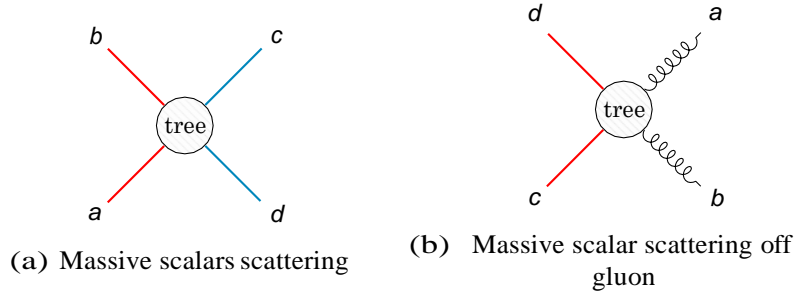


Figure 3.2: The four-point tree amplitudes in scalar QCD.

### Two massive scalars

The ordered four-point tree-amplitude for two pairs of massive scalars can be easily computed with a simple product of the three-point color-ordered Feynman rules [58, 87]. The result, up to normalization and phase, is given by

$$A_{4,2}^{\text{tree}}(k_1^{m_1}, k_2^{m_1}, k_3^{m_2}, k_4^{m_2}) = \frac{(k_1 - k_2) \cdot k_3}{2(k_1 + k_2)^2}. \quad (3.3)$$

In this section we will introduce the bootstrapping framework amplitudes to reconstruct this amplitude – overkill in this case, but as we will see this technique is quite generalizable and indeed takes us to loop-level.

### Bootstrapping the two pairs of massive scalars four-point amplitude

Writing down the graphs that contribute to the two massive scalar pairs amplitude, we see that one graph *topology*, or graph type, appears. The topology has a massless propagator, and for canonical external legs  $(a, b, c, d)$  is given the kinematic numerator function

$$= n_{4,2}(a, b, c, d). \quad (3.4)$$

We note that this is the only graph that contributes to the amplitude, but to maintain bose-symmetry of the full-amplitude this kinematic weight must obey the same (anti-)symmetry properties as it's color weight with both massive scalars dressed in the adjoint.

We will now give an ansatz to the numerator function in Equation (3.4). The graph has no external gluons, so the ansatz will consist solely of Lorentz products of momenta,

$$n_{4,2}(a, b, c, d) = \alpha_1 t_{ab} + \alpha_2 t_{bb} + \alpha_3 t_{bc} + \alpha_4 t_{cc}, \quad (3.5)$$

where  $t_{ij} \equiv (k_i \cdot k_j)$ , and  $\alpha_k$  are the free coefficients of the ansatz.

We determine some of the coefficients in Equation (3.5) by using the isomorphisms of the graph in Equation (3.4). The isomorphisms are expressed as relabelings of the

numerator function

$$\begin{aligned}
n_{4,2} &= -n_{4,2}(b, a, c, d), & n_{4,2} &= -n_{4,2}(c, d, b, a), \\
n_{4,2} &= -n_{4,2}(a, b, d, c), & n_{4,2} &= -n_{4,2}(d, c, a, b), \\
n_{4,2} &= n_{4,2}(b, a, d, c), & n_{4,2} &= n_{4,2}(d, c, b, a), \\
n_{4,2} &= n_{4,2}(c, d, a, b),
\end{aligned} \tag{3.6}$$

where we have suppressed the canonical arguments  $(a, b, c, d)$  on the left-hand side of each equation. Writing out the symmetry relations in terms of the ansatz in Equation (3.5) fixes three of the coefficients

$$\alpha_4 = 0, \quad \alpha_1 = \alpha_2 = \frac{\alpha_3}{2}, \tag{3.7}$$

and the numerator function is determined up to an overall factor

$$n_{4,2}(a, b, c, d) = \frac{\alpha_3}{2} (t_{ab} + t_{bb} + 2t_{bc}). \tag{3.8}$$

The numerator in Equation (3.8) now obeys the symmetries of the graph for this amplitude. The overall factor  $\alpha_3$  is completely determined by considering the cut of the only propagator in the ordered amplitude,

$$A_{4,2}^{\text{tree}}(a^{m_1}, b^{m_1}, c^{m_2}, d^{m_2}) = \frac{n_{4,2}(a, b, c, d)}{(a+b)^2}. \tag{3.9}$$

Satisfying factorization means that the sum over on-shell physical (cut) gluonic states of the three-point amplitudes is equal to  $n_{4,2}$  evaluated under the cut condition:

$$\sum_{s \in \text{states}} A_{3,2}(a^{m_1}, b^{m_1}, l^s) A_{3,2}(-l^s, c^{m_2}, d^{m_2}) = n_{4,2}(a, b, c, d)|_{(a+b)=0}^{\text{cut}} \tag{3.10}$$

The sum runs over the polarization states of the  $D$ -dimensional polarization vectors and is given (e.g. [39, 70, 88] and references therein) by the physical state projector

$$P^{\mu\nu}(p, q) = \underset{\text{pols.}}{\varepsilon^\mu(-p)\varepsilon^\nu(p)} = \eta^{\mu\nu} - \frac{q^\mu p^\nu + p^\mu q^\nu}{q \cdot p}, \tag{3.11}$$

where  $q$  is an arbitrary null reference momenta. Any such reference momenta must cancel out of any physical expression once the cut conditions and conservation of momenta have been imposed. It turns out for the cuts we consider in this chapter, when each side is dressed with color-dual kinematic weights, the above general projector is equivalent to a much simpler gauge-dependent projector,

$$\underset{\text{pols.}}{\varepsilon^\mu(-p)\varepsilon^\nu(p)} \rightarrow \eta^{\mu\nu}. \tag{3.12}$$

This projector is a gauge-dependent choice, so if ever used in construction its appropriateness must be ensured (c.f. [88]) or all gauge-compatibility must be verified via comparison with the above general projector (or equivalent constraints) as we have in this chapter on a cut-by-cut basis. This completely fixes  $\alpha_3 = -1$ , matching via bootstrap exactly what is given by Feynman rules in Equation (3.5). The numerator

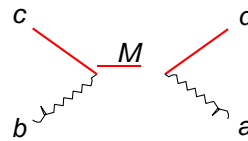
function is therefore

$$n_{4,2}(a, b, c, d) = -\frac{1}{2} (t_{ab} + t_{bb} + 2t_{bc}). \quad (3.13)$$

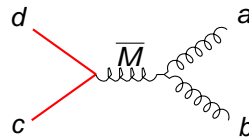
The functional ordered amplitude for two massive scalar pairs at tree level follows from simply dividing the kinematic numerator by the single graph's massless propagator.

### One massive scalar

The amplitude for one massive scalar pair scattering with a gluon represents a more lively application of bootstrapping approach, as it requires contributions from two distinct graph topologies whose kinematics are related by a color-dual identity. The relevant topologies are distinguished by whether the propagator is massive,  $M$ , or massless,  $\bar{M}$ ,



$$= n_{4,1}^M(a, b, c, d), \quad (3.14)$$



$$= n_{4,1}^{\bar{M}}(a, b, c, d). \quad (3.15)$$

It suffices to consider only one of the duality equations in order to identify a basis graph:

$$n_{4,1}^{\bar{M}}(a, b, c, d) = n_{4,1}^M(a, b, c, d) - n_{4,1}^M(b, a, c, d). \quad (3.16)$$

As  $n_{4,1}^{\bar{M}}$  can be expressed entirely in terms of  $n_{4,1}^M$ , we identify  $M$  as the basis graph and proceed to develop a kinematic ansatz for its numerator weight,  $n_{4,1}^M$ .

As shown in Equation (3.14), two of the external legs are gluons, so the ansatz will contain products of their polarization vectors. Each polarization vector appears once, and only once, in every term. We therefore apply the following ansatz

$$n_{4,1}^M(a, b, c, d) = \left( \alpha_1 t_{ab} + \alpha_2 t_{bc} + \alpha_3 t_{cc} t_{\varepsilon_a \varepsilon_b} + \alpha_4 t_{be} t_{a \varepsilon_b} \right. \\ \left. + \alpha_5 t_{ce} t_{a \varepsilon_b} + \alpha_6 t_{be} t_{ce} + \alpha_7 t_{ce} t_{ce} \right), \quad (3.17)$$

where  $\alpha_i$  are the free coefficients of the ansatz, and  $\varepsilon_p = \varepsilon(p)$  is the polarization vector of the particle with momenta  $p$ .

Similarly to the previous amplitude, we identify the isomorphisms of each of the contributing graphs,

$$\begin{aligned} n_{4,1}^{\bar{M}} &= -n_{4,1}^{\bar{M}}(b, a, c, d), & n_{4,1}^{\bar{M}} &= n_{4,1}^{\bar{M}}(b, a, d, c), \\ n_{4,1}^{\bar{M}} &= -n_{4,1}^{\bar{M}}(a, b, d, c), & n_{4,1}^{\bar{M}} &= n_{4,1}^{\bar{M}}(b, a, d, c), \end{aligned} \quad (3.18)$$

where we have again suppressed the canonical arguments  $(a, b, c, d)$  on the left-hand side of each equation. Constraining the single ansatz in terms of these relations offers

$$\alpha_5 = \alpha_7 - \alpha_6. \quad (3.19)$$



(a) Massive scalars scattering with (b) Massive scalar and gluon scattering with emitted gluon

Figure 3.3: The five-point tree amplitudes in scalar QCD.

To constrain the remaining coefficients of the numerator function one imposes factorization constraints as we did for the two-pairs of mass case considered earlier. This yields,

$$\alpha_1 = \alpha_3 = \alpha_4 = 0, \quad \alpha_6 = \alpha_7 = 2, \quad \alpha_2 = -1. \quad (3.20)$$

The basis numerator weight for the scattering of a massive scalar and gluon is then

$$n_{4,1}^M(a, b, c, d) = t_{ce_b}(t_{be_a} + t_{ce_a}) - \frac{1}{2} t_{bc} t_{\varepsilon_a \varepsilon_b}. \quad (3.21)$$

The resulting ordered amplitude follows,

$$\begin{aligned} A_{4,1}^{\text{tree}}(a, b, c^m, d^m) &= \frac{n_{4,1}^M(a, b, c, d)}{(b+c)^2 - m^2} + \frac{n_{4,1}^M(a, b, c, d)}{(a+b)^2} \\ &= \frac{(t_{be_a} + t_{ce_a})t_{ce_b} - \frac{1}{2} t_{bc} t_{\varepsilon_a \varepsilon_b}}{(b+c)^2 - m^2} + \\ &\quad \frac{t_{be_a} t_{ce_b} - t_{ce_a} t_{ae_b} + \frac{1}{2} (t_{ac} - t_{bc}) t_{\varepsilon_a \varepsilon_b}}{(a+b)^2}. \end{aligned} \quad (3.22)$$

The ordered amplitudes for a massive scalar and gluon scattering are known for explicit helicity configurations in  $D = 4$  spacetime dimensions. It is a useful exercise to compare our  $D$ -dimensional amplitude with appropriately chosen polarizations with the two independent four-dimensional amplitudes of ref. [64].

### 3.2.3 Five-point trees

At five-point tree level we again consider two distinct amplitudes with one and two massive scalar pairs, each now with an additional emitted gluon as shown in Figure 3.3. The amplitudes are bootstrapped using precisely the same procedure. The  $D$ -dimensional form of these tree level amplitudes we arrive at will allow a simple calculation of the unitarity cuts required for loop level.

#### Two massive scalars

We consider first the five-point amplitude with two massive scalar pairs. The graph topologies for this amplitude are shown in Figure 3.4. We now distinguish between the topology with two massless propagators ( $\overline{M}$ ), and the graph topology with one of the propagators massive ( $M$ ).

To identify a basis graph for this amplitude we write down one of the duality equations,

$$n_{5,2}^{\overline{M}}(a, b, c, d, e) = n_{5,2}^M(a, b, c, d, e) - n_{5,2}^M(a, c, b, d, e), \quad (3.23)$$

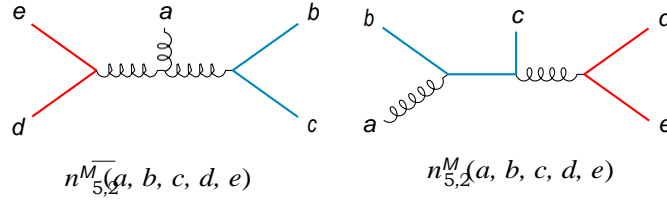


Figure 3.4: Graph topologies contributing to the amplitude for two massive scalars scattering with an emitted gluon.

from which see the massless propagator graph's kinematic weight,  $n_{5,2}^{\overline{M}}$ , can be entirely expressed in terms of the  $M$  graph's kinematics weight  $n_{5,2}^M$ . As such, we need only give the basis numerator  $n_{5,2}^M$  an ansatz, which we will constrain via color-dual relations and factorization. The rest of the amplitude follows directly. The ansatz is given in terms of Lorentz invariants of all momenta, including the polarization vector of the external gluon, labelled  $\varepsilon(a)$  in our canonical expression, which should appear once and only once in every term. We therefore begin with an ansatz of the form,

$$\begin{aligned} n_{5,2}^M(a, b, c, d, e) = & t_{be_a} (\alpha_1 t_{ab} + \alpha_4 t_{ac} + \alpha_7 t_{ad} + \alpha_{10} t_{bc} + \alpha_{13} t_{cc} + \alpha_{16} t_{cd} + \alpha_{19} t_{dd}) \\ & + t_{ce_a} (\alpha_2 t_{ab} + \alpha_5 t_{ac} + \alpha_8 t_{ad} + \alpha_{11} t_{bc} + \alpha_{14} t_{cc} + \alpha_{17} t_{cd} + \alpha_{20} t_{dd}) \\ & + t_{de_a} (\alpha_3 t_{ab} + \alpha_6 t_{ac} + \alpha_9 t_{ad} + \alpha_{12} t_{bc} + \alpha_{15} t_{cc} + \alpha_{18} t_{cd} + \alpha_{21} t_{dd}) . \end{aligned} \quad (3.24)$$

The isomorphisms of the graphs in Figure 3.4 are

$$\begin{aligned} n_{5,2}^M &= -n_{5,2}^{\overline{M}}(a, b, c, e, d), \quad n_{5,2}^{\overline{M}} = -n_{5,2}^M(a, d, e, b, c), \\ n_{5,2}^M &= -n_{5,2}^{\overline{M}}(a, b, c, e, d), \quad n_{5,2}^{\overline{M}} = n_{5,2}^M(a, d, e, c, b), \\ n_{5,2}^{\overline{M}} &= -n_{5,2}^M(a, c, b, d, e), \quad n_{5,2}^M = n_{5,2}^{\overline{M}}(a, e, d, b, c), \\ n_{5,2}^{\overline{M}} &= n_{5,2}^M(a, c, b, e, d), \quad n_{5,2}^M = -n_{5,2}^{\overline{M}}(a, e, d, c, b), \end{aligned} \quad (3.25)$$

where the canonical labeling  $(a, b, c, d, e)$  has been suppressed on the left-hand sides of the equations.

After imposing the symmetry constraints, eight coefficients remain to be determined. The five-point ordered amplitude  $A_{5,2}^{\text{tree}}(a, b, c, d, e)$  is given,

$$A_{5,2}^{\text{tree}}(a, b, c, d, e) = \frac{n_{5,2}^M(a, b, c, d, e)}{(d+e)^2((a+b)^2 - m_1^2)} + \frac{n_{5,2}^M(a, e, d, b, c)}{(b+c)^2((a+e)^2 - m_2^2)} + \frac{n_{5,2}^M(a, b, c, d, e)}{(b+c)^2(d+e)^2} \quad (3.26)$$

where  $m_1^2$  is the square mass of the scalar particle  $b, c$ , and  $m_2^2$  is the square mass of the scalar particle  $d, e$ . Factorization involving one-particle cuts of both the massive propagator and the massless propagator fixes the remaining coefficients.

The basis numerator function then takes the simple form matching results in the literature [89],

$$n_{5,2}^M(a, b, c, d, e) = \frac{1}{4} [t_{ab} t_{ce_a} + 2t_{ab} t_{de_a} + (t_{ab} + 2t_{ac} + 2t_{bc} + 2t_{cc} + 4t_{cd}) t_{be_a}], \quad (3.27)$$

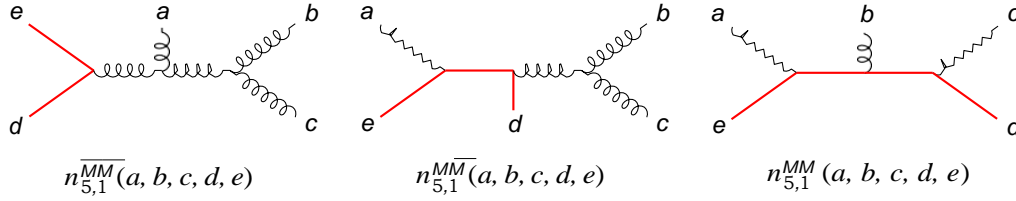


Figure 3.5: Graph topologies contributing to the amplitude for a massive scalar and gluon scattering, with an emitted gluon.

and the massless numerator function is given

$$n_{5,2}^M(a, b, c, d, e) = \frac{1}{4} [2(t_{bc} + 2t_{cd} + t_{cc})(t_{be_a} + t_{ce_a}) + t_{ab}(t_{be_a} + 3t_{ce_a} + 2t_{de_a}) + t_{ac}(t_{be_a} + 3t_{ce_a} - 2t_{de_a}) + 4t_{ad}t_{ce_a}]. \quad (3.28)$$

### One massive scalar

The five-point amplitude with one massive scalar pair has three possible graph topologies, all shown in Figure 3.5. The topologies are distinguished by whether they have zero ( $\overline{MM}$ ), one ( $M\overline{M}$ ), or two ( $MM$ ) massive propagators. To determine the basis graph under the kinematic algebra relations we need consider a subset of two kinematic color-dual relations, suppressing arguments  $(a, b, c, d, e)$  on the LHS of the equations,

$$\begin{aligned} n_{5,1}^{\overline{MM}} &= n_{5,1}^{M\overline{M}}(a, b, c, d, e) - n_{5,1}^{M\overline{M}}(a, b, c, e, d), \\ n_{5,1}^{MM} &= n_{5,1}^{MM}(a, b, c, d, e) - n_{5,1}^{MM}(a, c, b, d, e). \end{aligned} \quad (3.29)$$

From the duality relations we see that  $MM$  can be selected as the basis graph, and therefore proceed to give its numerator function a kinematic ansatz.

The amplitude has three external gluons, each of which should have a polarization vector in every term in the numerator ansatz. We construct an 81 term ansatz for  $n_{5,1}^{MM}$  from monomials of the forms  $t_{ie} t_{jc} t_{mf}$  and  $t_{e\epsilon} t_{jc} t_{mn}$ .

The graphs in Figure 3.5 have the following isomorphisms

$$\begin{aligned} n_{5,1}^{\overline{MM}} &= -n_{5,1}^{\overline{MM}}(a, b, c, e, d), & n_{5,1}^{\overline{MM}} &= -n_{5,1}^{\overline{MM}}(a, c, b, d, e), \\ n_{5,1}^{M\overline{M}} &= n_{5,1}^{M\overline{M}}(a, c, b, e, d), & n_{5,1}^{M\overline{M}} &= -n_{5,1}^{M\overline{M}}(a, c, b, d, e), \\ n_{5,1}^{MM} &= -n_{5,1}^{MM}(c, b, a, e, d), \end{aligned} \quad (3.30)$$

where the canonical labeling  $(a, b, c, d, e)$  has been omitted on the left-hand side of the equations. Imposing the symmetries fixes 38 of the 81 coefficients of the ansatz, the remaining physical 40 parameters are fixed by factorization involving only one-particle cuts. It is amusing to note that three remaining unconstrained coefficients never show up in a physical amplitude, representing residual generalized gauge freedom available to this five-point color-dual representation. The resulting  $D$ -dimensional ordered

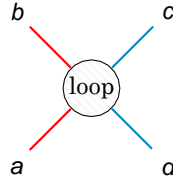


Figure 3.6: The four-point loop amplitude for massive scalar scattering in scalar QCD.

amplitude is given by

$$A_{5,1}^{\text{tree}}(a, b, c, d^m, e^m) = \frac{n_{5,1}^{MM}(a, b, c, d, e)}{((c+d)^2 - m^2)((a+e)^2 - m^2)} + \frac{n_{5,1}^{MM}(a, b, c, d, e)}{((a+e)^2 - m^2)(b+c)^2} + \frac{n_{5,1}^{MM}(a, b, c, d, e)}{(b+c)^2(d+e)^2} - \frac{n_{5,1}^{MM}(c, b, a, e, d)}{((c+d)^2 - m^2)(a+b)^2} + \frac{n_{5,1}^{MM}(c, b, a, d, e)}{(d+e)^2(a+b)^2}. \quad (3.31)$$

This amplitude can be numerically compared with the 4D amplitudes given in [64]<sup>1</sup>

### 3.3 Bootstrapping One-loop Integrands

#### 3.3.1 Loops (just like trees!)

Because the bootstrap approach – applied at tree-level in the previous section – is functional in terms of graph topologies, we can apply it directly towards constructing loop integrands. At loop level the role of tree-level one-particle factorization considerations is replaced by more general multi-leg unitarity cuts. At one-loop the numerator functions now take an additional argument compared to the same-multiplicity tree level case, namely the loop momentum  $\ell$ . The kinematic Jacobi-like relations are used to find a minimal set of basis graphs, which are in turn dressed with ansätze consistent with expected power counting. The ansätze are finally constrained using the remaining kinematic Jacobi-like relations, symmetries of the graph topologies, and a spanning set of generalized unitarity cuts.

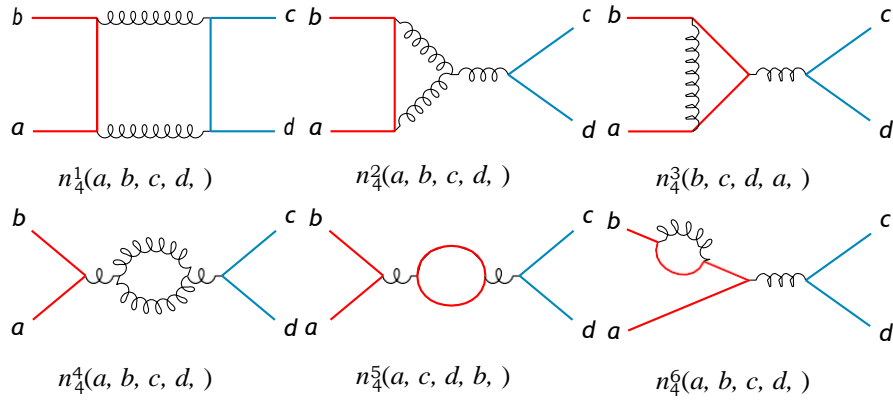
Recall that the full gauge amplitudes will be given by Equation (2.1), and the full  $N = 0$  supergravity amplitudes given by Equation (2.8). The subsequent sections will be concerned with identifying the appropriate color-dual kinematic weights,  $n(g)$ , of each graph topology relevant to one-loop four-point, and one-loop five-point amplitudes respectively.

#### 3.3.2 Four-point one-loop construction

In this section we determine a color-dual representation of the four-point one-loop amplitude for two pairs of massive scalars. The possible graph topologies of this amplitude are shown in Figure 5.1, including the snail graph<sup>2</sup> and excluding tadpoles. By inspecting the kinematic duality relations we find that we have some freedom in choosing the basis graphs for this amplitude. We will take as basis graphs:  $n_4^1(a, b, c, d, \ell)$  and  $n_4^3(a, b, c, d, \ell)$ . The remaining numerator functions can be written

<sup>1</sup>Verifying all of [64]’s five-point three-gluon and two-scalar amplitudes, with a corrected relative sign for the case where two of the external gluons are positive and one negative.

<sup>2</sup>We refer to graphs with a bubble on an external leg as snail graphs.

Figure 3.7: Graph topologies that contribute to  $\mathcal{A}_4^{1\text{-loop}}$ .

as linear combinations of these,

$$\begin{aligned}
n_4^2 &\equiv n_4^1(a, b, c, d, c+d) - n_4^1(a, b, d, c, c+d), \\
n_4^4 &\equiv n_4^1(a, b, c, d, c+d) + n_4^1(a, b, c, d, ) \\
&\quad - n_4^1(a, b, d, c, c+d) - n_4^1(a, b, d, c, ), \\
n_4^5 &\equiv n_4^3(a, c, d, b, a) + n_4^3(a, c, d, b, -b), \\
n_4^6 &\equiv n_4^1(a, b, c, d, ) - d \leftrightarrow c - n_4^3(a, c, d, b, ),
\end{aligned} \tag{3.32}$$

where all kinematic numerator weights on the LHS of the equalities functionally take arguments:  $(a, b, c, d, )$ .

The basis graphs  $n_4^1(a, b, c, d, )$  and  $n_4^3(a, b, c, d, )$  are given ansätze, based on power counting and the known form of tree level amplitudes in the previous section. All external particles are scalars, and we expect to see a monomial of degree two in Lorentz invariants per term. The number of independent monomials of the form  $t_{abcd}$  including inner products with loop momenta give 36 parameter ansatz for  $n_4^1$ . The basis numerator  $n_4^3$  is the same size, so the total number of free coefficients is therefore 72. As with the tree-level amplitudes we impose symmetries and color-kinematic constraints (see, e.g. Appendix 3.4.1), which fix 43 of the coefficients. This leaves 29 coefficients to constrain via generalized unitarity cuts.

The unitarity cuts are performed using the tree amplitudes generated in the previous section. Three unitarity cuts will be sufficient to determine the physical part of the numerators<sup>3</sup>, and they are illustrated in Figure 3.8. The first unitarity cut puts two massless internal legs on-shell, and the second and third cuts put two massive internal legs on-shell with *distinct* and *equal* masses, respectively.

The massless ordered cut in Figure 3.8a gets contributions from  $n_4^1$ ,  $n_4^2$  and  $n_4^4$ , and can be written as graphs dressed with numerator functions and corresponding propagator structures

$$\begin{aligned}
\mathcal{A}_4^{1\text{-loop}}(a, b, c, d, m_1, m_2, d_{m_2}) \Big|_{l^2 \rightarrow 0} &= \frac{n_4^2(a, b, c, d, -a-b-l_1)}{((b+l)^2 - m^2)(a+b)^2} - \frac{n_4^2(d, c, a, b, a+b+l_1)}{((c-l)^2 - m^2)(a+b)^2} \\
&\quad + \frac{n_4^4(a, b, c, d, l_1)}{((a+b)^2)^2} + \frac{n_4^1(a, b, c, d, l_1)}{((b+l_1)^2 - m_1^2)} - \frac{n_4^1(c, d, l_1)}{((c-l_1)^2 - m_2^2)} \tag{3.33}
\end{aligned}$$

<sup>3</sup>The numerators contain some generalized gauge freedom that cannot contribute to any integrated expression.



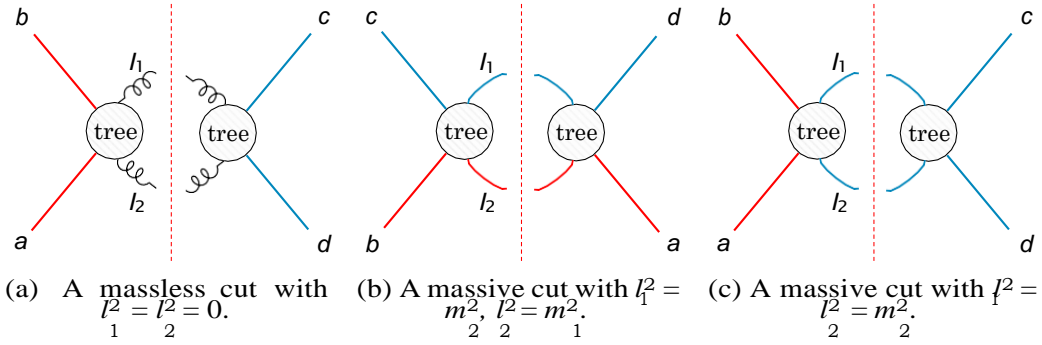


Figure 3.8: Generalized unitarity cuts on the four-point one-loop amplitude.

where  $m_1^2$  is the squared mass of the scalar  $a, b$  and  $m_2^2$  is the squared mass of the other scalar  $c, d$ . To determine coefficients, but also to verify the validity of our numerators so far, this cut should be equal to the product of two four-point trees with one massive scalar. We determined these tree amplitudes in the previous section, allowing us to easily work out,

$$A_4^{1\text{-loop}}(a^{m_1}, b^{m_1}, c^{m_2}, d^{m_2}) \Big|_{\substack{l_1^2 \rightarrow 0 \\ l_2^2 \rightarrow 0}}^{\text{cut}} = \sum_{s_1, s_2} A_{4,1}^{\text{tree}}(a^{m_1}, b^{m_1}, s_1^{s_1}, s_2^{s_2}, l_2) \times A^{\text{tree}}(-l_1^{s_1}, -l_2^{s_2}, c^{m_2}, d^{m_2}), \quad (3.34)$$

where the sum is over the possible states of the gluonic cut legs  $l_1, l_2$ . The sum runs over the polarization states of the  $D$ -dimensional polarization vectors just as we did when considering factorization at tree-level, so we can employ the same physical projectors (e.g. Eqs. (3.11) and (3.12)).

To further determine the coefficients of the amplitude we perform the massive cut in Figure 3.8b. This cut only gets a contribution from the box graph, which is now dressed in the following way

$$A_4^{1\text{-loop}}(a^{m_1}, b^{m_1}, c^{m_2}, d^{m_2}) \Big|_{\substack{l_1^2 \rightarrow m_1^2 \\ l_2^2 \rightarrow m_2^2}}^{\text{cut}} = \frac{n_4^1(a, b, c, d, l_1 - b)}{(b - l_1)^2 (a + l_1)^2}. \quad (3.35)$$

On the tree side of this cut, we get a product of the four-point trees with two massive scalars from the previous section,

$$A_4^{1\text{-loop}}(a^{m_1}, b^{m_1}, c^{m_2}, d^{m_2}) \Big|_{\substack{l_1^2 \rightarrow m_1^2 \\ l_2^2 \rightarrow m_2^2}}^{\text{cut}} = A_{4,2}^{\text{tree}}(a^{m_1}, l_1^{m_1}, l_2^{m_2}, d^{m_2})$$

4,2

The cut legs are now massive scalars with only one allowed state<sup>4</sup>, so the state sum is trivial and the cut fixes five coefficients.

After the massive and massless cut we are left with 13 undetermined coefficients. Some of these are fixed on the third and final cut shown in Figure 3.8c. This unitarity cut puts two massive internal lines on shell, now of the same type. There are two possibilities,  $l_1^2 = l_2^2 = m^2$  and  $l_1^2 = l_2^2 = -m^2$ , and we need only consider the latter, e.g.  $l_1^2, l_2^2 \rightarrow -m^2$ . Once this set of cuts is satisfied it fixes an additional eight coefficients.

<sup>4</sup>We are free to consider cuts where we fix the mass of the particle crossing the cut.

Because of the symmetry of the amplitude and the individual graphs, the corresponding unitarity cuts with  $l_1^2 = l_2^2 = m^2$  is also satisfied but puts no further constraints on the ansatz. Finally the amplitude numerators are determined up to five free coefficients, which represent generalized gauge freedom that cannot contribute to any integrated expression.

It is worth discussing this last cut in a little more detail. What do we mean by an ordered four-point tree when all external scalar masses are the same? This is the only distinction for one-loop four-point that occurs depending on when we allow the color version of Equation (2.5) to be satisfied. If we are to allow this, our ordered amplitudes can be thought of as *adjoint-type*, so e.g. we can have two channels contribute to an ordered color-stripped amplitude:

$$A_{4,\text{adj}}^{\text{tree}}(1^{m_1}, 2^{m_1}, 3^{m_1}, 4^{m_1}) = \frac{n_s}{s} + \frac{n_t}{t}. \quad (3.37)$$

where

$$\begin{aligned} n_s &= n_{4,2}(1^{m_1}, 2^{m_1}, 3^{m_1}, 4^{m_1}), \\ n_t &= n_{4,2}(4^{m_1}, 1^{m_1}, 2^{m_1}, 3^{m_1}), \end{aligned} \quad (3.38)$$

and  $s, t$  are Mandelstam invariants:

$$\begin{aligned} s &= (k_1 + k_2)^2, \\ t &= (k_2 + k_3)^2. \end{aligned} \quad (3.39)$$

If on the other hand, we demand that external scalars labeled 1 and 3 are particles distinct from anti-particle legs labeled 2 and 4, all still with the same mass, we have two distinct ordered color-stripped amplitudes with one channel each:

$$\begin{aligned} A_{4,2}^{\text{tree}}(1^{m_1}, \bar{2}^{m_1}, 3^{m_1}, \bar{4}^{m_1}) &= \frac{n_s}{s} \\ A_{4,2}^{\text{tree}}(1^{m_1}, \bar{4}^{m_1}, 3^{m_1}, \bar{2}^{m_1}) &= \frac{n_t}{t}. \end{aligned} \quad (3.40)$$

We can refer to these types of ordered trees as *fundamental-type*. As is perhaps not so surprising, the same kinematic weights written functionally can be used for both theories, the amplitudes differ simply in which graphs one allows to contribute. Demanding the kinematic analog of Equation (2.5) for functional numerators:

$$n_{4,2}(1^{m_1}, 2^{m_1}, 3^{m_1}, 4^{m_1}) = n_{4,2}(3^{m_1}, 1^{m_1}, 4^{m_1}, 2^{m_1}) + n_{4,2}(4^{m_1}, 1^{m_1}, 2^{m_1}, 3^{m_1}), \quad (3.41)$$

is simply an additional constraint that can be imposed on the kinematic dressings. If we could not satisfy these types of conditions, we would be unable to satisfy adjoint-type cuts, but it turns out both for four-point one-loop and five-point one-loop there is no problem establishing such constraints. As a result our same kinematic weights satisfy both adjoint-type and fundamental-type cuts, and indeed one can use adjoint-type cuts to constrain all parameters in our-bootstrap. The pattern we see here of adjoint-type ordered amplitudes being sums over individually gauge-invariant fundamental-type ordered amplitudes persists to higher multiplicity.

### 3.3.3 Five-point one-loop construction

In this section we will consider the five-point one-loop amplitude with two pairs of massive scalars. Compared to the construction of the four-point loop amplitude in

the previous section, at five-point the number of graph topologies is much larger and the external gluon contributes with a polarization vector that makes the form of the numerators more complicated.

The five-point one-loop amplitude has 33 possible graph topologies, shown in Figures 3.9-3.10, again including snails but not tadpoles. The two massive scalars are illustrated by a blue and red line representing the different masses, and we impose that the numerators be symmetric under the exchange of these lines. Note that some of the graphs with purely massive loops belong to two independent topologies that depend on the mass of the internal loop. For example,  $n_5^{24}$  and  $n_5^{25}$  are two distinct topologies. This plays a role in determining the Jacobi-like relationship between the graphs. Solving for these Jacobi-like relations we find that a possible set of basis graphs is  $n_5^1, n_5^2, n_5^8, n_5^{14}, n_5^{15}$  and  $n_5^{33}$ . Each basis graph is given a non-zero kinematic ansatz.

The ansatz for the kinematic numerators must contain the polarization vector of the external gluon,  $\varepsilon_a$ , and have the correct power counting. We therefore propose the following form

$$n_5^\lambda(a, b, c, d, e) = \sum_{p=1}^{312} \alpha_p^\lambda (k_i \cdot k_j)(k_l \cdot k_m)(k_n \cdot \varepsilon_a), \quad (3.42)$$

where  $\alpha_p^\lambda$  are the free coefficients, and  $k_a$  are the momenta of external particles or loop momenta. Each ansatz has 312 terms, so the total number of coefficients is 1872 for all six ansätze.

Imposing the symmetries of all graphs, along with the remaining relationships from the Jacobi-like relations, constrains 1190 of the coefficients. After imposing the symmetries, there are then 682 coefficients left to determine using generalized unitarity cuts.

The ordered unitarity cuts required to constrain the five-point amplitude are graphically depicted in Figure 3.11. One new feature at five-point one-loop is that ability to have two-particle cuts (bubble cuts) where one of the cut legs is massive and one is massless (c.f Figure 3.11b). Here are all the cuts that must be performed

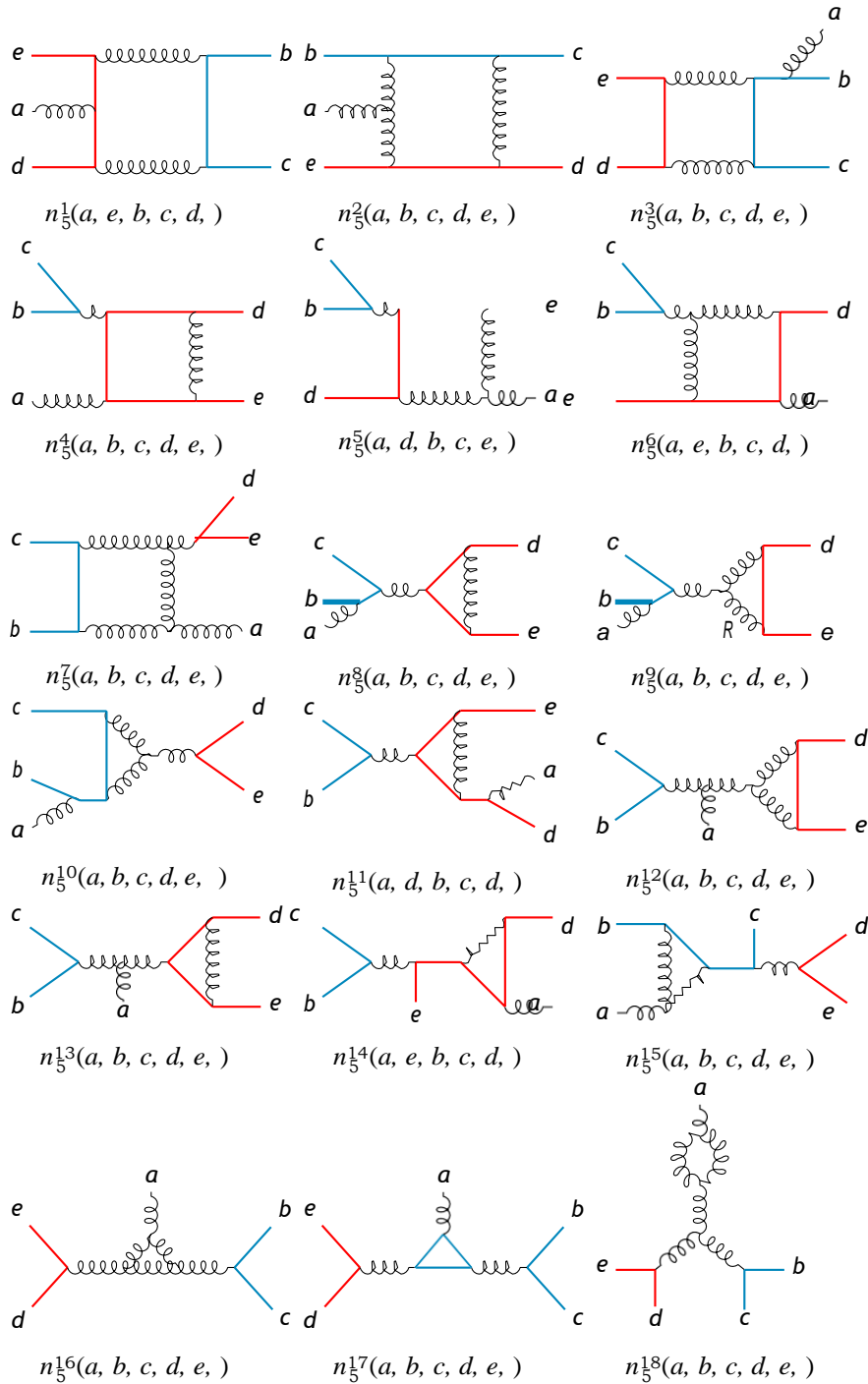


Figure 3.9: One-loop five-point graph topologies (excluding tadpoles) related by Jacobi and commutation relations (1-18).

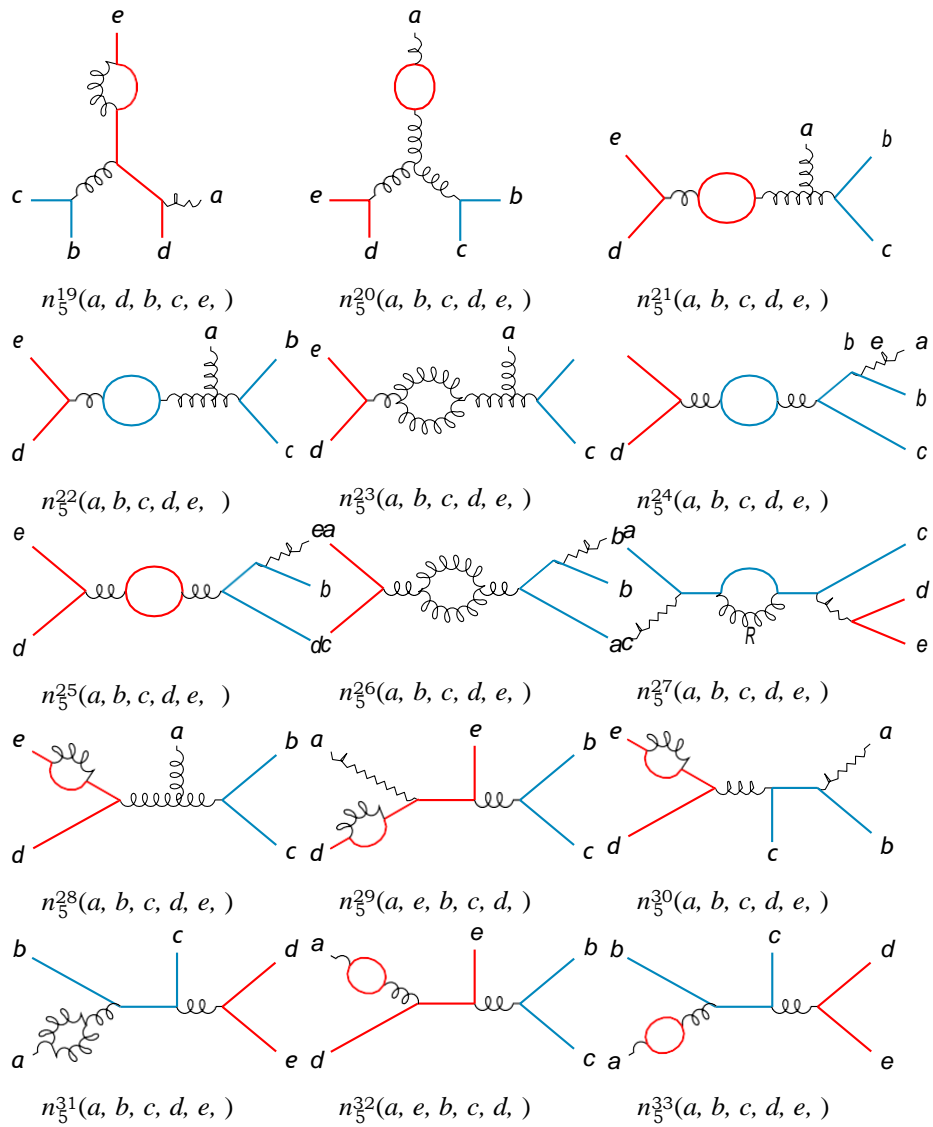


Figure 3.10: One-loop five-point graph topologies (excluding tadpoles) related by Jacobi and commutation relations (19-33).

expressed in terms of the tree amplitudes that contribute:

$$A_5^{1\text{-loop}}(a, b^{m_1}, c^{m_1}, m_2, e^{m_2}) \Big|_{l_1^2 \rightarrow 0}^{\text{cut}} = A_{4,1}^{\text{tree}}(d^{m_2}, e^{m_2}, s_1, s_2, l_1, l_2) \times A_{5,1}^{\text{tree}}(-l_2^{s_2}, -l_1^{s_1}, b^{m_1}, a, c^{m_1}), \quad (3.43)$$

$$A_5^{1\text{-loop}}(a, b^{m_1}, c^{m_1}, m_2, e^{m_2}) \Big|_{l_1^2 \rightarrow m_1^2}^{\text{cut}} = A_{4,1}^{\text{tree}}(a, b^{m_1}, m_1, s_2, l_1, l_2) \times A_{5,2}^{\text{tree}}(-l_2^{s_2}, -l_1^{m_1}, c^{m_1}, d^{m_2}, e^{m_2}), \quad (3.44)$$

$$A_5^{1\text{-loop}}(a, b^{m_1}, c^{m_1}, m_2, e^{m_2}) \Big|_{l_2^2 \rightarrow m_2^2}^{\text{cut}} = A_{4,2}^{\text{tree}}(c^{m_1}, m_2, m_1, l_1, l_2) \times A_{5,2}^{\text{tree}}(-l_2^{m_1}, -l_1^{m_2}, e^{m_2}, a, b^{m_1}), \quad (3.45)$$

$$A_5^{1\text{-loop}}(a, b^{m_1}, c^{m_1}, m_2, e^{m_2}) \Big|_{l_2^2 \rightarrow m_2^2}^{\text{cut}} = A_{4,2}^{\text{tree}}(d^{m_2}, e^{m_2}, l_1^{m_2}, l_2^{m_2}) \times A_{5,2}^{\text{tree}}(-l_2^{m_2}, -l_1^{m_2}, a, b^{m_1}, c^{m_1}), \quad (3.46)$$

$$A_5^{1\text{-loop}}(a, b^{m_1}, c^{m_1}, m_2, e^{m_2}) \Big|_{l_2^2 \rightarrow m_2^2}^{\text{cut}} = A_{4,2}^{\text{tree}}(d^{m_2}, e^{m_2}, l_1^{m_1}, l_2^{m_1})$$

5.2

After these cuts all but 123 of our original parameters are constrained. This is sufficient to ensure that all physical cuts are satisfied. The resulting integrand with all color-dual consistent gauge freedom is included in an ancillary file with the arXiv version of this chapter.

Note that the above cuts involve ordered partial amplitudes. It may seem surprising that we require no additional partial-amplitude orderings under the same kinematic constraints. After all at five-point tree-level, for a single pair of massive scalars, there are two independent ordered partial-amplitudes under amplitude relations. We witness here one of the benefits of using functional kinematic graph dressings tightly constrained by algebraic relations. In general one need only consider a smaller set of cuts (or factorization channels as at tree-level) to entirely constrain an integrand. Indeed for the maximally supersymmetric gauge theory at three-loop four-points only one maximal cut of one graph is required to constrain the entire color-dual integrand [90]. If one is concerned that additional ordered cuts may be required one can always examine the full color-dressed cut. Equivalently, for each set of kinematic cut conditions, one can verify that no additional orderings are required by simply considering the associated double-copy gravitational cut and noting the vanishing of any coefficients of remaining ansatz parameters. In any case we verify our final integrand on a set of physical spanning cuts as we discuss in the next section.

### 3.3.4 Verification

For both four-point one-loop and five-point one-loop, we consider the potential reduction to an integral basis by verifying the above integrands on all bubble, box, and triangle cuts with distinct color-orders under the following restrictions:

- Every bubble cut (two-particle cut) must involve a physical tree amplitude (multiplicity four or higher).
- Every triangle cut (three-particle cut) must involve the loop momenta flowing through each tree.

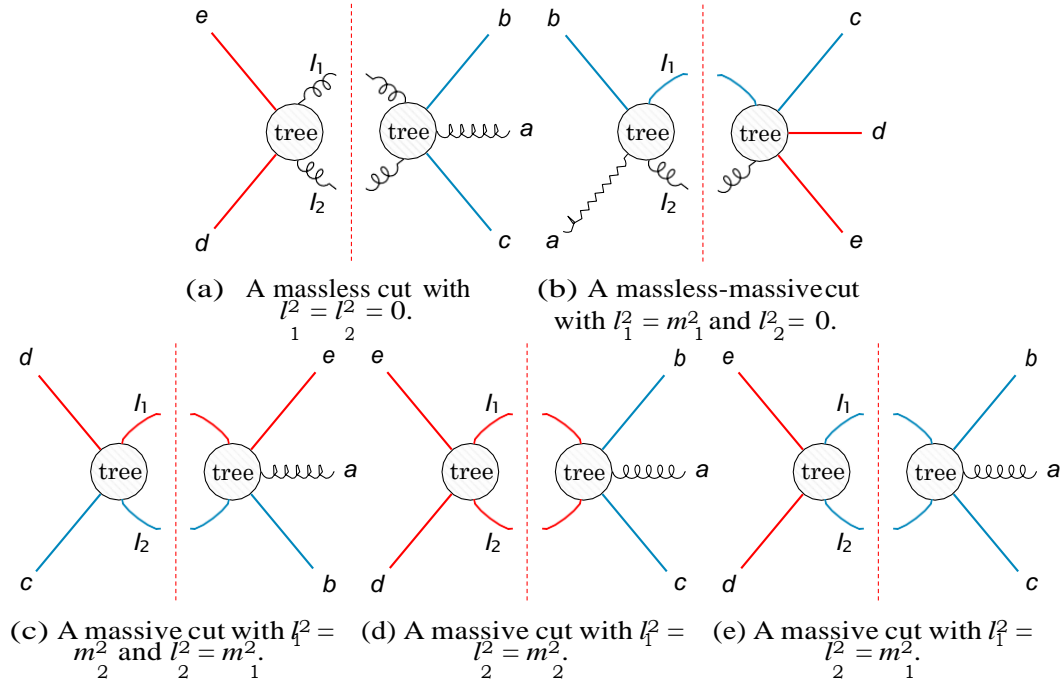


Figure 3.11: Generalized unitarity cuts on the five-point one-loop amplitude.

- Every box cut (four-particle cut) must involve the loop-momenta flowing through each tree.

This set of restrictions precludes snail diagrams (e.g. diagrams 18, 19, 20, 28, 29, 30, 31, 32, and 33 of Figures 3.9 and 3.10) as well as tadpole diagrams from contributing to the cuts. As practical applications of the gravitational double-copy of these amplitudes will involve the  $\eta \rightarrow 0$  limit, we expect this to be completely sufficient [39]. We verify on this spanning set of cuts that no remaining parameters contribute to physical cuts, and can be taken as pure gauge choice relative to any set of related physical observables.

We should emphasize that there are important questions around how to appropriately consider snail and tadpole contributions to the UV. We refer the interested reader to ref. [61] for analysis handling similar issues in the context of unitarity based approaches.

### 3.4 Conclusion

In this chapter, we frame a constructive bootstrap solely in terms of factorization and color-dual representations for  $D$ -dimensional massive scalar QCD amplitudes, leading to integrands at one loop in massive scalar QCD. Specifically we found the first loop correction to scattering between two different massive scalar fields, as well as the first loop correction to such scattering with an emitted gluon. Along the way we recalculated a number of tree-level amplitudes in this theory, starting with the three-point amplitudes constrained entirely by mass-dimension and symmetry. By exploiting the duality between color and kinematics – known to hold at tree-level, but still conjectural at loop level, we found tremendously simplified representations – requiring a small number of basis graph topologies whose functional kinematic weights encode

the entire amplitude. We confirmed the validity of this approach at tree-level by comparing with results in the literature, and at loop level on a spanning set of physical cuts. Besides the computational simplicity in the gauge theory, and further evidence for the conjecture of loop-level color-dual representations, a critical advantage of our current approach is that once the gauge amplitudes have been constructed in this color-dual form, building the corresponding gravity integrand in  $N = 0$  supergravity is trivial: one simply exchanges the color-weights with kinematics weights graph by graph.

The gauge theory representations we constructed in this chapter have a number of intriguing properties. Notably these representations land naturally on a gauge that plays well with summing Yang-Mills states over a simplified projector (cf. Equation (3.12) relative to Equation (3.11)) which aids in unitarity-based constructions. Indeed all loop-level cuts were performed with the gauge-dependent simplified projector and verified against the gauge invariant physical one. Even more notably, through tree-level and one-loop we find that the same kinematic graph weights can apply to both fundamental and adjoint-type representations, the only difference being which graphs are allowed to contribute. This discovery resonates with the color-dual/double-copy program, where a small number of building blocks are at the heart of prediction intimately relating seemingly disparate theories. Finally these color-dual representations propagate cut information to graphs with ambiguous or ill-defined cuts like massive snail or tadpole graphs. While these do not contribute to physical cuts relevant to classical limits, such graphs will be relevant to quantum UV behavior and mass renormalization. This implies a generalized gauge choice. It will be intriguing to apply the approach presented here to massive quark amplitudes in QCD with care to reproduce standard regularization schemes.

There is significant current interest in massive scattering amplitudes in pure Einstein-Hilbert gravity due to relevance to precision gravitational wave physics. A natural next step will be to take our  $N = 0$  supergravity double-copy results and project out any unwanted massless states. More non-trivial will be to generalize this type of multiloop scattering amplitude methods to massive particles with arbitrary spin. While ambitious, important clarifying progress is already being made both in field theory and scattering communities (see, e.g., [48, 55, 91–102], and references therein). We expect color-dual methods to play an increasingly vital role in this exploration.

In summary, the combination of unitarity methods and the duality between color and kinematics is incredibly powerful. While originally discovered in the quest of understanding the UV behavior of maximally supersymmetric gravity theory in four-dimensions, the duality between color and kinematics is both dimension-agnostic as well as entirely independent of the presence or absence of supersymmetry. It is gratifying to discover that massive scattering amplitudes at loop-level can be compatible with these principles, and we look forward to continuing to extend our visibility into loop-level prediction now in increasingly more phenomenological theories.



## Appendix

### 3.4.1 Kinematic Jacobi-like relations at one-loop four-point

Here we tabulate the Jacobi relations satisfied by four-point one-loop, two pairs of massive external scalars. Five-point one-loop is included in a machine readable ancillary file.

$$\begin{aligned}
n_4^2(a, b, c, d) &= n_4^6(a, b, c, d, -a - b - ) + n_4^3(a, c, d, b, -a - b - ), \\
n_4^2(a, b, c, d) &= -n_4^2(a, b, c, d, c + d - ) + n_4^4(a, b, c, d, c + d - ), \\
n_4^2(a, b, c, d) &= -n_4^6(b, a, c, d, ) + n_4^3(a, c, d, b, - ), \\
n_4^2(a, b, c, d) &= n_4^1(a, b, c, d, c + d - ) - n_4^1(a, b, d, c, c + d - ), \\
n_4^6(a, b, c, d) &= n_4^2(a, b, c, d, c + d - ) - n_4^3(a, c, d, b, ), \\
n_4^3(a, c, d, b) &= n_4^2(a, b, c, d, - ) + n_4^6(b, a, c, d, - ), \\
n_4^3(a, c, d, b) &= -n_4^3(a, c, d, b, a - b - ) + n_4^5(a, c, d, b, b + ), \\
n_4^3(a, c, d, b) &= n_4^2(a, b, c, d, c + d - ) - n_4^6(a, b, c, d, ), \\
n_4^4(a, b, c, d) &= n_4^2(c, d, a, b, -c - d + ) - n_4^2(d, c, a, b, -c - d + ), \\
n_4^4(a, b, c, d) &= n_4^2(a, b, c, d, c + d - ) + n_4^2(a, b, c, d, ), \\
n_4^1(a, b, c, d) &= n_4^2(c, d, a, b, - ) + n_4^1(a, b, d, c, c + d - ), \\
n_4^1(a, b, c, d) &= n_4^2(a, b, c, d, c + d - ) + n_4^1(b, a, c, d, c + d - ), \\
n_4^5(a, c, d, b) &= n_4^3(a, c, d, b, -b - c - d - ) + n_4^3(a, c, d, b, a + c + d + )
\end{aligned} \tag{3.48}$$

## Chapter 4

# Extracting Einstein from the Loop-Level Double-Copy

The naive double-copy of (multi) loop amplitudes involving matter coupled to gauge theories will generically produce amplitudes in a gravitational theory that contains additional contributions from propagating antisymmetric tensor and dilaton states. We present a graph-based approach that combines the method of maximal cuts with double-copy construction to offer a systematic framework to isolate the pure Einstein-Hilbert gravitational contributions at loop level. Indeed this allows for a bootstrap of pure-gravitational results from the double-copy bootstrap of ref. [57]. We construct the amplitudes relevant to non-spinning black-hole pure-gravitational scattering from tree-level and one-loop integrands of the  $N = 0$  supergravity double-copy of massive scalar-QCD.

### 4.1 Introduction

The color-dual double copy construction [7, 103] of quantum field theory predictions can be used to build scattering amplitudes for a wide variety of theories from phenomenological effective field theories to formal completions of Yang-Mills and Gravity like open and closed string theories<sup>1</sup>. The first concrete hint of this web of theories was the construction of closed string tree-level amplitudes from sums over permutations of Chan-Paton-stripped open-string amplitudes via the celebrated relations of Kawai, Lewellen and Tye [68] (KLT). In the low energy limit these relations allow the expression of tree-level graviton amplitudes in terms of sums over permutations of ordered tree-level Yang-Mills amplitudes. In the color-dual approach of Bern, Carrasco and Johansson (BCJ) the building blocks of gravitational predictions are gauge theory kinematic graph weights that satisfy the *duality between color and kinematics*. This means that the gauge theory predictions can be expressed in a representation where, graph-by-graph, kinematic weights obey the same algebraic relations as the color weights. The gravitational double copy prediction is then obtained by exchanging the gauge theory's color factors for a second set of kinematic weights. This approach can be used to generate the field-theory limit of KLT relations at tree-level [7], by inverting the relationship between color-dual numerators and ordered-amplitudes, and generalizes to integrand representations at multiloop levels [103, 105]. The theory of massive scalars minimally coupled to Yang-Mills, massive scalar-QCD, is compatible with this duality both at tree level [58, 87], as well as at the one-loop integrand level [57].

The advent of precision gravitational wave science has invited a renewed interest in applying quantum insights to classical predictions (see, e.g., refs. [10–38, 40–54, 101,

<sup>1</sup>See, e.g., Section 5 of ref. [104] for a recent review of the color-dual web of theories.

106]). Indeed, the highest precision post-Minkowskian  $O(G^4)$  correction to the scattering of classical non-rotating black holes has involved a synthesis of effective field theory techniques, advanced multiloop integration innovation, and double-copy applied to tree-level scattering amplitudes [51]. Scattering amplitudes in massive scalar-QCD, where massive scalars are coupled via Yang-Mills, can be used via double-copy to construct the scattering of massive scalars coupled to gravitons, whose classical limit describes the evolution and interaction of non-rotating black holes. At tree level, color-dual amplitudes in massive scalar QCD have been presented for up to six-points with three pairs of massive scalars [87], and in ref. [57] it was conjectured that a simple bootstrap extends to all multiplicity and loop-level using only color-kinematics and factorization, verifying through 1-loop five-point.

The straightforward double copy of Yang-Mills scattering without any particular state management results in predictions of the so called  $\mathcal{N} = 0$  supergravity, where – in addition to gravitons – a massless scalar (often called a dilaton) and an anti-symmetric two-form (dual to an axion in four dimensions) can propagate. These contributions can be avoided for external gravitons at tree-level for massless theories by coordinating the external states of gluons, but become relevant at loop level. Such extra-state contributions affect even tree-level when gravitons are coupled to massive matter. Such long-range mediators can survive the classical limit, and so must be projected out or otherwise removed if one is targeting classical predictions equivalent to that of pure Einstein-Hilbert gravity. There can be additional differences in double-copy amplitudes, such as additional local contact terms only between massive states. Such massive-state local contact terms are irrelevant to long range classical physics and so will not concern us here.

There are many strategies for removing the extra states arising from naive double-copy. The first examples of gravitational multi-loop cut-construction involved tree-level cuts built from ordered gauge-theory cuts by applying field theory KLT relations (see, e.g. [107]). Cut construction for pure-gravity theories can progress by explicitly subtracting out contributions from unwanted states (c.f. refs. [108, 109]). At loop level, the classical limit of amplitude integrands for binary black holes has been calculated up to three-loops using generalized unitarity cuts and the double copy of tree-level amplitudes to construct pure-graviton integrands [51] via the method of maximal cuts [9] .

The method of maximal cuts [9] offers a hierarchical approach to perturbative quantization. Here we combine it with double-copy construction at the off-shell integrand level. Thus we construct pure Einstein-Hilbert gravity integrands by starting with compact expressions for the  $\mathcal{N} = 0$  supergravity integrands and systematically project out any non-gravitational propagating modes. This projective double-copy offers a systematic isolation of local gravitational contributions.

Of course, if one is only interested in classical gravitation, it is not necessary to build consistent loop-level integrands at all, not to mention the generation of off-shell  $\mathcal{N} = 0$  supergravity integrands. One can employ [51] a variant of the method of maximal cuts to directly target only the relevant classical contributions. If we aspire, however, to apprehend the connections between theories in the web of theories at the integrand level, it is natural to develop techniques to map out and relate graph by graph the relevant integrands of both  $\mathcal{N} = 0$  supergravity as well as Einstein-Hilbert as we present here.

It is a good question as to whether it is possible to double-copy directly to pure-gravity integrands. In the massless case Johansson and Ochirov introduced [110] a prescription involving ghostly matter to remove unwanted states at loop-level. Inspired by this approach, ref. [73] constructed Einstein-Hilbert gravitation amplitudes

involving massive matter through five-points at tree level by introducing a massless, ghostly scalar in the gauge theory. A side benefit of our approach is the generation of data which may clarify the path forward at loop-level involving massive matter. Starting from loop-level integrands of  $N = 0$  supergravity, we generate *difference integrands* corresponding to the propagation of unwanted states. This data may be helpful as a future loop-level double-copy target for state-ghost targeting of double-copy amplitudes with massive states.

We will review the method of maximal cuts in Section 4.2. We introduce our approach to projective double-copy construction via the method of maximal cuts in Section 4.3. In Section 4.4 we will demonstrate our approach first at tree-level in Section 4.4.1, then the one-loop correction to two distinct-mass scalar particles scattering gravitationally in Section 4.4.2, as well as including gravitational radiation in the related five-point one-loop amplitude integrand in Section 4.4.2. We conclude and discuss potential next steps in Section 4.5.

## 4.2 Review of the method of maximal cuts

The method of maximal cuts iteratively constructs tree-level and the integrands of multi-loop scattering amplitudes by inverting the sufficient verification condition of a loop-integrand satisfying all unitarity cuts. It is important to note that cut construction alone is only sufficient when there are no contact terms invisible to all factorization channels that one has not accounted for. Since unitarity cuts involving trees with uncut propagators span any unitarity cuts with additionally consistent cut propagators there is a natural hierarchy for construction. Namely one can build weights associated with graphs that first satisfy all possible cut conditions (all propagators put on shell), then consider what is required when when cut conditions are relaxed to satisfy more inclusive cuts. Any cut-constructible missing information (encodable potentially in local Feynman rules) must be proportional to newly uncut propagators in order to have vanished when such newly-relevant propagators were on-shell.

Consider a general unitarity cut with  $k$  uncut propagators:

$$C^{N^k MC} = \sum_{\text{states}} M_{m(1)}^{\text{tree}} \dots M_{m(p)}^{\text{tree}} \quad k \equiv \sum_{i=1}^p m(i) - 3, \quad (4.1)$$

where  $M_{m(i)}^{\text{tree}}$  are tree-level  $m(i)$  multiplicity gravity amplitudes,  $k$  is the number of propagators that remain off-shell, and the sum runs over the possible states of the cut.

The first step in the method of maximal cuts is therefore to perform the maximal cuts of all relevant topologies of the amplitude, and compare with the sum over states of the product of trees described above. Thus for each maximal cut, which can be represented by a cubic graph, all propagators are put on-shell. The tree amplitudes in a maximal cut Equation (4.1) are all three-point amplitudes, and so only one cubic graph contributes to each cut. The contributions of maximal cuts can be unambiguously assigned to those/ cubic topologies. For local representations there is no choice other than how to represent conservation of momentum zeros under cut conditions. The only potential missing contributions must be proportional to inverse-propagators (momentum zeros for all maximal cuts). To identify them we subsequently relax cut conditions. This subsequent step involves performing the next-to-maximal cuts (NMC) and assigning their contributions to any of the cubic graphs that contribute to that cut. For each next to maximal cut, only one of the cut

conditions in a maximal cut is released, effectively returning propagators off-shell, so for full (orderless) cuts — as relevant for gravitational or color-dressed theories — at most<sup>2</sup> three graphs could contribute to each cut. For each such cut the only potentially new information will be proportional to the inverse of the newly uncut propagator, and this can be assigned or distributed amongst the three cubic topologies. One proceeds similarly, for the N<sup>2</sup>MC two propagators are held off-shell, and so on, until all potentially missing information is accounted for.

### 4.3 Projective double-copy

If one were to attempt to bootstrap pure Einstein-Hilbert gravitational amplitudes for four external gravitons from three-point amplitudes, using the method of maximal cuts alone, one runs into trouble immediately due to the four-point contact term required for linearized diffeomorphism invariance. Famously, gravitation requires additional contact terms at all multiplicity. At tree-level one can exploit analyticity properties to guarantee gauge-invariance via on-shell recursion [3, 113]. Naive double-copy, which generalizes straightforwardly to loop-level, alleviates such worry, at the cost of potentially extra modes relative to pure-Einstein-Hilbert gravitation, and fixing a choice of theory dependent contact terms between massive-scalars. Any weight given to massive-scalar contacts are of course irrelevant in the classical limit. All supergravity theories, including the so-called  $N = 0$  supergravity double-copy of pure Yang-Mills, share tree-level all-graviton amplitudes with pure Einstein-Hilbert gravitation. This of necessity changes at loop-level, where every state in the theory can contribute to loops. Famously, even at tree-level, this universality is also no longer the case when coupling to massive matter [73]. Critically, identifying these extra-mode contributions on any given amplitude is accessible through the method of maximal cuts.

We bootstrap pure-gravitational scattering between massive scalars via double-copy and the method of maximal cuts by only allowing gravitons to flow through the cuts involving massless propagators. To this end we use the  $D_s$ -dimensional physical state projector, described in [106] and references therein, to sew together the tree amplitudes,

$$P^{\mu\nu\rho\sigma}(p, q) = \underset{\text{pols.}}{\varepsilon^{\mu\nu}(-p)\varepsilon^{\rho\sigma}(p)} = \frac{1}{2}(P^{\mu\rho}P^{\nu\sigma} + P^{\mu\sigma}P^{\nu\rho}) - \frac{1}{D_s - 2}P^{\mu\nu}P^{\rho\sigma}, \quad (4.2)$$

where

$$P^{\mu\nu} = \eta^{\mu\nu} - \frac{q^\mu p^\nu + p^\mu q^\nu}{p \cdot q}, \quad (4.3)$$

where  $q$  is an arbitrary null reference momenta that should factor out of any physical expression once the cut conditions and conservation of momenta have been imposed. In certain cases, when we can add terms to the tree-amplitudes that vanish on-shell such that the  $q$ -dependent terms vanish when contracted with the tree-amplitudes, the state projector is equivalent to a simpler projector

$$\underset{\text{pols.}}{\varepsilon_{\mu\nu}(-p)\varepsilon_{\rho\sigma}(p)} = \frac{1}{2}\eta_{\mu\rho}\eta_{\nu\sigma} + \frac{1}{2}\eta_{\mu\sigma}\eta_{\nu\rho} - \frac{1}{D_s - 2}\eta_{\mu\nu}\eta_{\rho\sigma}. \quad (4.4)$$

The state projector projects out non-gravitational states so that only gravitons are allowed to cross the cuts. We can then attribute any discrepancies between

<sup>2</sup>Flavor conservation can further restrict the number of potential graphs contributing to any cut.

products of trees and the cut amplitude, or amplitude integrand, to excess states. We correct for these contributions by subtracting them from new higher-level contact terms as necessary. One can assign these contact contributions to cubic parent graphs in a manner that obeys the symmetries of those graphs (via ansatz and explicit symmetrization).

The initial contact contribution, involving non gravitationally mediated massless states, to each graph is given by that graph's maximal cut – where all propagators are cut:

$$\Delta_g^{MC} = M_g^{MC} - \underbrace{M_3^{\text{tree}} \dots M_3^{\text{tree}}}_{\text{projected states}}, \quad (4.5)$$

where  $M_g^{MC}$  is the maximal cut of graph  $g$ . The Einstein-Hilbert numerators,  $n^G$ , that satisfy these cut conditions are given by subtracting off a topology-symmetrized  $\tilde{\Delta}^{MC}$  from the  $N = 0$  numerator of the graph

$$n_g^G = n_g^N - \tilde{\Delta}_g^{MC}. \quad (4.6)$$

Any errors in  $n^G$  must be proportional to contact terms, but critically can not involve contact terms due to all-graviton interaction, as those are correctly accounted for in the  $N = 0$  supergravity numerators.

Higher cuts proceed as above, but the initial contribution is a  $\Delta_{\text{contact}}^{N, MC}$  | which must be assigned to cubic parent graph  $n_g^G$  via inverse propagators. For these higher point contact corrections we use  $\tilde{\Delta}_g$  to represent the symmetrized corrections including the inverse propagators that target a particular graph  $g$ . The procedure terminates when all physical cut conditions are released.

## 4.4 Extracting Einstein-Hilbert at Tree and Loop Level

Here we carry out the program of bootstrapping pure gravity amplitudes from double copies of massive scalars coupled to gluons, by projecting out excess states at the level of the numerator dressings. In [57] a set of color-dual kinematic numerators was determined for amplitudes with gluons and massive scalar particles in scalar QCD. The ‘naive double copy’ numerators are simply squares of these

$$n_g^{N=0} = (n_g^{QCD})^2, \quad (4.7)$$

where  $g$  is a cubic graph topology contributing to the amplitude, and  $n_g^{QCD}$  is the kinematic numerator dressing from the gauge theory amplitude. The pure gravity

three-point graph numerators are simply given by the double copy of the corresponding kinematic dressings found in [57]

$$n^G \begin{array}{c} \square \\ \square \\ \square \end{array} \begin{array}{c} k_3 \\ \text{wavy} \\ \text{red} \\ k_2 \quad k_1 \end{array} = (k_1 \cdot \varepsilon_3)^2, \quad (4.8)$$

$$n^G \begin{array}{c} \square \\ \square \\ \square \end{array} \begin{array}{c} k_2 \\ \text{wavy} \\ k_1 \quad k_3 \end{array} = \left( (k_3 \cdot \varepsilon_1)(\varepsilon_2 \cdot \varepsilon_3) - (k_3 \cdot \varepsilon_2)(\varepsilon_1 \cdot \varepsilon_3) + (k_2 \cdot \varepsilon_3)(\varepsilon_1 \cdot \varepsilon_2) \right)^2, \quad (4.9)$$

We can now bootstrap from the above results to find the scattering amplitudes for massive scalars coupled gravitationally, including all appropriate gravitational self-interaction terms.

#### 4.4.1 Tree-level

In addition to the graviton, the naive double-copy of the four-point tree-level amplitude with two massive scalars of distinct mass admits non-gravitational mediators, which we project out on cuts using the physical graviton state projector as described in Section 4.3. The tree-level case is relatively simple even at higher multiplicity, as only one channel is ever cut at a time. The entire procedure can be understood by simply considering the four-point example in detail. We tabulate all results with external massive scalars through six-point.

The graph representation used here consists solely of cubic graphs, so the four-point amplitude involves a single graph topology,

$$n \begin{array}{c} \square \\ \square \\ \square \end{array} \begin{array}{c} b \\ \text{red} \\ \text{wavy} \\ a \quad c \\ \text{blue} \\ d \end{array} = n_{4,2}(a, b, c, d), \quad (4.10)$$

which is dressed with a *functional kinematic numerator*  $n_{4,2}(a, b, c, d)$ . The numerator function takes the ordered external legs  $a, b, c, d$  as arguments, by which it is completely determined. The functional expression consists of Lorentz products of kinematic variables – such as momenta and polarization vectors – and must obey the same isomorphisms, or symmetries, as the corresponding graph topology. In [57] this kinematic numerator was determined for massive scalars coupled to gluons

$$n_{4,2}^{QCD}(a, b, c, d) = -\frac{1}{2} (k_a \cdot k_b + 2k_b \cdot k_c + m_1^2), \quad (4.11)$$

where  $m_1^2$  is the squared mass of the scalar  $a, b$ , and  $p_i \cdot p_j$  is the Lorentz product of momenta. The  $N = 0$  supergravity numerator is the square of the QCD numerator

$$n_{4,2}^{N=0}(a, b, c, d) = \left( n_{4,2}^{QCD}(a, b, c, d) \right)^2 = \frac{1}{4} (k_a \cdot k_b + 2k_b \cdot k_c + m_1^2)^2. \quad (4.12)$$

For this amplitude the projective double-copy requires fixing the only factorization channel of the graph. We find the product of trees as described above using the state projector in Equation (4.2),

$$\begin{aligned}
 \begin{array}{c} b \\ \diagdown \\ \text{---} \\ \diagup \\ a \end{array} & \begin{array}{c} \text{---} \\ \diagdown \\ \text{---} \\ \diagup \\ c \\ d \end{array} = M_3^{\text{trees}}(a, b, q^s) M_3^{\text{trees}}(-q^s, \bar{c}, d) \\
 & = (k_b \cdot k_d)^2 - \frac{m_1^2 m_2^2}{(D_s - 2)}
 \end{aligned} \tag{4.13}$$

Recall,  $D_s$  is the number of space-time dimensions arising from the trace of the metric,  $\delta_{\mu}^{\mu} = D_s$ , in the physical state projector. The cut amplitude is given by

$$M_{4,2}^{\text{tree}}(a, b, c, d) \Big|_{q^2=0}^{\text{cut}} = n_{4,2}^{N=0}(a, b, c, d) \Big|_{q^2=0}^{\text{cut}} = (k_b \cdot k_d)^2. \tag{4.14}$$

The extra-state difference between the factorized numerators is identified,

$$\Delta_{4,2} = M_{4,2}^{\text{tree}}(a, b, c, d) \Big|_{q^2=0}^{\text{cut}} - M_3^{\text{trees}}(a^{m_1}, b^{m_1}, \bar{q}) M_3^{\text{trees}}(-\bar{q}, c^{m_2}, d^{m_2}) = \frac{m_1^2 m_2^2}{(D_s - 2)}, \tag{4.15}$$

where massive particles are denoted in the tree-labels by a superscript  $m_i$ , and the two  $M_3^{\text{tree}}$  are the 3-point gravity tree amplitudes given in Equation (4.8). We then proceed to update the numerator function for pure-gravity exchange by subtracting the extra-state dimension

$$n_{4,2}^G(a, b, c, d) = n_{4,2}^{N=0}(a, b, c, d) - \Delta_{4,2} = \frac{1}{4} (k_a \cdot k_b + 2k_b k_c + m_1^2)^2 - \frac{m_1^2 m_2^2}{(D_s - 2)} \tag{4.16}$$

The full amplitude for two-to-two scattering at tree level in Einstein-Hilbert gravity (c.f. ref. [73]) is then found to be,

$$M_4^{\text{tree}}(a^{m_1}, b^{m_1}, c^{m_2}, d^{m_2}) = \frac{\frac{1}{4} (k_a \cdot k_b + 2k_b k_c + m_1^2)^2 - \frac{m_1^2 m_2^2}{(D_s - 2)}}{(a+b)^2}. \tag{4.17}$$



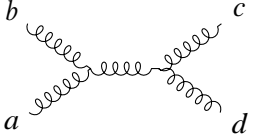
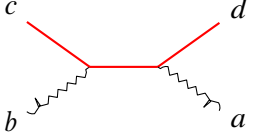
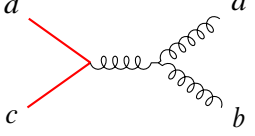
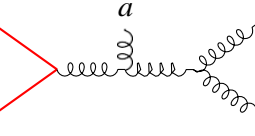
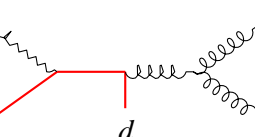
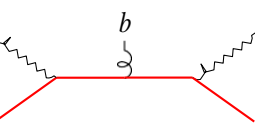
Graph topology	$\mathcal{N} = 0$ supergravity numerator	$\Delta$
	$\frac{1}{4} 2(\varepsilon_a \cdot \varepsilon_b)(k_c \cdot \varepsilon_c)(k_d \cdot \varepsilon_d) - (k_a \cdot \varepsilon_a)(k_b \cdot \varepsilon_b)(k_c \cdot \varepsilon_c)(k_d \cdot \varepsilon_d)$ $- (\varepsilon_a \cdot \varepsilon_d) 2(k_d \cdot \varepsilon_c)(k_a \cdot \varepsilon_b) + (k_a \cdot k_b)(\varepsilon_b \cdot \varepsilon_c)$ $- 2(k_c \cdot \varepsilon_d)((\varepsilon_b \cdot \varepsilon_c)(k_b \cdot \varepsilon_a) - (\varepsilon_a \cdot \varepsilon_c)(k_a \cdot \varepsilon_b))$ $+ (\varepsilon_b \cdot \varepsilon_d)(k_a \cdot k_b)(\varepsilon_a \cdot \varepsilon_c) + 2(k_d \cdot \varepsilon_c)(k_b \cdot \varepsilon_a)$ $- (\varepsilon_c \cdot \varepsilon_d)(2(k_d \cdot \varepsilon_a)(k_c \cdot \varepsilon_b) - 2(k_c \cdot \varepsilon_a)(k_d \cdot \varepsilon_b))$ $+ ((k_a \cdot k_b) + 2(k_c \cdot k_d))(\varepsilon_a \cdot \varepsilon_b)$	0
	$(k_c \cdot \varepsilon_c)(k_d \cdot \varepsilon_d) + \frac{1}{2}(k_c \cdot k_d)(\varepsilon_c \cdot \varepsilon_d)$	0
	$(k_a \cdot \varepsilon_a)(k_b \cdot \varepsilon_b) - (k_c \cdot \varepsilon_c)(k_d \cdot \varepsilon_d) - \frac{1}{2}(k_c \cdot k_d)(\varepsilon_c \cdot \varepsilon_d)$	0
	$(k_b \cdot \varepsilon_a)^2(k_b \cdot \varepsilon_c)^2(k_d \cdot \varepsilon_b)^2 + \dots + \frac{1}{4}(k_c \cdot k_e)^2(k_e \cdot \varepsilon_a)^2(\varepsilon_b \cdot \varepsilon_c)^2$	0
	$(k_b \cdot \varepsilon_a)^2(k_b \cdot \varepsilon_c)^2(k_d \cdot \varepsilon_b)^2 + \dots + \frac{1}{4}(k_c \cdot k_d)^2(k_d \cdot \varepsilon_a)^2(\varepsilon_b \cdot \varepsilon_c)^2$	0
	$(k_b \cdot \varepsilon_a)^2(k_c \cdot \varepsilon_b)^2(k_d \cdot \varepsilon_c)^2 + \dots + \frac{1}{4}(k_c \cdot k_d)^2(k_d \cdot \varepsilon_a)^2(\varepsilon_b \cdot \varepsilon_c)^2$	0

Table 4.1: Tree amplitude graphs for one massive scalar at four and five-point, where  $k_{ij} = k_i + k_j$  and  $k_{ij}^- = k_i - k_j$ . The correction  $\Delta$  should be subtracted from the  $\mathcal{N} = 0$  supergravity dressing to obtain the pure graviton numerator.

Higher multiplicity proceeds as above where first one considers any corrections from maximal cuts and proceeds to release all cut conditions. The  $\mathcal{N} = 0$  supergravity dressings and excess state contributions  $\Delta$  are shown in Table 4.1 for amplitudes with one massive scalar. As seen from the table there are no excess state corrections for the tree amplitudes with a single scalar line. This is not unexpected, as the states are expected to propagate between scalar lines.

Graph topology	$\mathcal{N} = 0$ supergravity numerator	$\Delta$
	$\frac{1}{4} \left( \frac{k_a \cdot k_b}{a} + 2 \frac{k_b \cdot k_c}{b} + \frac{m^2}{c} \right)^2$	$\frac{m_1^2 m_2^2}{D_s - 2}$
	$\frac{1}{16} \left( \frac{k_{bc}^- \cdot k_1^-}{bc} \right) \left( \frac{k_{de}^- \cdot \varepsilon_1}{de} \right) + 2 \left( \frac{k_c \cdot k_{de}^-}{c} \right) \left( \frac{k_b \cdot \varepsilon_a}{b} \right) - 2 \left( \frac{k_b \cdot k_{de}^-}{b} \right) \left( \frac{k_c \cdot \varepsilon_a}{c} \right)$	$\frac{m^2 m_2^2}{D_s - 2} (k_{de} \cdot \varepsilon_a)^2$
	$\frac{1}{16} \left( \frac{k_{ce} \cdot k}{ce} \right) \left( \frac{k_{de}^- \cdot \varepsilon}{de} \right) + 2 \left( \frac{k \cdot k_{de}^-}{c} \right) \left( \frac{k \cdot \varepsilon}{de} \right)$	$\frac{m^2 m_2^2}{D_s - 2} (k_b \cdot \varepsilon_a)^2$

Table 4.2: Tree amplitude graphs for two massive scalars, at four and five-point, where  $k_{ij} = k_i + k_j$  and  $k_{ij}^- = k_i - k_j$ . The correction  $\Delta$  should be subtracted from the  $\mathcal{N} = 0$  supergravity dressing to obtain the pure graviton numerator.

The tree-level dressings for four-point and five-point amplitudes with two scalar lines are shown in Table 4.2, and the corrections for the six-point amplitude with two massive scalars are shown in Table 4.3. These graphs *do* require corrections from  $\mathcal{N} = 0$  SG. We can now easily calculate the first correction to massive scalar scattering with radiation. The amplitude gets contributions from the second topology in Table 4.2 and four differently-labeled versions of the third topology in Table 4.2, using  $k_{ij}^- \equiv k_i - k_j$ ,

$$\begin{aligned}
M_5^{\text{tree}}(k_1, k_2, k_3, k_4, k_5) = & \frac{2 \left( \frac{k_3 \cdot k_{45}^-}{k_3} \right) \left( \frac{k_2 \cdot \varepsilon_1}{k_2} \right) + (k_1 \cdot k_2) \left( \frac{k_{45}^- \cdot \varepsilon_1}{k_{45}^-} \right)^2 - \frac{1}{D_s - 2} 16 m^2 m_1^2 (k_2 \cdot \varepsilon_1)^2}{\left( \frac{k_2 \cdot k_{45}^-}{k_2} \right) \left( \frac{k_3 \cdot \varepsilon_1}{k_3} \right) + (k_1 \cdot k_3) \left( \frac{k_{45}^- \cdot \varepsilon_1}{k_{45}^-} \right)^2 - \frac{m_1^2}{D_s - 2} 16 m^2 m^2 (k_3 \cdot \varepsilon_1)^2} \\
& + \frac{16 (k_4^2 + k_5^2) \left( \frac{k_1 \cdot k_3}{k_1} \right)^2 - \frac{m_1^2}{D_s - 2} 16 m^2 m^2 (k_5 \cdot \varepsilon_1)^2}{\left( \frac{k_4 \cdot k_{23}^-}{k_4} \right) \left( \frac{k_5 \cdot \varepsilon_1}{k_5} \right) + (k_1 \cdot k_5) \left( \frac{k_{23}^- \cdot \varepsilon_1}{k_{23}^-} \right)^2 - \frac{m_1^2}{D_s - 2} 16 m^2 m^2 (k_5 \cdot \varepsilon_1)^2} \\
& + \frac{2 \left( \frac{k_4 \cdot k_{23}^-}{k_4} \right) \left( \frac{k_5 \cdot \varepsilon_1}{k_5} \right) + (k_1 \cdot k_5) \left( \frac{k_{23}^- \cdot \varepsilon_1}{k_{23}^-} \right)^2 - \frac{m_1^2}{D_s - 2} 16 m^2 m^2 (k_4 \cdot \varepsilon_1)^2}{\left( \frac{k_4 \cdot k_{23}^-}{k_4} \right) \left( \frac{k_5 \cdot \varepsilon_1}{k_5} \right) + (k_2 + k_3) \left( \frac{k_{23}^- \cdot \varepsilon_1}{k_{23}^-} \right)^2 - \frac{m_1^2}{D_s - 2} 16 m^2 m^2 (k_4 \cdot \varepsilon_1)^2} \\
& + \frac{2 \left( \frac{k_4 \cdot k_{23}^-}{k_4} \right) \left( \frac{k_5 \cdot \varepsilon_1}{k_5} \right) + (k_2 + k_3) \left( \frac{k_{23}^- \cdot \varepsilon_1}{k_{23}^-} \right)^2 - \frac{m_1^2}{D_s - 2} 16 m^2 m^2 (k_4 \cdot \varepsilon_1)^2}{16 (k + k)^2 (k + k)^2 - m_2^2} \\
& + \frac{\left( \frac{k_{23}^- \cdot k_1}{k_{23}^-} \right) \left( \frac{k_{45}^- \cdot \varepsilon_1}{k_{45}^-} \right) + 2 \left( \frac{k_3 \cdot k_{45}^-}{k_3} \right) \left( \frac{k_2 \cdot \varepsilon_1}{k_2} \right) - 2 \left( \frac{k_2 \cdot k_{45}^-}{k_2} \right) \left( \frac{k_3 \cdot \varepsilon_1}{k_3} \right)}{16 (k_2 + k_3)^2 (k_4 + k_5)^2} - \frac{1}{D_s - 2} 16 m^2 m_2^2 (k_{45} \cdot \varepsilon_1)^2
\end{aligned} \tag{4.18}$$

Graph topology	$\Delta$
	$\frac{1}{4} \frac{m^2 \eta^2}{D_s - 2} (k_b \cdot k_f - k_a \cdot k_f) (\varepsilon_a \cdot \varepsilon_b) - 2 ((k_{cde} \cdot \varepsilon_b) k_f \cdot \varepsilon_a - (k_{cde} \cdot \varepsilon_a) k_f \cdot \varepsilon_b) \quad 1_2$
	$\frac{1}{64} \frac{m^2 \eta^2}{D_s - 2} (k_{cd} \cdot k_{de} - 4k_a \cdot k_f) (\varepsilon_a \cdot \varepsilon_b) - 8(k_f \cdot \varepsilon_a)(k_{cde} \cdot \varepsilon_b) \quad 1_2$
	$\frac{1}{4} \frac{m^2 \eta^2}{D_s - 2} (2 k_{be} \cdot k_{ef} + k_{cd} \cdot k_{ef}) (\varepsilon_a \cdot \varepsilon_b) - 2(k_{ef} \cdot \varepsilon_a)(k_{cd} \cdot \varepsilon_b) + 2(k_{cd} \cdot \varepsilon_a)(k_{ef} \cdot \varepsilon_b) \quad 1_2$
	$\frac{1}{64} \frac{m^2 \eta^2}{D_s - 2} (k_{bcd} \cdot k_e + k_{cd} \cdot k_d - 3k_a \cdot k_f) (\varepsilon_a \cdot \varepsilon_b) - 8(k_f \cdot \varepsilon_a)(k_{cd} \cdot \varepsilon_b) \quad 1_2$
	$\frac{1}{64} \frac{m^2 \eta^2}{D_s - 2} (k_b \cdot k_e + k_a \cdot k_f) (\varepsilon_a \cdot \varepsilon_b) + 8(k_f \cdot \varepsilon_a)(k_e \cdot \varepsilon_b) \quad 1_2$
	$\frac{1}{16} \frac{m^2 \eta^2}{D_s - 2} (2k_{bcd} \cdot k_{ef} + k_c \cdot k_{cd} + 3k_e \cdot k_{ef}) (\varepsilon_a \cdot \varepsilon_b) - 4(k_{ef} \cdot \varepsilon_a)(k_{cd} \cdot \varepsilon_b) \quad 1$
	$\frac{1}{64} \frac{m^2 \eta^2}{D_s - 2} (k_{bcd} \cdot k_{de} - 2k_a \cdot k_f) (\varepsilon_a \cdot \varepsilon_b) - 8(k_f \cdot \varepsilon_a)(k_c \cdot \varepsilon_b) \quad 1_2$

Table 4.3: The graph topologies for the six-point tree amplitude for two distinct-mass scalars, and the corresponding contributions from non-gravitational states  $\Delta$ , where  $k_{ij} = k_i + k_j$ .

#### 4.4.2 Loop Level

The physical cuts relevant to one-loop are relatively straightforward. For both four-point one-loop and five-point one-loop reduction to standard integral basis means satisfying cuts to tree-level under the following restrictions:

- Every bubble cut (two-particle cut) involves physical tree amplitudes (multiplicity four or higher). These are  $N^2\text{MC1-N}^2\text{MC4}$  in Figure 4.4 for the four-point amplitude, and  $N^3\text{MC1-N}^3\text{MC5}$  in Figure 4.11 for the five-point amplitude.

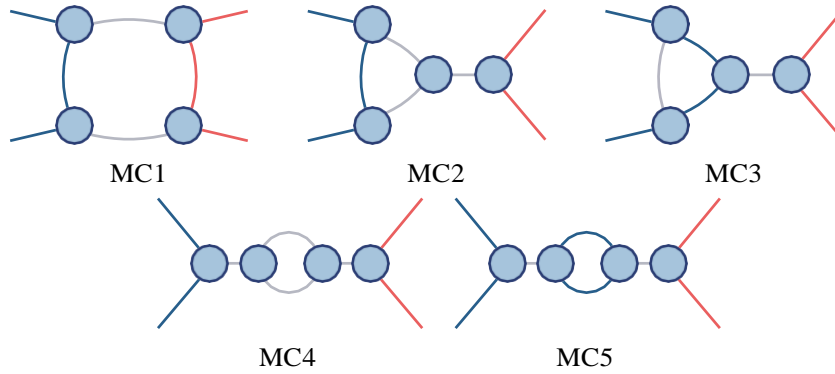


Figure 4.1: All distinct maximal cuts of the one-loop four-point amplitude, not including tadpole graphs. Blue blobs represent three point amplitudes, and exposed legs represent on-shell propagators.

- Every triangle cut (three-particle cut) must involve the loop momenta flowing through each tree. These are cuts NMC1, NMC2 and NMC3 in Figure 4.2 for the four-point amplitude, and  $N^2$ MC1- $N^2$ MC11 in Figure 4.9.
- Every box cut (four-particle cut) for the five-point amplitude, must involve the loop-momenta flowing through each tree. These are cut MC1 in Figure 4.1 for the four-point amplitude and cuts NMC1-NMC7 in Figure 4.7.

This set of restrictions precludes one-loop snail<sup>3</sup> diagrams as well as tadpole diagrams from contributing to the cuts. Any such contributions are not cut constructible with standard (non-regulated) approaches — even in arbitrary dimensions — representing a distinct set of considerations, but one absolutely complementary and compatible with unitary methods as per ref. [61]. As such for each multiplicity at one loop, we only concern ourselves with the series of maximal cuts which can contribute to these physical cuts. This entirely spans any information relevant to the classical  $n \rightarrow 0$  limit.

### Four-point one-loop

Projective double copy allows us to construct the Einstein-Hilbert gravity numerator dressings for the graph topologies of the one-loop four-point amplitude that could possibly be relevant in the classical limit. The maximal cuts expose the information that is inherent to each graph topology, *i.e.* terms that cannot be moved to other cubic graphs. The  $N$ -maximal cuts in turn provide contact terms that can be distributed amongst the uncut propagators of the given cut. At this point a representation choice can thus be made as to where to assign these contributions. Some  $N$ -maximal cuts are delicate, in that they have infinite poles that blow up as cut conditions are released. The information that is missed by omitting these cuts can, however, be retrieved at the level of  $N^2$ -maximal cuts. This type of information shows up as a propagator with some kinematic coefficient, and must therefore be attributed to the corresponding graph topology. We find that the Einstein-Hilbert numerators are corrected by up to  $N^2$ -maximal cuts relative to the  $N = 0$  supergravity kinematic weights.

<sup>3</sup>Apparently one-particle reducible topologies can contribute in an all cubic diagram basis, but only when dressed with appropriate inverse-propagators to actually be encoding one-particle irreducible contact-diagrams [74].

The first step is to calculate all maximal cuts. At one-loop the four-point amplitude has five cubic graph topologies which can ever contribute to the physical cuts<sup>4</sup>, whose topologies can label potential maximal cuts. We present these in Figure 4.1.

For the first consideration of physically relevant information, we now provide details for calculation of the cut MC1 (cf. Figure 4.1) as an example. All propagators are on-shell and so the left-hand side of Equation 4.1 is simply the numerator of the box

$$\mathcal{M}_4^{1\text{-loop}\uparrow\text{cut}}_{\text{MC1}} = n_{N=0} \left( \begin{array}{c} 2 \\ 1 \end{array} \left| \begin{array}{c} 3 \\ 4 \end{array} \right. \right)_{\text{MC1}}^{\uparrow\text{cut}} = (k_1 \cdot k_4)^4, \quad (4.19)$$

where  $l$  is the loop momenta and we have imposed the cut conditions  $l^2 = 0$ ,  $(-k_1)^2 = m_1^2$ ,  $(-k_1 - k_2)^2 = 0$  and  $(l + k_4)^2 = m_2^2$ . The right-hand side of Equation 4.1 is the state sum over the product of three-point tree amplitudes,

$$\begin{aligned} \mathcal{M}_{\text{MC1}}^{\text{trees}\uparrow} &= \sum_{\text{states}} \mathcal{M}_3^{\text{tree}}(l_3^{m_1}, l_1^{m_1}, l_1^{s_3}) \mathcal{M}_3^{\text{tree}}(-l_3^{m_1}, k_1^{m_1}, l_2^{s_2}) \\ &\quad \times \mathcal{M}_3^{\text{tree}}(-l_2^{s_2}, k_3^m, -l_4^m) \mathcal{M}_3^{\text{tree}}(l_4^m, k_4^m, -l_3^m) \\ &= \sum_{\text{states}} (l_1 \cdot \varepsilon(l_3))^2 (l_1 \cdot \varepsilon(l_2))^2 (l_4 \cdot \varepsilon(-l_2))^2 (l_4 \cdot \varepsilon(-l_3))^2. \end{aligned} \quad (4.20)$$

Note that  $\varepsilon(l_i) \neq \varepsilon(-l_i)$ . Using the state projector to sum over polarizations, we find

$$\mathcal{M}_{\text{MC1}}^{\text{trees}\uparrow} = \frac{m_1^2 m_2^2}{D_s - 2} \mathbf{1}_2$$

Similarly to tree-level, the contribution from non-gravitational states is given by the difference between Equation (5.83) and Equation (4.21)

$$\begin{aligned} \hat{\Delta}^{\text{MC1}} &= \mathcal{M}_4^{1\text{-loop}\uparrow\text{cut}}_{\text{MC1}} - \mathcal{M}_{\text{MC1}}^{\text{trees}\uparrow} \\ &= 2 \frac{m_1 m_2 (k_1 \cdot k_4)^2}{D_s - 2} - \frac{(m_1^2 m_2^2)^2}{(D_s - 2)^2}. \end{aligned} \quad (4.22)$$

As mentioned, the functional numerators must obey all the isomorphisms of the graph topologies they describe – such as  $k_1 \leftrightarrow k_2$ ,  $k_3 \leftrightarrow k_4$  for the box graph – and  $\hat{\Delta}^{\text{MC1}}$  is symmetrized accordingly. In this particular case the expression already obeys the relevant isomorphisms, and we have

$$\hat{\Delta}^{\text{MC1}} = -\frac{(m_1^2 m_2^2)^2}{(D_s - 2)^2} + \frac{2m_1^2 m_2^2}{D_s - 2} (k_1 \cdot k_4)^2. \quad (4.23)$$

The constructed Einstein-Hilbert numerator is then given by

$$n_G^{\text{box}} = n_{N=0}^{\text{box}} - \hat{\Delta}^{\text{MC1}}. \quad (4.24)$$

The  $\Delta$  contributions before symmetrization from the maximal cuts of the one-loop amplitude can be found in Table 4.4.

<sup>4</sup>We do not include here contacts associated with cubic graphs like bubbles on external legs nor massive tadpole graphs.

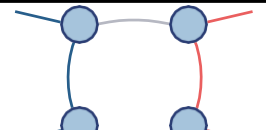
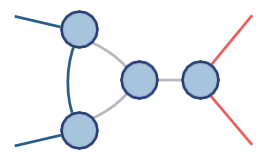
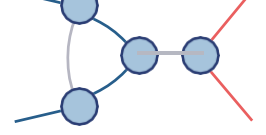
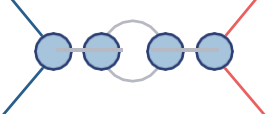
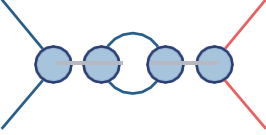
Graph topology	Maximal cut $\Delta$
	$\frac{2}{D_s - 2} m_1^2 m_2^2 (k \cdot k)^2 - \frac{m_1^4 m_2^4}{(D_s - 2)^2}$
	$\frac{1}{D_s - 2} m_1^4 (k \cdot k_4)^2$
	$-\frac{m_1^4}{D_s - 2} (k \cdot k_4 + k_2 \cdot k_4)^2 + m_1 m_2^2 \frac{1}{2} - \frac{m_1^6 m_2^2}{(D_s - 2)^2}$
	$\frac{1}{2} ((D_s - 2)^2 - (D_s - 2) + 2) (k \cdot k_4)^2$
	$\frac{m_1^4 (k \cdot k_4)^2 + m_1 m_2^2 (\frac{3}{2} k \cdot k_4)^2}{D_s - 2} - \frac{m_1^6 m_2^2}{(D_s - 2)^2}$

Table 4.4: The  $\Delta$  contributions from the maximal cuts of the one-loop four-point amplitude, not including tadpole graphs. Blue blobs represent three point amplitudes, and exposed legs represent on-shell propagators.

Updating numerators on the  $N^k$ -maximal cuts is a similar procedure, and the next-to-maximal cuts (NMC) can be found in Figure 4.2. In the Figure, the light blue blobs represent three-point tree amplitudes, and darker blobs represent higher-point trees where cut conditions have been released. The maximal cuts fix all the information inherent to each graph, and excess state contributions from higher-level cuts are therefore contact terms. As we have chosen to represent the amplitudes exclusively in terms of cubic graphs, these terms are associated with uncut propagators of the cut graph topologies. For example, consider the next-to-maximal cut NMC1, which yields the following additional information

$$\begin{aligned}
 \Delta^{\text{NMC1}} &= \frac{n_G \begin{matrix} 2 & & 3 \\ | & & | \\ 1 & & 4 \end{matrix}}{(-k_3)^2} + \frac{n_G \begin{matrix} 2 & & 4 \\ | & & | \\ 1 & & 3 \end{matrix}}{(-k_4)^2} + \frac{n_G \begin{matrix} 2 & & 3 \\ | & & | \\ 1 & & 4 \end{matrix}}{(k_3 + k_4)^2} \\
 &= -\frac{M^{\text{tree}}(k^{m_1}, l^{m_1}, l^{s_3}) M^{\text{tree}}(s^{-l^{m_1}}, l^{k^{m_1}}, l^{s_2}) M^{\text{tree}}(l^{-s_2}, l^{-l^{s_3}}, k^{m_2}, k^{m_4})}{8(D_s - 2) m^4 m^2} (k_3 + k_4)^2 - \frac{1}{(D_s - 2)^2}
 \end{aligned}
 \tag{4.25}$$

where  $k_{ij} = k_i + k_j$ . The resulting expression is a contact term which we are free to attribute to an uncut propagator in the box or triangle graph. We choose the triangle graph, whose uncut propagator is  $(k_3 + k_4)^2$ . The correction to the Einstein-Hilbert

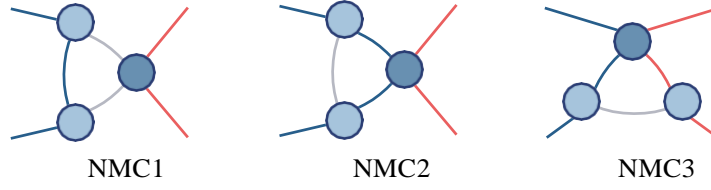


Figure 4.2: Next-to-maximal cuts of the one-loop four-point amplitude. Light blue blobs represent three-point amplitudes, dark blobs represent four-point amplitudes, and exposed legs represent on-shell propagators.

numerator of the MC2 topology is then given by

$$\hat{\Delta}_{\text{NMC}} = -(\mathbf{k}_3 + \mathbf{k}_4)^2 \frac{m_1^2 (m_1^2 - 4m_2^2) (k_3 + k_4)^2}{8(D_s - 2)} + \frac{m_2^2 m_1^4}{(D_s - 2)^2}, \quad (4.26)$$

where we have highlighted the propagator prefactor of the expression, which is kept explicit to ensure the vanishing of this term in the maximal cut MC2.

Here one can choose representations that satisfy either<sup>5</sup> adjoint-type or fundamental-type scalar single-copy origins. For expedience in this thesis we collapse to adjoint-type scalars as the expressions are relatively compact. The remaining next-to-maximal cuts in Figure 4.2 give similar corrections to the gravity numerators, and are shown in Table 4.5 with the corresponding  $\hat{\Delta}_{\text{NMC}}$  terms and the topology to which the new term is attributed.

Graph topology	N-Maximal cut $\hat{\Delta}$	Attributed to
	$-(\mathbf{k}_3 + \mathbf{k}_4)^2 \times \frac{m_1^2 (m_1^2 - 4m_2^2) (k_3 + k_4)^2}{8(D_s - 2)} + \frac{m_1^4 m_2^2}{(D_s - 2)^2}$	
	$(\mathbf{k}_1 + \mathbf{k}_2 + \mathbf{l})^2 \times \frac{m_1^2 m_2^2 (\cdot k_1 - \cdot k_4) + 2(3k_1 \cdot k_4 - k_2 \cdot k_4)}{16(D_s - 2)}$ $+ \mathbf{l}^2 \times \frac{m_1^2 m_2^2 (\cdot k_3 - \cdot k_2) + 8k_1 \cdot k_4}{16(D_s - 2)}$	
	$(\mathbf{k}_3 + \mathbf{k}_4)^2 \times \frac{m_1^2 (4m_2^2 (k_3 + k_4)^2 - m_1^2 (k_3 + k_4)^2 + 16m_2^2)}{16(D_s - 2)}$	

Table 4.5: The symmetrized  $\hat{\Delta}$  contributions from the well-defined next-to-maximal cuts of the one-loop four-point amplitude attributed to inverse propagators. Blue blobs represent three point amplitudes, and exposed legs represent on-shell propagators.

<sup>5</sup>Or both.

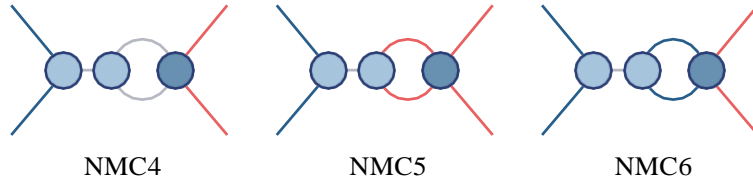


Figure 4.3: Delicate next-to-maximal cuts of the one-loop four-point amplitude excluding snail and tadpole cuts. Light blue blobs represent three point amplitudes, and darker blobs represent four-point amplitudes. Exposed legs represent on-shell propagators.

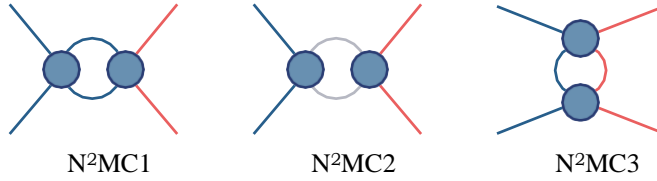


Figure 4.4: All next-to-next-to-maximal cuts of the one-loop four-point amplitude, not including tadpole graphs. Light blue blobs represent three point amplitudes, and darker blobs represent four and five-point amplitudes. Exposed legs represent on-shell propagators.

Some next-to-maximal cuts are delicate. Cuts involving one collapsed propagator of bubble graphs such as NMC4-6 in Figure 4.3, have infinite poles that blow up as cut conditions are imposed on the fully dressed graphs. By construction the numerator dressings are made up of a minimal kinematic basis where conservation of momentum has been imposed. This means that inverse propagators in the numerators – which should cancel against propagators in the denominator – are rewritten in a form where these cancellations do not occur. The cuts, as written, therefore naively go to infinity as propagators in the denominator are sent to zero. Fortunately any potentially physically relevant information in these types of cuts can instead be extracted using the  $N^2$ -maximal cuts (cf. Figure 4.4).

Consider for example the  $N^2$ -maximal cut  $N^2MC1$  in Figure 4.4. This cut is equivalent to NMC6 with an additional propagator,  $(k_1 + k_2)^2$ , put off-shell. The excess state term  $\Delta$  for this cut is

$$\Delta^{N^2MC1} = -\frac{m_1^2}{16(D_s - 2)} \frac{12m^2 m_1^2}{(k_3 + k_4)^2} - 6m_2^2 + m_1^2, \quad (4.27)$$

where we see that this is not a pure contact term. We see the contribution of a manifest propagator, so in this  $N^2MC$  we have found the excess state contribution to one of the propagators in a previously skipped NMC cut. We attribute this information to the topology MC5 (massive bubble), by multiplying by appropriate combinations of the two uncut propagators  $(k_1 + k_2)^2 = (k_3 + k_4)^2$  which yields two distinct contact terms:

$$\begin{aligned} \hat{\Delta}^{N^2MC1} = & (k_3 + k_4)^2 \times \frac{-3m_1 m_2}{4(D_s - 2)} \\ & + (k_1 + k_2)^2 (k_3 + k_4)^2 \times \frac{(6m_1^2 m_2^2 - m_1^4)}{16(D_s - 2)}. \end{aligned} \quad (4.28)$$

As the first is proportional to a single uncut propagator, we see that it contains information relevant to a cut like NMC6. Of course because of conservation of momentum



it vanishes when  $(k_1 + k_2)^2$  is on-shell, which is why it was sensible to wait until this  $N^2$ -maximal cut to figure out where it belongs. The second term is proportional to the two propagators whose cut conditions are released at  $N^2$ -maximal level, and so is inherently a  $N^2$ MC correction.

Of the  $N^2$ -maximal cuts shown in Figure 4.4 the cuts  $N^2$ MC1 and  $N^2$ MC2 yield numerator corrections, and the remaining cut can be used for verification. The symmetrized corrections for the  $N^2$ MC are shown in Table 4.6, with the propagator prefactors that correspond to attributing the cut information to the topologies shown in the right column.

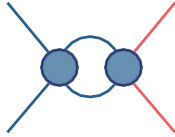
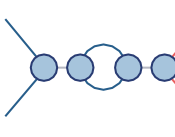
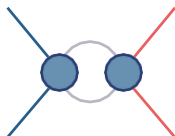
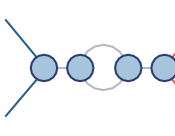
Graph topology	$N^2$ -Maximal cut $\hat{\Delta}$	Attributed to
	$- (\mathbf{k}_{34})^2 \times \frac{3m_1^4 m_2^2}{4(D_s - 2)} - (\mathbf{k}_{34})^2 \times \frac{m_1^2 (m_1^2 - 6m_2^2)}{16(D_s - 2)}$	
	$(\mathbf{k}_{34})^2 \times \left[ - \frac{sP_{14} - 4(m_1^2 P_{34} + m_2^2 P_{12})}{8(D_s - 2)} \right. \\ + \frac{D_s - 2}{s} \left( \frac{16}{8(k_2 \cdot k_4)} \frac{13}{13} - (m_1^2 P_{34} + m_2^2 P_{12}) \right) \\ - \frac{1}{16} \left( \frac{8(k_4 \cdot k_{12})(\cdot k_{13}) + 16}{13} + 3P_{14} \right) \\ + 4 \left( \frac{16(k_2 \cdot k_4)}{13} - 3(m_1^2 P_{34} + m_2^2 P_{12}) \right) \\ \left. - 4(k_2 \cdot k_4)s^2 \right] \\ + (\mathbf{k}_{34})^2 \times \frac{2^{12} (D_s - 2)^2 (s - 4P_{14})}{128} \\ + \frac{D_s - 2}{128} \left( \frac{8su - 9s^2 + 32(k_2 \cdot k_4)^2 + 12P_{14}}{8} \right) \\ - \frac{32(k_2 \cdot k_4)^2 - 16m_1^2 m_2^2 + 8P_{14}}{64 + 8su + 4sm^2 - 9s^2} \\ - \frac{sm_{12}^2 - 16m_1^2 m_2^2 - P_{14}}{8(D_s - 2)} - \frac{m_1^2 m_2^2}{(D_s - 2)^2}$	

Table 4.6: The symmetrized  $\hat{\Delta}$  contributions from the well-defined  $N^2$ -maximal cuts of the one-loop four-point amplitude attributed to inverse propagators. Blue blobs represent three point amplitudes, and exposed legs represent on-shell propagators. Here  $_{13} = (\cdot k_1)(\cdot k_3)$ ,  $m_{12}^2 \equiv m_1^2 + m_2^2$ ,  $s \equiv (k_3 + k_4)^2$ ,  $u \equiv (k_2 + k_4)^2$ ,  $k_{ij} = k_i + k_j$ ,  $k_{ij}^- = k_i - k_j$ ,  $P_{12} = (\cdot k_1)^2 + (\cdot k_2)^2$ ,  $P_{34} = (\cdot k_3)^2 + (\cdot k_4)^2$ , and  $P_{14} = (\cdot k_1)^2 + (\cdot k_2)^2 + (\cdot k_3)^2 + (\cdot k_4)^2$ .

All five maximal cuts of the four-point one-loop amplitude, not including snail or tadpole graphs, are shown in Figure 4.1. All the cuts in the figure give corrections

which are inherent to the gravity numerators of these topologies. The three next-to-maximal cuts shown in Figure 4.2 are well-defined, and removing cut conditions do not result in infinite poles. The first of these cuts, NMC1, exposes a correction that can be attributed to one of two graph topologies (corresponding to MC1 and MC2 in Figure 4.1). The remaining two well-defined cuts – NMC2, NMC3 – also give corrections, but they involve four-point tree amplitudes with two massive scalars, which means only one topology contributes to each of these cuts. In Figure 4.3 we show three delicate next to maximal cuts, whose relevant information can be more easily extracted by further relaxing cut conditions. Finally, the  $N^2$ -maximal cuts are shown in Figure 4.4. The two first cuts –  $N^2$ MC1 and  $N^2$ MC2 – give corrections to the numerators, including information from the skipped  $N$ -maximal cuts. The third cut,  $N^2$ MC3, receives no correction.

### Five-point one-loop

We proceed with the projective double copy to find the one-loop gravitational radiative correction to the two-to-two scattering of massive scalars. The procedure at five-points is the same as demonstrated at four-points, again starting with the maximal cuts. The 24 maximal cuts relevant to the physical cuts for this five-point amplitude are shown in Figures 4.5-4.6, excluding both tadpole and snail topologies. All the maximal cuts give excess state corrections to the corresponding graph numerators.

The 30 next-to-maximal cuts can be found in Figures 4.7-4.8, and all of these cuts give corrections to the numerators. There are 19  $N^2$ -maximal cuts which are shown in Figures 4.9-4.10. In contrast to the next-to-maximal cuts, not all of these yield corrections. The cuts  $N^2$ MC1,  $N^2$ MC3,  $N^2$ MC11 and  $N^2$ MC19 give no contributions, while the remaining 15 cuts do correct for excess states. At five-point one-loop the highest order of corrections come from  $N^2$ -maximal cuts. However, some delicate cuts must be ignored at NMC and  $N^2$ MC and the information extracted using  $N^3$ MC, as described in the previous section for the four-point amplitude. All  $N^3$ -max cuts are bubble cuts, and can be found in Figure 4.11. The corrected gravitational numerators can be found in auxiliary files.

## 4.5 Conclusion

In this thesis we demonstrate that the method of maximal cuts in combination with double-copy can be used to bootstrap graph dressings in Einstein-Hilbert gravity from the double copy of scalar QCD, in a combined procedure we refer to as projective double-copy. Specifically, we systematize the contribution of unitarity cuts of the amplitudes where only gravitational states are allowed to cross the cuts, while allowing the double-copy to provide all relevant gravitational contact terms. Starting with the maximal cuts where all propagators are put on-shell, we work our way up to the necessary  $N^k$ -maximal cuts by systematically releasing cut conditions on propagators. This allows us to project out all non-gravitational states from the graph dressings. For tree-level amplitudes with a single massive scalar we find that no correction is necessary up to five-point, while tree- and one-loop amplitudes with more than one massive scalar do contain excess states that are removed. We expect these integrands to be useful to understanding and developing optimized approaches to previously uncalculated classical predictions relevant to gravitational wave astrophysics.

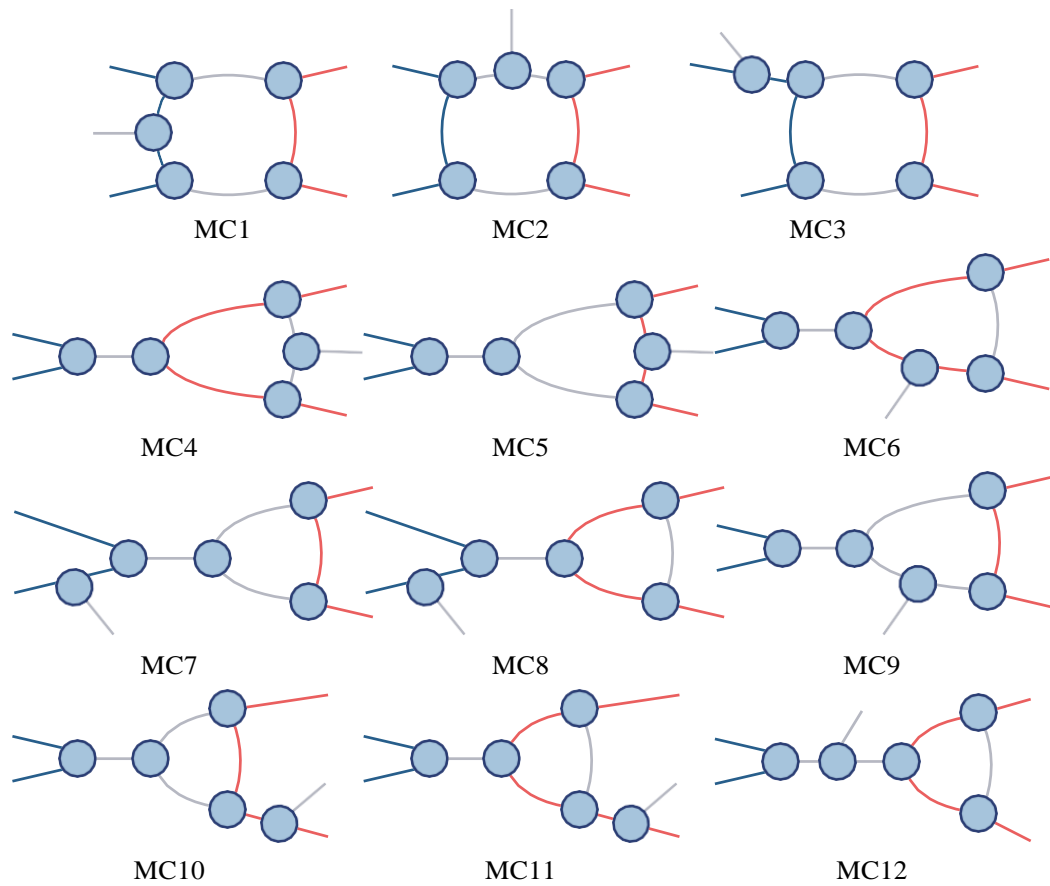


Figure 4.5: Maximal cuts MC1-MC12 of the one-loop five-point amplitude. Light blue blobs represent three point amplitudes, and darker blobs represent four and five-point amplitudes. Exposed legs represent on-shell propagators.

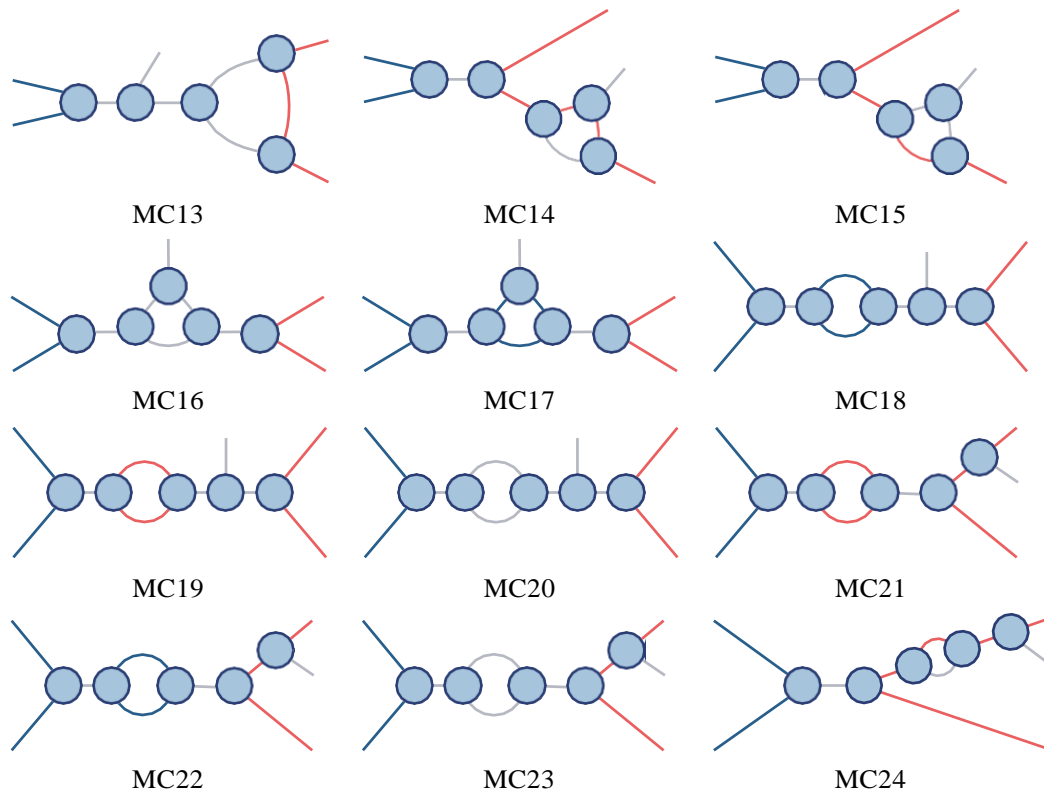


Figure 4.6: Maximal cuts MC13-MC24 of the one-loop five-point amplitude. Light blue blobs represent three point amplitudes, and darker blobs represent four and five-point amplitudes. Exposed legs represent on-shell propagators.

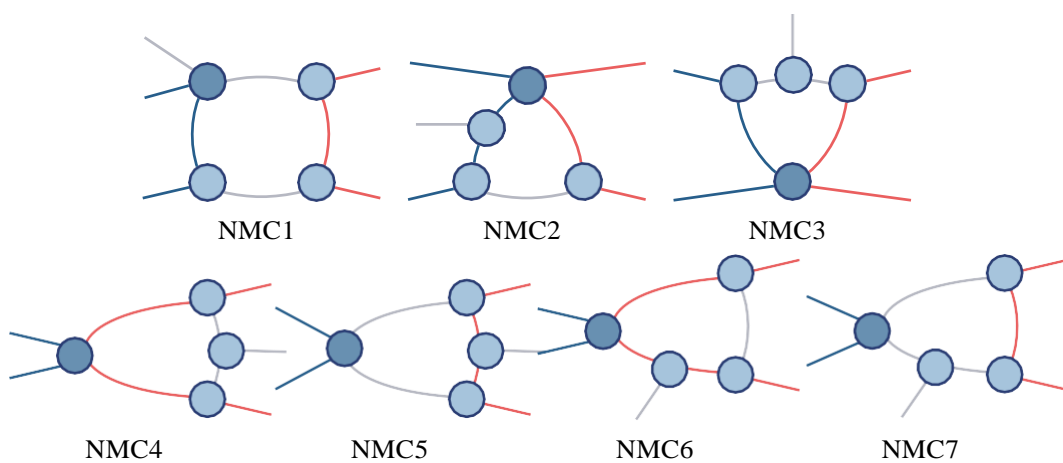


Figure 4.7: Next-to-maximal box cuts of the one-loop five-point amplitude. Light blue blobs represent three-point amplitudes, and darker blobs represent four and five-point amplitudes. Exposed legs represent on-shell propagators.

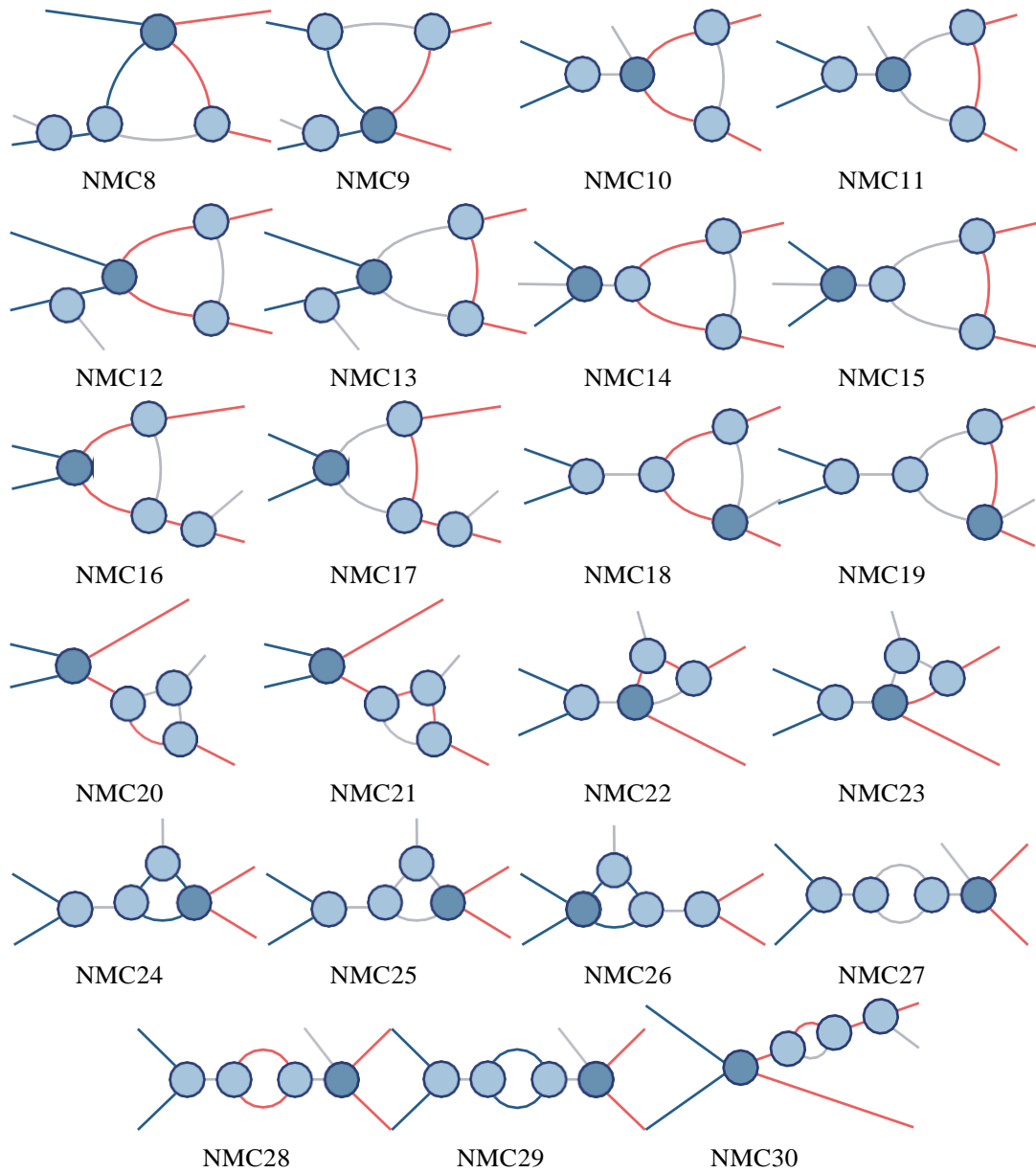


Figure 4.8: Next-to-maximal cuts of the one-loop five-point amplitude. Light blue blobs represent three-point amplitudes, and darker blobs represent four and five-point amplitudes. Exposed legs represent on-shell propagators.

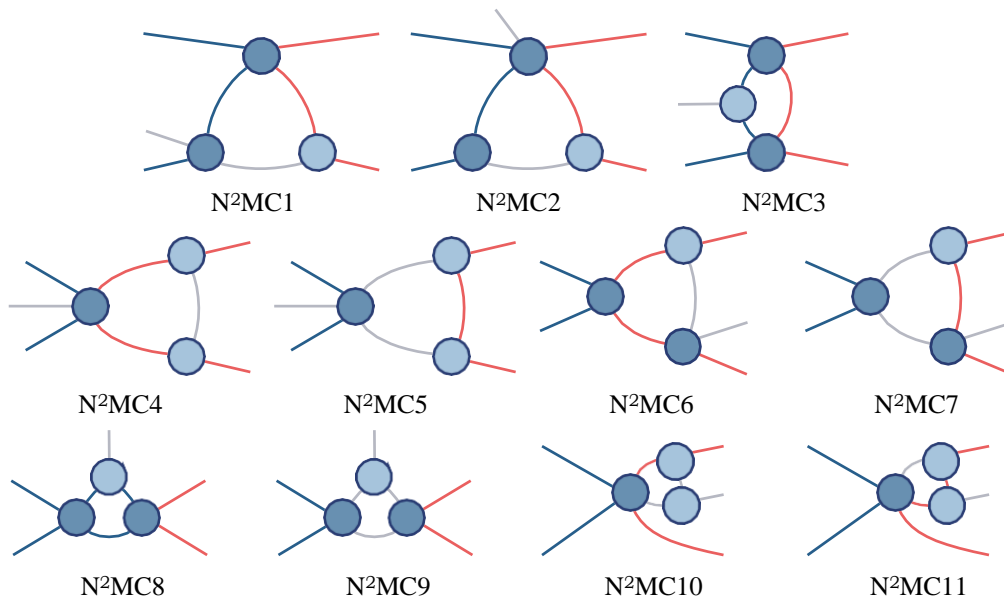


Figure 4.9:  $N^2$ -maximal triangle cuts of the one-loop five-point amplitude. Light blue blobs represent three-point amplitudes, and darker blobs represent four and five-point amplitudes. Exposed legs represent on-shell propagators.

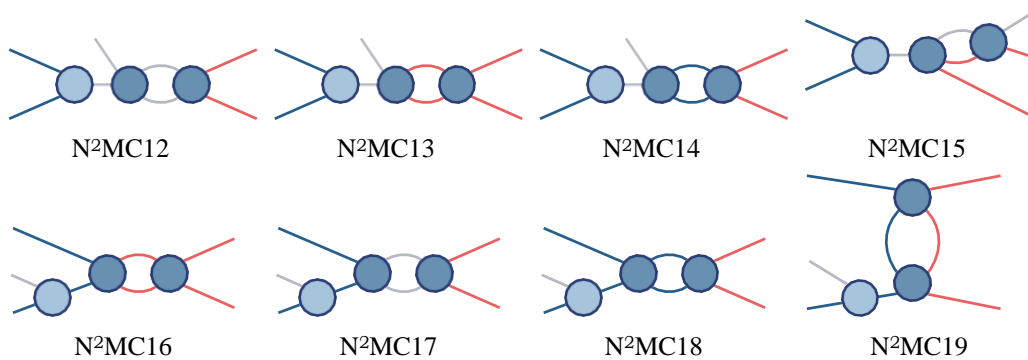


Figure 4.10:  $N^2$ -maximal cuts of the one-loop five-point amplitude. Light blue blobs represent three-point amplitudes, and darker blobs represent four and five-point amplitudes. Exposed legs represent on-shell propagators.

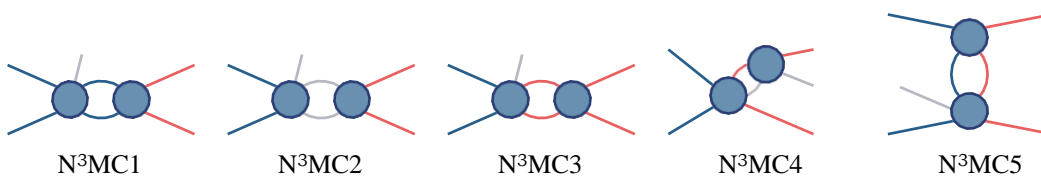


Figure 4.11:  $N^3$ -maximal bubble cuts of the one-loop five-point amplitude. Dark blue blobs represent four and five-point amplitudes. Exposed legs represent on-shell propagators.

The success and relative simplicity of this procedure promises possible verification for future double copy schemes. It would be intriguing to investigate whether including massless ghostly matter in the original theory in a strategic manner will remove the excess states at loop-level, and the method of maximal cuts can here provide a straightforward comparison for the resulting amplitudes.

## Chapter 5

# Classical limits

### 5.1 Introduction

The detection of gravitational wave-signals by the LIGO and VIRGO collaborations [1], along with the observation of a black hole by [114] in 2019, have made it an urgent matter to improve theoretical gravitational predictions. By combining numerical relativity and analytic predictions we can make gravitational wave templates to compare with experiment. From the analytic side we must provide theoretical predictions, either as a gravitational Hamiltonian, from which we can find the equations that govern the motion of gravitationally interacting bodies, or directly in the form of classical observables.

As techniques for calculating scattering amplitudes become increasingly powerful and allow the calculation of amplitudes up to several-loop level, many strategies for extracting the classically relevant information from scattering amplitudes have been developed. In particular, observables related to the binary problem are of great interest, and one of the successful applications of amplitude methods has been in determining the potential between two bodies. Early progress using amplitudes was made in [115, 116]. In certain cases full quantum amplitudes contain many quantum terms that are irrelevant to the classical limit, but which are still calculated to obtain the full amplitude. Effective Field Theory (EFT) methods are a way to avoid unnecessary calculation by allowing certain classical effects to be targeted in amplitude calculations, to which [117] was a major contribution.

In the inspiral phase of the two-body gravitational binary problem two heavy bodies spiral around each other emitting energy in the form of gravitational radiation, thereby reducing the radius of movement. In this region we can use the post-Newtonian (PN) expansion – a relativistic expansion in both Newton’s constant and the relative velocity between bodies – and post-Minkowskian (PM) expansion – an expansion only in Newton’s constant.

The above methods can be combined with amplitude techniques to find the two-body Hamiltonian. The conservative part of the potential has been determined up to third and fourth order in the PM expansion [51, 55]. The equations of motion from the conservative potential can then be used to calculate observables of a scattering process, such as the impulse and spin kick.

The potential region has an ill-defined high-energy limit, where radiation reaction effects must also be included [118]. The radiation effect has been calculated in [49, 52], and the scattering amplitude with all the necessary terms for a well-behaved expression has been calculated to third PM order in [54]. From the potential one can find the scattering angle between the colliding bodies [119–121].

Another important step towards finding gravitational waveforms is given in [36], where the authors present the Kosower-Maybee-O’Connell (KMOC) formalism for



calculating observables directly from on-shell scattering amplitudes. By expressing the observables as expectation values of carefully crafted incoming and outgoing states, factors of  $\hbar$  are restored in quantum expressions, and the limit  $\hbar \rightarrow 0$  yields the observable in the classical limit. In particular, there are two observables we can calculate using this method: the change in momentum during a collision, the *impulse*, and the radiated momentum from two-to-two scattering, for which the authors present results in QED. In [56] a similar formalism was developed for observables in Yang-Mills theory, namely the color impulse and radiated color. It is worth noting that the methods of amplitudes extend beyond the scattering of massive particles to include, for example, the scattering of massless particles, like classical light, from heavy objects like the sun [122].

### 5.1.1 Restoring $\hbar$ and classical point particles

Classical predictions can be thought of as the  $\hbar \rightarrow 0$  limit of predictions in some quantum theory. An important step in the KMOC formalism is therefore to restore powers of  $\hbar$ . When restoring  $\hbar$  in an expression, the coupling constants are multiplied by a factor of  $\hbar^{-1/2}$  because the dimensionless couplings are by definition proportional to  $\hbar^{-1/2}$ . Naively, it seems that higher order amplitudes contribute more to the classical observables. However, we also get  $\hbar$  from certain momenta which we will have to treat as wavenumbers classically, whereas point particles have momenta that is fixed as  $\hbar \rightarrow 0$ . The wavenumber associated with the particle of momentum  $p$  is given by

$$\bar{p} \equiv \frac{p}{\hbar}. \quad (5.1)$$

At the quantum level particles are described by wavefunctions which are in turn described by wavepackets, characterized by a smearing or spread in momenta  $\omega$  and a Compton wavelength  $\ell_c$ . The precision with which we know the particles position is given by  $\omega$ . This parameter should not be too big, so the particles wavefunctions do not interfere, but also not too small so that quantum effects do not occur for the wavefunction. Towards the classical limit particle momenta should reduce to the classical value

$$p_i^\mu \rightarrow m_i u_i^\mu \quad (5.2)$$

with classical four-velocities normalized to  $u^2 = 1$ .

The wavefunction must depend on at least one four-vector parameter, and in the simplest cases this will just be the four velocity  $u$  of the corresponding particle. The momentum shifts  $q_i = p'_i - p_i$  are difference between the momentum of the incoming particle  $p_i$  and the conjugate  $p'_i$ . In the classical limit this shift should go to zero, as the wavefunction and its conjugate should represent the same particle. We integrate over all  $q$ , so we take  $q_0$  to be a 'characteristic' value of  $q$ . We then require that  $\varphi(p + q)$  not differ much from  $\varphi(p)$ , or in other words that

$$\frac{q_0 \cdot u_i}{m \xi} \ll 1, \quad (5.3)$$

where  $\xi$  is the square of the ratio of the Compton wavelength to the intrinsic spread

$$\xi \equiv \frac{\ell_c^2}{w^2}. \quad (5.4)$$

Scaling the momentum by  $\mathfrak{n}$ , and using the wavenumber, we find

$$\bar{q}_0 \cdot u_i \omega \ll \bar{\xi}. \quad (5.5)$$

In general, when taking the  $\mathfrak{n} \rightarrow 0$  classical limit, we may meet with *singular terms*. These are terms with too many inverse powers of  $\mathfrak{n}$ . These meet with one of two fates: they are multiplied by functions that vanish in the regime of this limit, or they cancel in the sum of all contributions. When taking the limit, we benefit from two simplifications: setting momentum  $p^\mu$  to the classical values  $m u^\mu$ , and truncating at the lowest power of  $\mathfrak{n}$ . Inside on-shell delta functions  $\hat{\delta}^4(2p_i \cdot \bar{q} \pm \mathfrak{n} \bar{q}^2)$  we can neglect the  $\bar{q}^2$  term, so long as the factors multiplying these delta functions are not singular in  $\mathfrak{n}$ . We introduce a notation to allow for the manipulation of integrands in the  $\mathfrak{n} \rightarrow 0$  limit

$$\int \mathbf{r} f(p_1, p_2, \dots) \equiv \int d\Phi(p_1) d\Phi(p_2) |\varphi(p_1)|^2 |\varphi(p_2)|^2 f(p_1, p_2, \dots), \quad (5.6)$$

where the integration over  $p_i$  is implicit.

### 5.1.2 Color Impulse

In [56] the authors calculate the expression for the *color impulse*, *i.e.* the change in color of colliding particles. I will here give a brief resumé of the derivation. Consider the case where two distinct scalar fields,  $\alpha = 1, 2$ , couple to the Yang-Mills field, given by the action

$$S = \int d^4x \sum_{\alpha=1}^2 \left( D_\mu \phi^\dagger_\alpha D^\mu \phi_\alpha - \frac{m_\alpha^2}{\mathfrak{n}^2} \phi^\dagger_\alpha \phi_\alpha - \frac{1}{4} F_{\mu\nu}^a F^{a\mu\nu} \right), \quad (5.7)$$

where  $D_\mu = \partial_\mu + ig A_\mu^a T^a$  and  $T^a$  are the generator matrices in a representation  $R$ .

The color charge of a single particle can be written as

$$C^a = i \int d^3x \left( \phi^\dagger T^a_R \partial_0 \phi - (\partial_0 \phi^\dagger) T^a_R \phi \right) = \mathfrak{n} \int d\Phi(p) \left( a^\dagger(p) T^a_R a(p) - b^\dagger(p) T^a_{\bar{R}} b(p) \right), \quad (5.8)$$

where  $\bar{R}$  is the conjugate representation,  $T^a_{\bar{R}} = -T^a_R$ . This operator inherits the usual Lie algebra

$$[C^a, C^b] = i\mathfrak{n} f^{abc} C^c. \quad (5.9)$$

The inner products are then rescalings of the generators

$${}_i \langle C^a | p_j \rangle = (C^a)_i = \mathfrak{n} (T_R^a)_i. \quad (5.10)$$

We write a generic single particle state as

$$|\psi\rangle = \int d\Phi(p) \varphi(p) \chi_i |p^i\rangle, \quad (5.11)$$

where the vector  $\chi_i$  labels a general colour state, and normalisations are

$$\int d\Phi(p) |\varphi(p)|^2 = 1, \quad \chi_i^* \chi_i = 1. \quad (5.12)$$

The color charge of a particle, and the classical limit of the color charge, are then defined as

$$c^a \equiv \psi | C^a | \psi = \chi^{i*} (C^a)^j \chi_j, \quad (5.13)$$

where in the classical limit we require

$$\begin{aligned} \psi | C^a | \psi &= \text{finite} \\ \psi | \overset{a}{C} \overset{b}{C} | \psi &= \psi | C^a | \psi \psi | C^b | \psi + \text{negligible}. \end{aligned} \quad (5.14)$$

The initial state for multiple particles assumes the particles in the initial state have well-defined positions, momenta and colors. Each particle  $\alpha$  has a wavepacket  $\varphi_\alpha(p_\alpha)$  describing the momentum-space distribution, and a color wavepacket  $\chi_\alpha$ . Initially, the particles are separated by an impact parameter  $b$  much larger than the spread of wave packets in momentum space. The initial state is

$$|\Psi\rangle = \int d\Phi(p_1) \Phi(p_2) \varphi_1(p_1) \varphi_2(p_2) e^{ib \cdot p_1 / \Lambda} \chi_{1i} \chi_{2j} |p^i; p^j\rangle. \quad (5.15)$$

The color operator used on a state with multiple particles is the sum of the color operators of the individual particle states

$$C^a |p_1 \chi_1; p_2 \chi_2\rangle = |p_1^i p_2^j\rangle (C^a)_i^j \delta_{j\ell} \delta_{\ell k} \chi_{1i} \chi_{2j}, \quad (5.16)$$

which means the colors add

$$p_1 \chi_1; p_2 \chi_2 | C_{1+2}^a | p_1 \chi_1; p_2 \chi_2 = c_1^a + c_2^a. \quad (5.17)$$

The color impulse is given by

$$\Delta c_1^a \rightarrow \Delta c_1^a = i \int d^4 \bar{q} \delta(2p_1 \cdot \bar{q}) \delta^2(2p_2 \cdot \bar{q}) e^{-ib \cdot \bar{q}} G, \quad (5.18)$$

where the double brackets denote the classical limit as defined in Equation (5.6), and the color kernel  $G$  is defined to be

$$\begin{aligned} G^a &= n^2 [C^a, C(D)] A_D(p_1, p_2 \rightarrow p_1 + q, p_2 - q) \\ &- in^4 \prod_{X=i,1,2}^D \int d^4 \bar{\omega}_i \delta(2p_1 \cdot \bar{\omega}_i + n \bar{\omega}_i^2) \delta^{(4)}(\bar{\omega}_1 + \bar{\omega}_2 - \bar{r}_X) C(D)^\dagger [C^a, C(D)] \\ &\times A_{D^\dagger}^*(p_1 + q, p_2 - q \rightarrow p_1 + \omega_1, p_2 + \omega_2, r_X) A_D(p_1, p_2 \rightarrow p_1 + \omega_1, p_2 - \omega_2, r_X). \end{aligned} \quad (5.19)$$

### 5.1.3 Color Radiation

KMOC considers the radiation of momenta, but we can also study the total color radiated to infinity. We shall start with radiated momenta or energy, and imagine a collision with detectors that detect radiated photons for QED or gravitons for gravity. Radiated particles are called *messengers*, and the momentum operator of the radiated field is  $K^\mu$ . The expectation value of the radiated momenta is then, inserting a complete set of states,

$$R^\mu = \int_X \int d\Phi(k) \Phi(r_1) \Phi(r_2) k^\mu \langle k r_1 r_2 | T | \psi \rangle^2. \quad (5.20)$$

To study the radiated gluon we need an operator for the gluon radiation field. We restrict to the adjoint representation,

$$F^a = i\eta \int_{\sigma=\pm}^{\mathbf{r}} f^{abc} \mathbf{d}\Phi(k) a_{\sigma}^{bt}(k) a^c(k), \quad (5.21)$$

where  $\sigma$  labels helicity. Assuming there are no bosons in the initial state, the expectation value of the radiation is

$$R_{\text{col}^a} = \Psi |T^\dagger F^a T| \Psi. \quad (5.22)$$

The conservation of color means we can write

$$\Delta c_1^a + \Delta c_2^a = - R_{\text{col}^a}. \quad (5.23)$$

The classical limit of the radiation expectation value is

$$R_{\text{col}}^a = -i \int_{\sigma}^{\mathbf{r}} f^{abc} \mathbf{n}^{-2} \mathbf{d}\Phi(k) R^{*b}(k, \sigma) R^c(k, \sigma), \quad (5.24)$$

where radiation kernels inherit the color index of the external gluon

$$R^a(k, \sigma) = \mathbf{n}^{\frac{3}{2}} \int^{\mathbf{r}} \hat{\mathbf{d}} q_1 \hat{\mathbf{d}} q_2 \delta(2p_1 \cdot q_1 + q_1^2) \delta(2p_2 \cdot q_2 + q_2^2) \hat{\delta}^{(4)}(k - q_1 - q_2) e^{ib \cdot q_1 / \mathbf{n}} \\ \times \int_D C^a(D) A_D(p_1 + q_1, p_2 + q_2 \rightarrow p_1, p_2; k, \sigma). \quad (5.25)$$

## 5.2 Reproducing the classical impulse and radiation

The graph representation of amplitudes and integrands we have developed in the previous chapters can be used to reproduce results from [56] for the classical impulse at leading order

$$\Delta c_1^{a,(0)} = g^2 \int^{\mathbf{r}} f^{abc} c_1^b c_2^c u_1 \cdot u_2 \int^{\mathbf{r}} \hat{\mathbf{d}} \bar{q} \hat{\delta}(u_1 \cdot \bar{q}) \hat{\delta}(u_2 \cdot \bar{q}) \frac{e^{-ib \cdot \bar{q}}}{\bar{q}^2}, \quad (5.26)$$

the impulse kernel at next-to-leading order

$$G^{a,(1)} = g^4 \int^{\mathbf{r}} \int^{\mathbf{f}} \frac{1}{\mathbf{d}^{-2}(\bar{c} - \bar{q})^2} 4i f^{abc} C_2^c C_1^d (C_1 \cdot C_2) \\ \times \hat{\delta}(p_1 \cdot \bar{c}) \frac{m_1^2 + (p_1 \cdot p_2)^2 \cdot (\bar{c} - \bar{q})}{(p_2 \cdot \bar{c} - i\varepsilon)^2} + i \hat{\delta}(p_2 \cdot \bar{c}) \\ + \hat{\delta}(p_2 \cdot \bar{c}) \frac{m_2^2 + (p_1 \cdot p_2)^2 \cdot (\bar{c} - \bar{q})}{(p_1 \cdot \bar{c} + i\varepsilon)^2} - i \hat{\delta}(p_1 \cdot \bar{c}) \\ - 2i f^{acd} f^{dbe} \left( C_1^e C_2^b C_2^c - C_2^e C_1^b C_1^c \right) (p_1 \cdot p_2)^2 \hat{\delta}(p_1 \cdot \bar{c}) \hat{\delta}(p_2 \cdot \bar{c}), \quad (5.27)$$

as well as the leading order radiation kernel

$$\begin{aligned}
 R^{a,(0)}(\bar{k}) = & -g^3 \int_{c_1 \cdot c_2}^{\mathbf{r}} \hat{d}^4 \bar{q}_1 \hat{d}^4 \bar{q}_2 \delta^{(4)}(\bar{k} - \bar{q}_1 - \bar{q}_2) \hat{\delta}(u_1 \cdot \bar{q}_1) \hat{\delta}(u_2 \cdot \bar{q}_2) e^{ib \cdot \bar{q}_1} \varepsilon_{\mu}^h \\
 & \times \frac{\bar{q}_2 \cdot \bar{k} \cdot u_1}{i f^{abc} c^b c^c} - \frac{(u_1 \cdot u_2)}{2k \cdot u_2 u_1} - \frac{\bar{q}_2 \cdot \bar{k} \cdot u_1}{\bar{k} \cdot u_1} + \frac{k \cdot u_1 u_2 - k \cdot u_2 u_1}{\bar{q}_2^2} \\
 & + \frac{1}{\bar{q}_2^2 \bar{q}_1^2} \left[ 2k \cdot u_2 u_1 - u_1 \cdot u_2 \bar{q}_1 + u_1 \cdot u_2 \bar{k} \cdot u_1 \right] + (1 \leftrightarrow 2) . \quad (5.28)
 \end{aligned}$$

The calculation in this chapter differs from [56], as we only use cubic graphs and the graph numerators we have developed in previous chapters. I will present all three calculations in some detail. This is meant also as a motivation for ongoing work – to calculate the classical radiative correction at one-loop.

### 5.2.1 Leading order impulse calculation

The expression for the color impulse is given in Equation (5.86), and at tree-level only the first term in the expression contributes. The leading order kernel with factors of  $\mathfrak{n}$  extracted from the kinematics is therefore

$$G^{a,(0)} = \mathfrak{n}^2 g^2 [C^a, C(D)] A_D^{(0)}(p_1, p_2 \rightarrow p_1 + \mathfrak{n}\bar{q}, p_2 - \mathfrak{n}\bar{q}). \quad (5.29)$$

We calculate the color-stripped amplitude  $\bar{A}_D^{(0)}(p_1, p_2 \rightarrow p_1 + \mathfrak{n}\bar{q}, p_2 - \mathfrak{n}\bar{q})$  using our graph dressings, and as only the  $t$ -channel graph contributes we can set up

$$\bar{A}^{\text{tree}}(-p_1, p_1 + \mathfrak{n}\bar{q}, p_2 - \mathfrak{n}\bar{q}, -p_2) \sim \begin{array}{c} p_1 + \mathfrak{n}\bar{q} \quad p_2 - \mathfrak{n}\bar{q} \\ \diagdown \quad \diagup \\ \text{---} q \text{---} \\ \diagup \quad \diagdown \\ p_1 \quad p_2 \end{array}, \quad (5.30)$$

so that the color-stripped amplitude is given by

$$\bar{A}^{\text{tree}}(-p_1, p_1 + \mathfrak{n}\bar{q}, p_2 - \mathfrak{n}\bar{q}, -p_2) = \frac{\mathfrak{n} \left( (\bar{q} \cdot p_1) - 2(\bar{q} \cdot p_2) + \mathfrak{n}\bar{q}^2 \right) - 2(p_1 \cdot p_2)}{2\mathfrak{n}^2 \bar{q}^2}. \quad (5.31)$$

By conservation of momentum we have that  $p_1 \cdot \bar{q} = -\mathfrak{n}\bar{q}^2/2$  and  $p_2 \cdot \bar{q} = \mathfrak{n}\bar{q}^2/2$ , so we rewrite the expression

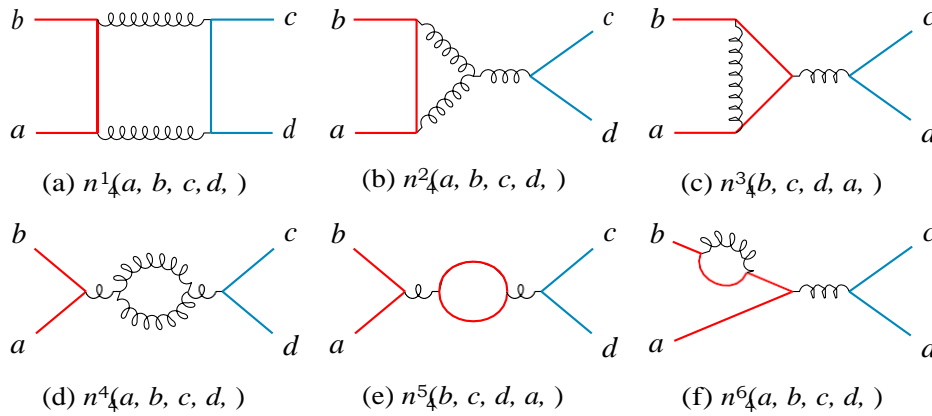
$$\bar{A}^{\text{tree}}(-p_1, p_1 + \mathfrak{n}\bar{q}, p_2 - \mathfrak{n}\bar{q}, -p_2) = -\frac{1}{4} \frac{\mathfrak{n}^2 \bar{q}^2 + 4p_1 \cdot p_2}{\mathfrak{n}^2 \bar{q}^2}. \quad (5.32)$$

The color factor of the graph in Equation (5.30) is

$$C(t) = C_1 \cdot C_2, \quad (5.33)$$

where  $C_i$  is the color factor related to the particle with momenta  $p_i$ , so the color impulse factor is

$$[C_1^a, C(t)] = [C_1^a, C_1^b] C_2^c = i f^{abc} C_1^c C_2^b. \quad (5.34)$$


 Figure 5.1: Cubic graph topologies that contribute to  $A_4^{1\text{-loop}}$ .

Inserting the expressions into the kernel means the factors of  $\mathfrak{n}$  cancel, and the color impulse in Equation (5.86) gives

$$\begin{aligned} \Delta c_1^{a,(0)} &= i \int \frac{d^4 \bar{q}}{(2\pi)^4} \delta(2p_1 \cdot \bar{q}) \delta(2p_2 \cdot \bar{q}) e^{-ib \cdot \bar{q}} G \\ &= i \int \frac{d^4 \bar{q}}{(2\pi)^4} \delta(2p_1 \cdot \bar{q}) \delta(2p_2 \cdot \bar{q}) e^{-ib \cdot \bar{q}} \mathfrak{n} g^2 (i\mathfrak{n} f^{abc} C_1 C_2) \times \left( \frac{1}{4} \frac{\hat{\mathbf{T}}}{\mathfrak{n}^2 \bar{q}^2} 4p_1 \cdot p_2 + \mathfrak{n}^2 \bar{q}^2 \right) \end{aligned} \quad (5.35)$$

where the double brackets indicate that we evaluate the expression in the classical limit, where we Laurent expand around  $\mathfrak{n}$ . Massive momenta are replaced by four-velocities,  $p_i \rightarrow m_i u_i$ , and we arrive at the same expression as Equation (5.26)

$$\begin{aligned} \Delta c_1^{a,(0)} &= -g^2 \int \frac{d^4 \bar{q}}{(2\pi)^4} \frac{1}{m_1} \delta(2u_1 \cdot \bar{q}) \frac{1}{m_2} \delta(2u_2 \cdot \bar{q}) e^{-ib \cdot \bar{q}} (f^{abc} C_1 C_2) \times \left( -\frac{1}{4} \frac{\hat{\mathbf{T}}}{\bar{q}^2} 4m_1 m_2 u_1 \cdot u_2 \right. \\ &= -\frac{1}{4} g f^{abc} C_1 C_2 u_1 \cdot u_2 \int \frac{d^4 \bar{q}}{(2\pi)^4} \delta(u_1 \cdot \bar{q}) \delta(u_2 \cdot \bar{q}) \frac{e^{-ib \cdot \bar{q}}}{\bar{q}^2} \left. \right) \end{aligned} \quad (5.36)$$

### 5.2.2 Next-to-leading order impulse calculation

At next-to-leading order the classical color kernel with factors of  $\mathfrak{n}$  from couplings removed is given by

$$\begin{aligned} G^{a,(1)} &= g^4 \int \frac{d^4 \bar{q}}{(2\pi)^4} \delta(2p_1 \cdot \bar{q}) \delta(2p_2 \cdot \bar{q}) e^{-ib \cdot \bar{q}} [C_1^a, C_2] \bar{A}_\Gamma^{(1)}(p_1, p_2 \rightarrow p_1 + \mathfrak{n}\bar{q}, p_2 - \mathfrak{n}\bar{q}) \\ &\quad - i g^4 \mathfrak{n}^2 \int \frac{d^4 \bar{q}}{(2\pi)^4} \delta(2p_1 \cdot \bar{q}) \delta(2p_2 \cdot \bar{q}) e^{-ib \cdot \bar{q}} [C_1, C_2] \bar{A}_\Gamma^{(1)}(p_1 + \mathfrak{n}\bar{q}, p_2 - \mathfrak{n}\bar{q}) \\ &\quad \times \bar{A}_\Gamma^{(1)*}(p_1 + \mathfrak{n}\bar{q}, p_2 - \mathfrak{n}\bar{q} \rightarrow p_1 + \mathfrak{n}\bar{q}, p_2 - \mathfrak{n}\bar{q}) \bar{A}_\Gamma^{(1)}(p_1, p_2 \rightarrow p_1 + \mathfrak{n}\bar{q}, p_2 - \mathfrak{n}\bar{q}). \end{aligned} \quad (5.37)$$

The first term in the impulse is a one-loop amplitude, and the second term we can view as a two-particle cut of the four-point amplitude. We will calculate the classical one-loop amplitude integrand and the cut separately, and then combine the terms. Here we calculate the one-loop integrand using the kinematic numerators found in the previous chapters, and discuss how to find the optimal color basis for the classical limit.

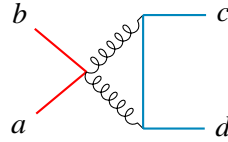


Figure 5.2: Quartic graph topology for  $A_4^{1\text{-loop}}$  included in [56].

All the cubic topologies that contribute to the quantum integrand at one-loop level are shown in Fig. 5.1, and the additional contact term which would be included in a Feynman rule calculation is shown in Figure 5.2. As discussed previously, we can assign this contact term to cubic graphs, and so the topology is not included in the calculation using our representation. The amplitude is built of these topologies with different momentum labels and exchanges of the scalar particles (*e.g.* for the massless triangle (b) in 5.1 the same graph with the masses/colors flipped also contributes). We therefore write down the full color-dressed integrand, represented by all cubic topologies<sup>1</sup> with all distinct orderings<sup>2</sup>

$$\begin{aligned}
 A &= C \int \frac{d^4k}{(2\pi)^4} \frac{1}{k^2} \frac{1}{(k-a)^2} \frac{1}{(k-b)^2} \frac{1}{(k-c)^2} \frac{1}{(k-d)^2} I_{b_1}^{(1)} + C \int \frac{d^4k}{(2\pi)^4} \frac{1}{k^2} \frac{1}{(k-a)^2} \frac{1}{(k-b)^2} \frac{1}{(k-c)^2} \frac{1}{(k-d)^2} I_{b_2}^{(1)} + C \int \frac{d^4k}{(2\pi)^4} \frac{1}{k^2} \frac{1}{(k-a)^2} \frac{1}{(k-b)^2} \frac{1}{(k-c)^2} \frac{1}{(k-d)^2} I_{t_1}^{(1)} \\
 &+ C \int \frac{d^4k}{(2\pi)^4} \frac{1}{k^2} \frac{1}{(k-a)^2} \frac{1}{(k-b)^2} \frac{1}{(k-c)^2} \frac{1}{(k-d)^2} I_{t_2}^{(1)} + C \int \frac{d^4k}{(2\pi)^4} \frac{1}{k^2} \frac{1}{(k-a)^2} \frac{1}{(k-b)^2} \frac{1}{(k-c)^2} \frac{1}{(k-d)^2} I_{t_1}^{(1)} + C \int \frac{d^4k}{(2\pi)^4} \frac{1}{k^2} \frac{1}{(k-a)^2} \frac{1}{(k-b)^2} \frac{1}{(k-c)^2} \frac{1}{(k-d)^2} I_{t_2}^{(1)} \\
 &+ C \int \frac{d^4k}{(2\pi)^4} \frac{1}{k^2} \frac{1}{(k-a)^2} \frac{1}{(k-b)^2} \frac{1}{(k-c)^2} \frac{1}{(k-d)^2} I_o^{(1)} + C \int \frac{d^4k}{(2\pi)^4} \frac{1}{k^2} \frac{1}{(k-a)^2} \frac{1}{(k-b)^2} \frac{1}{(k-c)^2} \frac{1}{(k-d)^2} I_{\hat{o}_1}^{(1)} + C \int \frac{d^4k}{(2\pi)^4} \frac{1}{k^2} \frac{1}{(k-a)^2} \frac{1}{(k-b)^2} \frac{1}{(k-c)^2} \frac{1}{(k-d)^2} I_{\hat{o}_2}^{(1)} \\
 &+ C \int \frac{d^4k}{(2\pi)^4} \frac{1}{k^2} \frac{1}{(k-a)^2} \frac{1}{(k-b)^2} \frac{1}{(k-c)^2} \frac{1}{(k-d)^2} I_{s_1}^{(1)} + C \int \frac{d^4k}{(2\pi)^4} \frac{1}{k^2} \frac{1}{(k-a)^2} \frac{1}{(k-b)^2} \frac{1}{(k-c)^2} \frac{1}{(k-d)^2} I_{s_2}^{(1)} + C \int \frac{d^4k}{(2\pi)^4} \frac{1}{k^2} \frac{1}{(k-a)^2} \frac{1}{(k-b)^2} \frac{1}{(k-c)^2} \frac{1}{(k-d)^2} I \\
 &+ C \int \frac{d^4k}{(2\pi)^4} \frac{1}{k^2} \frac{1}{(k-a)^2} \frac{1}{(k-b)^2} \frac{1}{(k-c)^2} \frac{1}{(k-d)^2} I_{s_4}^{(1)}.
 \end{aligned} \tag{5.38}$$

The color factors of the graphs in Equation (5.88) are related via symmetries and Jacobi relations, and the kinematic numerators are related by the corresponding BCJ relations. Thus far, we have presented the BCJ relations of the kinematic numerators as relationships between canonically labeled kinematic numerator functions, which favor the box-graph topology as a basis graph. However, when finding the classical limit it is advantageous to write color factors in terms of a basis that maximises the power of  $\mathfrak{n}$ , to exclude these graph contributions from the classical limit of the amplitude early on. We begin by restoring the  $\mathfrak{n}$ -factors in the Jacobi-like relations

<sup>1</sup>Excluding tadpole graphs.

<sup>2</sup>Orderings that cannot be related internally via an isomorphism of the graph.

(pure-gluon vertices now get dressed with  $f^{abc} \rightarrow \eta f^{abc}$ )

$$\begin{aligned}
 C_b(a, b, c, d) &= \eta C_t(a, b, c, d) + C_b(a, b, d, c), & \eta C_o(a, b, c, d) &= 2 C_f(a, b, c, d), \\
 C_b(a, b, c, d) &= \eta C_t(c, d, a, b) + C_b(a, b, d, c), & \eta C_o(a, b, c, d) &= 2 C_t(c, d, a, b), \\
 \eta C(a, b, c, d) &= C(a, b, c, d) + C(a, c, d, b), & 2 C_t(a, c, d, b) &= \mathcal{E}(a, c, d, b). \\
 C_f^t(a, c, d, b) &= \eta C_t^f(a, b, c, d) + \hat{C}_s^f(b, a, c, d),
 \end{aligned}
 \tag{5.39}$$

These seven equations are canonically labelled (functional), so we can set up a slightly larger set of equations where all orderings not related by isomorphisms are included. Note that we now treat color factors of the same type with different orderings as different elements - similarly to tree level kinematic numerators (the Mandelstam variables  $s$ ,  $t$  and  $u$ ). Using all orderings we get 12 equations, which we can solve for the color factors which maximize the power of  $\eta$

$$\begin{aligned}
 C_b(c, d, a, b) &\rightarrow \frac{1}{2} \eta C_o(a, b, c, d), & C_b(a, b, c, d) &\rightarrow \frac{1}{2} \eta^2 C_o(a, b, c, d) + C_b(a, b, d, c), \\
 C_t(a, b, c, d) &\rightarrow \frac{1}{2} \eta C_o(a, b, c, d), & C_f(d, c, a, b) &\rightarrow \frac{1}{2} (C_o(c, a, b, d) - \eta C_o(a, b, c, d)), \\
 C_f(c, a, b, d) &\rightarrow \frac{1}{2} C_o(c, a, b, d), & C_f(c, d, a, b) &\rightarrow \frac{1}{2} (\eta^2 C_o(a, b, c, d) - C_o(c, a, b, d)), \\
 C_f(a, c, d, b) &\rightarrow \frac{1}{2} C_o(a, c, d, b), & C_f(b, a, c, d) &\rightarrow \frac{1}{2} (C_o(a, c, d, b) - \eta^2 C_o(a, b, c, d)), \\
 & & C_f(a, b, c, d) &\rightarrow \frac{1}{2} (\eta^2 C_o(a, b, c, d) - C_o(a, c, d, b)),
 \end{aligned}
 \tag{5.40}$$

which can be shown graphically as

$$C_{\square} \begin{array}{c} b \\ \square \\ a \end{array} \begin{array}{c} c \\ \square \\ d \end{array} \rightarrow \frac{1}{2} \eta^2 C_{\square} \begin{array}{c} b \\ \square \\ a \end{array} \begin{array}{c} c \\ \square \\ d \end{array} + C_{\square} \begin{array}{c} b \\ \square \\ a \end{array} \begin{array}{c} c \\ \square \\ d \end{array}, \tag{5.41}$$

and the triangles

$$\begin{aligned}
 C_{\triangle} \begin{array}{c} b \\ \square \\ a \end{array} \begin{array}{c} c \\ \square \\ d \end{array} &\rightarrow \frac{1}{2} \eta C_{\triangle} \begin{array}{c} b \\ \square \\ a \end{array} \begin{array}{c} c \\ \square \\ d \end{array}, & C_{\triangle} \begin{array}{c} b \\ \square \\ a \end{array} \begin{array}{c} c \\ \square \\ d \end{array} &\rightarrow \frac{1}{2} C_{\triangle} \begin{array}{c} b \\ \square \\ a \end{array} \begin{array}{c} c \\ \square \\ d \end{array}, \\
 C_{\triangle} \begin{array}{c} b \\ \square \\ a \end{array} \begin{array}{c} c \\ \square \\ d \end{array} &\rightarrow \frac{1}{2} \eta C_{\triangle} \begin{array}{c} b \\ \square \\ a \end{array} \begin{array}{c} c \\ \square \\ d \end{array}, & C_{\triangle} \begin{array}{c} b \\ \square \\ a \end{array} \begin{array}{c} c \\ \square \\ d \end{array} &\rightarrow \frac{1}{2} C_{\triangle} \begin{array}{c} b \\ \square \\ a \end{array} \begin{array}{c} c \\ \square \\ d \end{array},
 \end{aligned}
 \tag{5.42}$$



and finally the snails

$$\begin{aligned}
 C \begin{array}{c} b \\ \diagup \\ a \end{array} \begin{array}{c} c \\ \diagdown \\ d \end{array} &\rightarrow -\frac{1}{2}n^2 C \begin{array}{c} b \\ \diagup \\ a \end{array} \begin{array}{c} c \\ \diagdown \\ d \end{array} + \frac{1}{2} C \begin{array}{c} b \\ \diagup \\ a \end{array} \begin{array}{c} c \\ \diagdown \\ d \end{array}, \\
 C \begin{array}{c} b \\ \diagup \\ a \end{array} \begin{array}{c} c \\ \diagdown \\ d \end{array} &\rightarrow \frac{1}{2}n^2 C \begin{array}{c} b \\ \diagup \\ a \end{array} \begin{array}{c} c \\ \diagdown \\ d \end{array} - \frac{1}{2} C \begin{array}{c} b \\ \diagup \\ a \end{array} \begin{array}{c} c \\ \diagdown \\ d \end{array}, \\
 C \begin{array}{c} b \\ \diagup \\ a \end{array} \begin{array}{c} c \\ \diagdown \\ d \end{array} &\rightarrow -\frac{1}{2}n^2 C \begin{array}{c} b \\ \diagup \\ a \end{array} \begin{array}{c} c \\ \diagdown \\ d \end{array} + \frac{1}{2} C \begin{array}{c} b \\ \diagup \\ a \end{array} \begin{array}{c} c \\ \diagdown \\ d \end{array}, \\
 C \begin{array}{c} b \\ \diagup \\ a \end{array} \begin{array}{c} c \\ \diagdown \\ d \end{array} &\rightarrow \frac{1}{2}n^2 C \begin{array}{c} b \\ \diagup \\ a \end{array} \begin{array}{c} c \\ \diagdown \\ d \end{array} - \frac{1}{2} C \begin{array}{c} b \\ \diagup \\ a \end{array} \begin{array}{c} c \\ \diagdown \\ d \end{array}.
 \end{aligned} \tag{5.43}$$

We see that the color basis is

$$C \begin{array}{c} b \\ \diagup \\ a \end{array} \begin{array}{c} c \\ \diagdown \\ d \end{array}, C \begin{array}{c} a \\ \diagup \\ b \end{array} \begin{array}{c} c \\ \diagdown \\ d \end{array}, C \begin{array}{c} b \\ \diagup \\ a \end{array} \begin{array}{c} c \\ \diagdown \\ d \end{array}, C \begin{array}{c} b \\ \diagup \\ a \end{array} \begin{array}{c} c \\ \diagdown \\ d \end{array}. \tag{5.44}$$

We can write the full amplitude in Equation (5.88) in terms of this new color basis. We first restore the  $n$  factors to the color factors, then use Jacobi relations to write the color in terms of the basis, *e.g.* we write for the massless triangle

$$C \begin{array}{c} b \\ \diagup \\ a \end{array} \begin{array}{c} c \\ \diagdown \\ d \end{array} \rightarrow n C \begin{array}{c} b \\ \diagup \\ a \end{array} \begin{array}{c} c \\ \diagdown \\ d \end{array} \rightarrow \frac{1}{2}n^2 C \begin{array}{c} b \\ \diagup \\ a \end{array} \begin{array}{c} c \\ \diagdown \\ d \end{array}. \tag{5.45}$$

The amplitude is then

$$\begin{aligned}
 A^{(1)} &= n^2 C \begin{array}{c} b \\ \diagup \\ a \end{array} \begin{array}{c} c \\ \diagdown \\ d \end{array} (I_{t1}^{(1)} + I_{t2}^{(1)} + I_{s1}^{(1)} - I_{s2}^{(1)} + I_{s3}^{(1)} - I_{s4}^{(1)} + I_o^{(1)} + I_{b1}^{(1)}) \\
 &+ C \begin{array}{c} a \\ \diagup \\ b \end{array} \begin{array}{c} c \\ \diagdown \\ d \end{array} (I_{b1} + I_{b2}) + C \begin{array}{c} b \\ \diagup \\ a \end{array} \begin{array}{c} c \\ \diagdown \\ d \end{array} (I_{s2} - I_{s1} + I_{\hat{t}1} + I_{\hat{o}1}) \\
 &+ C \begin{array}{c} b \\ \diagup \\ a \end{array} \begin{array}{c} c \\ \diagdown \\ d \end{array} (I_{s4}^{(1)} - I_{s3}^{(1)} + I_{\hat{t}2}^{(1)} + I_{\hat{o}2}^{(1)}). \tag{5.46}
 \end{aligned}$$

Recall that the kinematic numerators are related via the BCJ relations, so the amplitude can be written in terms of basis graph numerators

$$\begin{aligned}
A^{(1)} = & n^2 C \left[ \text{triangle graph} \left( \frac{n_f(b, c, d, a, ) - n_b(b, a, c, d, ) + n_b(b, a, d, c, )}{2^2(a+b)^2 (a^2 - m_1^2) ((a+)^2 - m_1^2)} \right. \right. \\
& \left. \left. - \frac{n_f(a, c, d, b, ) - n_b(a, b, c, d, ) + n_b(a, b, d, c, )}{2^2(a+b)^2 (b^2 - m_1^2) ((b+)^2 - m_1^2)} + \dots \right) \right. \\
& + C \left[ \text{box graph} \left( \frac{n_b(a, b, c, d, )}{2^2(a+b+)^2 ((b+)^2 - m_1^2) ((c-)^2 - m_2^2)} \right) \right. \\
& \left. + \frac{n_b(a, b, d, c, )}{2^2(a+b+)^2 ((b+)^2 - m_1^2) ((d-)^2 - m_2^2)} \right) \left. \right. \\
& + C \left[ \text{triangle graph} \left( \frac{n_f(a, c, d, b, ) - (n_b(a, b, c, d, ) + n_b(a, b, d, c, ))}{2^2(a+b)^2 (b^2 - m_1^2) ((b+)^2 - m_1^2)} \right) \right. \\
& \left. - \frac{n_f(b, c, d, a, ) - n_b(b, a, c, d, ) + n_b(b, a, d, c, )}{2^2(a+b)^2 (a^2 - m_1^2) ((a+)^2 - m_1^2)} + \dots \right) \left. \right. \\
& + C \left[ \text{triangle graph} \left( \frac{n_f(c, a, b, d, ) - n_b(c, d, a, b, ) + n_b(c, d, b, a, )}{2^2(a+b)^2 (d^2 - m_2^2) ((d+)^2 - m_2^2)} \right) \right. \\
& \left. - \frac{n_f(d, a, b, c, ) - n_b(d, c, a, b, ) + n_b(d, c, b, a, )}{2^2(a+b)^2 (c^2 - m_2^2) ((c+)^2 - m_2^2)} + \dots \right) \left. \right. \quad , \quad (5.47)
\end{aligned}$$

where  $n_f$  is the kinematic numerator function for the massive triangle graph, and  $n_b$  is the kinematic numerator function for the box graph.

At this point we relabel the momenta in terms of the incoming momenta  $p_1, p_2$ , and the momentum shift  $q$

$$\{k_1 \rightarrow -p_1, k_2 \rightarrow p_1 + q, k_3 \rightarrow p_2 - q, k_4 \rightarrow -p_2, \rightarrow -\} . \quad (5.48)$$

As described above, we restore the  $n$  factors to the loop momenta and the momentum exchange

$$\rightarrow n^{\bar{\quad}}, q \rightarrow n\bar{q} . \quad (5.49)$$

We also symmetrize the full expression by substituting  $\bar{\quad} \rightarrow \bar{q} - \bar{\quad}$ , and averaging over the two expressions while imposing the on-shell conditions  $p_1 \cdot \bar{q} = -\frac{n}{2}\bar{q}^2$  and  $p_2 \cdot \bar{q} = \frac{n}{2}\bar{q}^2$ . Note that we symmetrize *before* taking the series expansion – this is important, as the symmetrization combined with conservation of momenta introduces new powers of  $n$ ,

$$p_i \cdot \bar{\quad} \rightarrow p_i \cdot (\bar{q} - \bar{\quad}) \rightarrow -\frac{n}{2}\bar{q}^2 - p_i \cdot \bar{\quad} . \quad (5.50)$$

Having now restored the powers of  $n$ ,<sup>3</sup> we find the Laurent series around  $n$

$$\underline{A}^{(1)} \equiv \underline{A}_{-1}^{(1)} + \underline{A}_0^{(1)} + \underline{O}(n^0) . \quad (5.51)$$

<sup>3</sup>We also multiply the full expression by  $n^4$  from the integration measure  $d^D J \rightarrow d^D \bar{J}$  since we will be interested in the four-dimensional result.

The leading order term in this expansion is

$$\begin{aligned}
 \mathbf{A}_{-1}^{(1)} = & - \frac{(p_1 \cdot p_2)}{n^2} \frac{1}{d} \frac{1}{2^{-2} (\bar{q}^-)^2} \mathbf{C} \left[ \begin{array}{c} a \\ \text{---} \\ b \end{array} \right] \left[ \begin{array}{c} c \\ \text{---} \\ d \end{array} \right] (p_1 \cdot p_2) \delta(\cdot p_1) \delta(\cdot p_2) \\
 & + \frac{1}{16\bar{q}^2} \mathbf{C} \left[ \begin{array}{c} b \\ \text{---} \\ a \end{array} \right] \left[ \begin{array}{c} c \\ \text{---} \\ d \end{array} \right] m_1^2 \left( (\bar{q}^-)^2 + \epsilon^2 \right) \hat{\delta}(p_1 \cdot \bar{q}) \left( 1 - \frac{1}{\epsilon} - i \bar{q} \cdot (\bar{q}^-) \hat{\delta}(\cdot p_1) \right) \\
 & + \mathbf{C} \left[ \begin{array}{c} b \\ \text{---} \\ a \end{array} \right] \left[ \begin{array}{c} c \\ \text{---} \\ d \end{array} \right] m_2^2 \left( (\bar{q}^-)^2 + \epsilon^2 \right) \delta(p_2 \cdot \bar{q}) \left( 1 - \frac{1}{\epsilon} + i \bar{q} \cdot (\bar{q}^-) \delta(\cdot p_2) \right), \tag{5.52}
 \end{aligned}$$

where

$$\begin{aligned}
 i\delta(x) &= \frac{1}{x - i\epsilon} - \frac{1}{x + i\epsilon} \\
 &\sim \frac{1}{x} - \frac{1}{x} \\
 -i\delta(x) &= \frac{1}{(x - i\epsilon)^2} - \frac{1}{(x + i\epsilon)^2}. \tag{5.53}
 \end{aligned}$$

The term proportional to the box color factor will prove to cancel against the cut box, so no superclassical terms,  $\mathcal{O}(n^{-2})$ , survive. As per the discussion in Section 5.2.1 of [36] the remaining terms are pure quantum contributions that go into renormalizing the vertex and photon self-energy terms, and we will therefore not include them in further discussion here.

The next-to-leading order term in  $n$  is

$$\begin{aligned}
 \mathbf{A}_0^{(1)} = & \frac{1}{n} \frac{1}{d} \frac{1}{i\bar{c}_4} \frac{1}{2^{-2} (\bar{q}^-)^2} \mathbf{C} \left[ \begin{array}{c} a \\ \text{---} \\ b \end{array} \right] \left[ \begin{array}{c} c \\ \text{---} \\ d \end{array} \right] \left( \frac{im^2 (\cdot p_2)^2 \hat{\delta}(\cdot p_1)}{8 (\cdot p_2)^2 + \epsilon^2} - \frac{im^2 (\cdot p_1)^2 \hat{\delta}(\cdot p_2)}{8 (\cdot p_1)^2 + \epsilon^2} \right) \\
 & + \frac{1}{4} (p_1 \cdot p_2) (\cdot p_1) (\cdot p_2) \left( \frac{\epsilon^2 - p_1 \cdot p_2 - ((\bar{q}^-) \cdot p_1 + i\epsilon)^2}{2 (\cdot p_1)^2 + \epsilon^2} - \frac{((p_2) \cdot i\bar{q}) (\cdot p_1 - p_2 + \epsilon^2)}{2 (\cdot p_2)^2 + \epsilon^2} \right) \\
 & + \mathbf{C} \left[ \begin{array}{c} b \\ \text{---} \\ a \end{array} \right] \left[ \begin{array}{c} c \\ \text{---} \\ d \end{array} \right] \left( \frac{im_1^2 (\cdot p_2)}{16\bar{q}^2} \delta(\cdot p_1) + \frac{q^- \cdot (\bar{q}^-)}{(o - i \cdot p_1)^2} + \dots \right) \\
 & + \mathbf{C} \left[ \begin{array}{c} b \\ \text{---} \\ a \end{array} \right] \left[ \begin{array}{c} c \\ \text{---} \\ d \end{array} \right] \left( \frac{im_2^2 (\cdot p_1)}{16\bar{q}^2} \delta(\cdot p_2) + \frac{q^- \cdot (\bar{q}^-)}{(\epsilon + i \cdot p_2)^2} + \dots \right). \tag{5.54}
 \end{aligned}$$

### The cut box

The second term in the next-to-leading order impulse in Equation (5.37) involves the two-particle cut of the one-loop amplitude, which is given by the product of two

four-point tree amplitudes

$$\begin{aligned} \mathcal{B} &= -in^2 \int d^4 \hat{p} \delta(2p_1 \cdot \hat{p} + n^2) \delta(2p_2 \cdot \hat{p} - n^2) \\ &\quad \times \bar{A}_{\hat{p}}(p_1 + n\bar{q}, p_2 - n\bar{q} \rightarrow p_1 + n^-, p_2 - n^-) \\ &\quad \times \bar{A}_{\hat{p}}(p_1, p_2 \rightarrow p_1 + n^-, p_2 - n^-). \end{aligned} \quad (5.55)$$

We use the four-point tree-level amplitudes developed in the previous chapters, and expand around  $n$

$$\mathcal{B} = \mathcal{B}_{-1} + \mathcal{B}_0 + \mathcal{O}(n^0), \quad (5.56)$$

where

$$\mathcal{B}_{-1} = \frac{(p_1 \cdot p_2)^2}{n^2} \int d^4 \hat{p} \frac{1}{-2(\hat{p} - \bar{q})^2} \delta(p_1 \cdot \hat{p}) \delta(p_2 \cdot \hat{p}), \quad (5.57)$$

and

$$\mathcal{B}_0 = \frac{(p_1 \cdot p_2)^2}{16n} \int d^4 \hat{p} \frac{(p_1 - p_2) \cdot (\hat{p} \cdot \bar{q})}{-2(\hat{p} - \bar{q})^2} \left( \frac{\delta \cdot p_1}{\delta \cdot p_1} \frac{\delta \cdot p_2}{\delta \cdot p_2} - \frac{\delta \cdot p_1}{\delta \cdot p_1} \frac{\delta \cdot p_2}{\delta \cdot p_2} \right). \quad (5.58)$$

### Combining terms

To combine the terms we use the color operator on the box color factor

$$\begin{aligned} C_1^a, C_1^b \left( \text{Diagram} \right) &= in f^{acd} \left( 2C_1^d C_2^c (C_1 \cdot C_2) - in f^{dbe} \left( C_1^e C_2^b C_2^c \frac{1}{2} C_1^e C_2^b C_1^c \right) \right) \\ &= 2n \text{Col}_1 + n^2 \text{Col}_2 + \mathcal{O}(n^3), \end{aligned} \quad (5.59)$$

where

$$\text{Col}_1 = if^{acd} C_1^d C_2^c (C_1 \cdot C_2), \quad \text{Col}_2 = f^{acd} f^{dbe} \left( C_1^e C_2^b C_2^c \frac{1}{2} C_1^e C_2^b C_1^c \right) \quad (5.60)$$

The commutation for the cut box expression is

$$\begin{aligned} \mathcal{C}(\text{tree})[C_1^a, \mathcal{C}(\text{tree})] &= in f^{acd} \left( C_1^d C_2^c (C_1 \cdot C_2) - in f^{dbe} \left( C_1^e C_2^b C_2^c \frac{1}{2} C_1^e C_2^b C_1^c \right) \right) \\ &= n \text{Col}_1 + n^2 \text{Col}_2 + \mathcal{O}(n^3). \end{aligned} \quad (5.61)$$

In terms of these color commutations we set up

$$\begin{aligned} \mathcal{G}^{a,(1)} &= \mathcal{G}_{1\text{-loop}}^{a,(1)} + \mathcal{G}_{\text{cut box}}^{a,(1)} \\ &= n \text{Col}_1 (2\mathcal{A}^{(1)} + \mathcal{A}_{\mathcal{B}}^{(1)}) + n^2 \text{Col}_2 (\mathcal{A}^{(1)} + \mathcal{A}_{\mathcal{B}}^{(1)}). \end{aligned} \quad (5.62)$$

The kinematic part of the leading box term is

$$\mathcal{A}_{0 \text{ box color}}^{(1)} = - \frac{(p_1 \cdot p_2)^2}{2n^2} \int d^4 \hat{p} \frac{-\delta(\hat{p} \cdot p_1) \delta(\hat{p} \cdot p_2)}{-2(\hat{p} - \bar{q})^2}, \quad (5.63)$$

so we find that

$$n \left( 2\mathcal{A}^{(1)} + \mathcal{A}_{\mathcal{B}}^{(1)} \right) \Big|_{n=2} = 0 \quad (5.64)$$

and

$$n^2 \left( A^{(1)} + A_B \right) \Big|_{n^2} = \frac{(p_1 \cdot p_2)^2}{2} \hat{d}^4 \frac{\hat{\delta}(\bar{\cdot} \cdot p_1) \hat{\delta}(\bar{\cdot} \cdot p_2)}{(-\bar{\cdot} - \bar{q})^2}. \quad (5.65)$$

We finally consider the coefficient of  $\text{Col}_1$  in Eq. 5.62

$$\begin{aligned} n \left( A^{(1)} \right) \Big|_{n^2} &= \frac{i(p_1 \cdot p_2)^2}{16\epsilon} \hat{d}^4 \frac{1}{(-\bar{\cdot} - \bar{q})^2} \\ &\times \frac{\left( m_1^2 (-\bar{\cdot} \cdot p_2)_2 + m_2^2 (-\bar{\cdot} \cdot p_1)_2 - 4c_4 B \right)}{2} \delta'(-\bar{\cdot} \cdot p_1) \delta'(-\bar{\cdot} \cdot p_2) \\ &- \frac{(-\bar{\cdot} - \bar{q})}{\epsilon^2} \hat{\delta}'(-\bar{\cdot} \cdot p_1)_2 \hat{\delta}'(-\bar{\cdot} \cdot p_2)_2 + (-\bar{\cdot} \cdot p_1)(-\bar{\cdot} \cdot p_2) \hat{\delta}'(-\bar{\cdot} \cdot p_1) \hat{\delta}'(-\bar{\cdot} \cdot p_2) \end{aligned}, \quad (5.66)$$

where  $B = (p_1 \cdot p_2)(-\bar{\cdot} \cdot p_2)(-\bar{\cdot} \cdot p_1)$ , and the coefficient  $c_4$  is a non-vanishing free coefficient that was not fixed by physical cuts and partially stand-in for what ultimately end up to be scheme-dependent considerations. We therefore set  $c_4$  to zero (total derivative). The color kernel is then

$$\begin{aligned} G^{a,(1)} &= g \frac{4(p_1 \cdot p_2)^2}{2} \hat{d}^4 \frac{1}{(-\bar{\cdot} - \bar{q})^2} \\ &\times f^{acd} f^{dbe} \left( C_1^e C_2^b C_2^c - C_2^e C_1^b C_1^c \right) \hat{\delta}(\bar{\cdot} \cdot p_1) \hat{\delta}(\bar{\cdot} \cdot p_2) \\ &- \frac{1}{8\epsilon} f^{acd} C_1^c C_2^c \frac{\left( m_1^2 (-\bar{\cdot} \cdot p_2)_2 + m_2^2 (-\bar{\cdot} \cdot p_1)_2 \right)}{(p_1 \cdot p_2)^2} \delta'(-\bar{\cdot} \cdot p_1) \delta'(-\bar{\cdot} \cdot p_2) \\ &- \frac{(-\bar{\cdot} - \bar{q})}{\epsilon^2} \hat{\delta}'(-\bar{\cdot} \cdot p_1)_2 \hat{\delta}'(-\bar{\cdot} \cdot p_2)_2 + (-\bar{\cdot} \cdot p_1)(-\bar{\cdot} \cdot p_2) \hat{\delta}'(-\bar{\cdot} \cdot p_1) \hat{\delta}'(-\bar{\cdot} \cdot p_2) \end{aligned} \quad (5.67)$$

This result matches the expression in 5.27 at leading order in  $\epsilon$ .

### 5.2.3 Leading order radiation calculation

The leading order color radiation is given in terms of amplitudes stripped of coupling constants,

$$\begin{aligned} R^{a,(0)}(\bar{k}) &= n^2 g^3 \hat{d}^4 \bar{q}_1 \hat{d}^4 \bar{q}_2 \hat{\delta}(2p_1 \cdot \bar{q}_1 + n\bar{q}_1^2) \hat{\delta}(2p_2 \cdot \bar{q}_2 + n\bar{q}_2^2) \\ &\times \hat{\delta}^4(\bar{k} - \bar{q}_1 - \bar{q}_2) e^{ib\bar{q}_1} C^a(D) \bar{A}_D^{(0)}(p_1 + q_1, p_2 + q_2 \rightarrow p_1, p_2; k, \sigma). \end{aligned} \quad (5.68)$$

Only terms in the amplitude proportional to  $1/n^2$  or smaller will survive the classical limit. In our graph representation, the full color-dressed five-point amplitude in terms

of only cubic graphs is given by

$$\begin{aligned}
 A^{(0)}(\bar{k}^a) = & C \left[ \begin{array}{c} \square \\ \square \\ \square \end{array} \begin{array}{c} b \\ a \\ a \end{array} \begin{array}{c} c \\ | \\ c \end{array} \begin{array}{c} d \\ | \\ d \end{array} \begin{array}{c} \square \\ \square \\ \square \end{array} \right] A_1 + C \left[ \begin{array}{c} \square \\ \square \\ \square \end{array} \begin{array}{c} a \\ a \\ a \end{array} \begin{array}{c} | \\ | \\ | \end{array} \begin{array}{c} d \\ | \\ d \end{array} \begin{array}{c} \square \\ \square \\ \square \end{array} \right] A_2 \\
 & + C^a \left[ \begin{array}{c} \square \\ \square \\ \square \end{array} \begin{array}{c} c \\ b \\ b \end{array} \begin{array}{c} e \\ | \\ e \end{array} \begin{array}{c} a \\ | \\ a \end{array} \begin{array}{c} d \\ | \\ d \end{array} \begin{array}{c} \square \\ \square \\ \square \end{array} \right] A_3 + C^a \left[ \begin{array}{c} \square \\ \square \\ \square \end{array} \begin{array}{c} b \\ b \\ b \end{array} \begin{array}{c} c \\ | \\ c \end{array} \begin{array}{c} e \\ | \\ e \end{array} \begin{array}{c} d \\ | \\ d \end{array} \begin{array}{c} \square \\ \square \\ \square \end{array} \right] A_4 \\
 & + C^a \left[ \begin{array}{c} \square \\ \square \\ \square \end{array} \begin{array}{c} c \\ b \\ b \end{array} \begin{array}{c} | \\ | \\ | \end{array} \begin{array}{c} a \\ | \\ a \end{array} \begin{array}{c} e \\ | \\ e \end{array} \begin{array}{c} d \\ | \\ d \end{array} \begin{array}{c} \square \\ \square \\ \square \end{array} \right] A_5, \quad (5.69)
 \end{aligned}$$

which we can write more simply as

$$A^{(0)}(\bar{k}^a) = C_1 A_1 + C_2 A_2 + C_3 A_3 + C_4 A_4 + C_5 A_5. \quad (5.70)$$

As with the four-point amplitudes there are Jacobi relations and symmetries between the color factors, notably

$$\begin{aligned}
 C \left[ \begin{array}{c} \square \\ \square \\ \square \end{array} \begin{array}{c} e \\ | \\ e \end{array} \begin{array}{c} a \\ | \\ a \end{array} \begin{array}{c} b \\ | \\ b \end{array} \begin{array}{c} \square \\ \square \\ \square \end{array} \right] &= C \left[ \begin{array}{c} \square \\ \square \\ \square \end{array} \begin{array}{c} b \\ | \\ b \end{array} \begin{array}{c} c \\ | \\ c \end{array} \begin{array}{c} d \\ | \\ d \end{array} \begin{array}{c} \square \\ \square \\ \square \end{array} \right] - C \left[ \begin{array}{c} \square \\ \square \\ \square \end{array} \begin{array}{c} c \\ | \\ c \end{array} \begin{array}{c} b \\ | \\ b \end{array} \begin{array}{c} d \\ | \\ d \end{array} \begin{array}{c} \square \\ \square \\ \square \end{array} \right] \quad (5.71)
 \end{aligned}$$

and for the kinematic numerators, which satisfy the BCJ relations, we have

$$\begin{aligned}
 N \left[ \begin{array}{c} \square \\ \square \\ \square \end{array} \begin{array}{c} e \\ | \\ e \end{array} \begin{array}{c} a \\ | \\ a \end{array} \begin{array}{c} b \\ | \\ b \end{array} \begin{array}{c} d \\ | \\ d \end{array} \begin{array}{c} \square \\ \square \\ \square \end{array} \right] &= N \left[ \begin{array}{c} \square \\ \square \\ \square \end{array} \begin{array}{c} b \\ | \\ b \end{array} \begin{array}{c} c \\ | \\ c \end{array} \begin{array}{c} d \\ | \\ d \end{array} \begin{array}{c} e \\ | \\ e \end{array} \begin{array}{c} \square \\ \square \\ \square \end{array} \right] - N \left[ \begin{array}{c} \square \\ \square \\ \square \end{array} \begin{array}{c} c \\ | \\ c \end{array} \begin{array}{c} b \\ | \\ b \end{array} \begin{array}{c} d \\ | \\ d \end{array} \begin{array}{c} e \\ | \\ e \end{array} \begin{array}{c} \square \\ \square \\ \square \end{array} \right]. \quad (5.72)
 \end{aligned}$$

which allow us to express both the color factors and kinematic numerators in terms of a smaller basis of elements.

For the color factors we choose the color basis

$$\begin{aligned}
 C^a \left[ \begin{array}{c} \square \\ \square \\ \square \end{array} \begin{array}{c} b \\ a \\ a \end{array} \begin{array}{c} c \\ | \\ c \end{array} \begin{array}{c} d \\ | \\ d \end{array} \begin{array}{c} \square \\ \square \\ \square \end{array} \right] &= C^a \left[ \begin{array}{c} \square \\ \square \\ \square \end{array} \begin{array}{c} a \\ c \\ c \end{array} \begin{array}{c} | \\ | \\ | \end{array} \begin{array}{c} d \\ | \\ d \end{array} \begin{array}{c} \square \\ \square \\ \square \end{array} \right] + C^a \left[ \begin{array}{c} \square \\ \square \\ \square \end{array} \begin{array}{c} c \\ b \\ b \end{array} \begin{array}{c} a \\ | \\ a \end{array} \begin{array}{c} d \\ | \\ d \end{array} \begin{array}{c} \square \\ \square \\ \square \end{array} \right] \\
 C_1 &= C_2 + C_3, \quad (5.73) \\
 C^a \left[ \begin{array}{c} \square \\ \square \\ \square \end{array} \begin{array}{c} c \\ b \\ b \end{array} \begin{array}{c} d \\ | \\ d \end{array} \begin{array}{c} e \\ | \\ e \end{array} \begin{array}{c} a \\ | \\ a \end{array} \begin{array}{c} \square \\ \square \\ \square \end{array} \right] &= C^a \left[ \begin{array}{c} \square \\ \square \\ \square \end{array} \begin{array}{c} c \\ b \\ b \end{array} \begin{array}{c} | \\ | \\ | \end{array} \begin{array}{c} e \\ | \\ e \end{array} \begin{array}{c} a \\ | \\ a \end{array} \begin{array}{c} d \\ | \\ d \end{array} \begin{array}{c} \square \\ \square \\ \square \end{array} \right] + C^a \left[ \begin{array}{c} \square \\ \square \\ \square \end{array} \begin{array}{c} c \\ b \\ b \end{array} \begin{array}{c} a \\ | \\ a \end{array} \begin{array}{c} d \\ | \\ d \end{array} \begin{array}{c} \square \\ \square \\ \square \end{array} \right] \\
 C_4 &= C_5 + C_3.
 \end{aligned}$$

so the amplitude becomes

$$\begin{aligned}
 A^{(0)}(\bar{k}^a) &= C_1 A_1 + C_2 A_2 + \frac{1}{2} C_3 A_3 + (m_1 \leftrightarrow m_2) \\
 &= (C_2 + C_3) A_1 + C_2 A_2 + \frac{1}{2} C_3 A_3 + (m_1 \leftrightarrow m_2) \\
 &= C_2 (A_1 + A_2) + \frac{1}{2} C_3 (A_3 + 2A_1) + (m_1 \leftrightarrow m_2), \quad (5.74)
 \end{aligned}$$

where  $(m_1 \leftrightarrow m_2)$  indicates the swapping of the two massive particles. The color factors are easily read off the graphs

$$\begin{aligned}
 C_2 &= \mathcal{C}^a \begin{array}{c} \square \\ a \\ \diagup \quad \diagdown \\ c \quad b \\ \diagdown \quad \diagup \\ d \\ e \end{array} \square = C_{\mathfrak{F}}(C_1 \cdot C_2) \\
 C_3 &= \mathcal{C}^a \begin{array}{c} \square \\ c \\ \diagup \quad \diagdown \\ b \quad a \\ \diagdown \quad \diagup \\ d \\ e \end{array} \square = f^{abc} C_1^b C_2^c.
 \end{aligned} \tag{5.75}$$

The graphs are dressed with the kinematic numerators developed in previous chapters, and we restore the powers of  $\mathfrak{n}$  in the expressions,  $p \rightarrow \mathfrak{n}\bar{p}$ ,  $q_i \rightarrow \mathfrak{n}\bar{q}_i$  and  $k \rightarrow \mathfrak{n}\bar{k}$ . Laurent expanding around  $\mathfrak{n} = 0$ , the kinematic prefactor of the first color factor in Equation (5.74) is at leading order in  $\mathfrak{n}$

$$A_3 + 2A_1 = \frac{\varepsilon_\mu(\bar{k})}{\mathfrak{n}^3 \bar{q}_1^2 \bar{q}_2^2} (p_1 \cdot p_2) \frac{(\bar{k} \cdot p_1) \bar{q}_1^\mu - \bar{q}_1^2 p_1^\mu}{\bar{k} \cdot p_1} - (k \cdot p_2) p_1^\mu + (k \cdot p_1) p_2^\mu + \mathcal{O}(\mathfrak{n}^{-2}). \tag{5.76}$$

The second kinematic term in Equation (5.74) is Laurent expanded around  $\mathfrak{n}$  in the same way, and at leading order in  $\mathfrak{n}$  becomes

$$\begin{aligned}
 A_{1+} + A_2 = & \frac{1}{2 \mathfrak{n}^2} \frac{\varepsilon_\mu(\bar{k})}{\bar{q}_2^2 (p_1 \cdot \bar{k})} (p_1 \cdot p_2) \bar{q}_1^\mu - \frac{(p_1 \cdot p_2)(\bar{q}_1 \cdot \bar{k})}{p_1 \cdot \bar{k}} p_1^\mu \\
 & + (p_1 \cdot \bar{k}) p_2^\mu - (p_2 \cdot \bar{k}) p_1^\mu + \mathcal{O}(\mathfrak{n}^{-1}), \tag{5.77}
 \end{aligned}$$

where  $\varepsilon^\mu$  is the polarization vector of the outgoing radiation. Conservation of momenta and the on-shell property of the radiation gives  $\bar{q}_1^2 = \bar{q}_2^2 = 2\bar{k} \cdot \bar{q}_1$  and  $\varepsilon(\bar{k}) \cdot \bar{q}_1 = -\varepsilon(\bar{k}) \cdot \bar{q}_2$ , so we get

$$\begin{aligned}
 A_{1+} + A_2 = & \frac{1}{4\mathfrak{n}^2} \frac{\varepsilon_\mu(\bar{k})}{\bar{q}_2^2 (p_1 \cdot \bar{k})} [2(\bar{k} \cdot p_1) p_2^\mu - 2(\bar{k} \cdot p_2) p_1^\mu - 2(p_1 \cdot p_2) \bar{q}_2^\mu \\
 & - \frac{(\bar{q}_1^2 - \bar{q}_2^2)(p_1 \cdot p_2)}{(\bar{k} \cdot p_1)} p_1^\mu] + \mathcal{O}(\mathfrak{n}). \tag{5.78}
 \end{aligned}$$

Combining the terms we find the classical limit of the five-point amplitude

$$\begin{aligned}
 \mathbf{A}^{(0)}(\bar{k}^a) &= \frac{\varepsilon_\mu(\bar{k})}{\mathfrak{n}^2} \frac{f^{abc} C_1^b C_2^c}{2\bar{q}_2^2} (p_1 \cdot p_2) \frac{(\bar{k} \cdot p_1) \bar{q}_1^\mu - \bar{q}_1^2 p_1^\mu}{\bar{k} \cdot p_1} - (\bar{k} \cdot p_2) p_1^\mu + (\bar{k} \cdot p_1) p_2^\mu \\
 &+ \frac{1}{2} \frac{C_1^a (C_1 \cdot C_2)}{(p_1 \cdot k)} [2(\bar{k} \cdot p_1) p_2^\mu - 2(\bar{k} \cdot p_2) p_1^\mu - 2(p_1 \cdot p_2) \bar{q}_2^\mu - \frac{(\bar{q}_1^2 - \bar{q}_2^2)(p_1 \cdot p_2)}{(\bar{k} \cdot p_1)} p_1^\mu] + (m_1 \leftrightarrow m_2). \tag{5.79}
 \end{aligned}$$

We substitute the amplitude in the kernel

$$\begin{aligned}
R^{a,(0)}(\bar{k}) = & g^3 \int_{\mathbf{d}} \hat{d}^4 \bar{q}_1 \hat{d}^4 \bar{q}_2 \delta(2u_1 \cdot \bar{q}_1) \delta(2u_2 \cdot \bar{q}_2) \delta^{(4)}(\bar{k} - \bar{q}_1 - \bar{q}_2) e^{ib\bar{q}_1} \\
& \int_{\mathbf{f}} \frac{\varepsilon_\mu(\bar{k})}{2\bar{q}_2^2} \frac{c^a(c_1 \cdot c_2)}{m_1(u_1 \cdot \bar{k})} \left( (k \cdot u_1)u_2^\mu - (\bar{k} \cdot u_2)u_1^\mu - (u_1 \cdot u_2) \left( q_2^\mu - \frac{\bar{k} \cdot \bar{q}_2}{\bar{k} \cdot u_1} u_1^\mu \right) \right) \\
& + \frac{f^{abc} c_1^b c_2^c}{\bar{q}^2} \left( (u_1 \cdot u_2) \bar{q}_1^\mu - (u_1 \cdot u_2) \frac{\bar{q}_1^\lambda u_1^\mu}{\bar{k} \cdot u_1} - (\bar{k} \cdot u_2) u_1^\mu + (\bar{k} \cdot u_1) u_2^\mu + (m_1 \leftrightarrow m_2) \right), \tag{5.80}
\end{aligned}$$

which matches Equation (5.28).

### 5.3 Conclusion

In this chapter, we use the BCJ satisfying amplitude representations developed in the previous chapters to reproduce the results in [56]. Specifically we use the KMOC formalism applied to observables in Yang-Mills theory to calculate the classical color impulse at leading and next-to-leading order, and the color radiation at leading order. We confirm that our representation, which consists purely of cubic graphs, lands on the same classical observables as the amplitude representations used in [56], which additionally allow quartic vertices. An important take-away for the classical observables in Yang-Mills is that we can simplify our calculations by choosing a clever color basis. The color factors of the contributing graphs obey Jacobi relations, and the number of independent color factors is therefore smaller than the total number. From previous calculations we have built up the intuition that we favour *e.g.* box graphs as basis elements in one-loop calculations. However, when finding an optimal color basis we favor graphs with pure-gluon vertices as these have a higher relative power of  $\hbar$  and can thus be discarded from the classical calculation at an early stage.

These calculations serve as a warm-up for finding the color radiation at next-to-leading order. As the five-point one-loop amplitude requires many more graphs than the corresponding four-point amplitude, having a systematic way of choosing an advantageous color-basis is a helpful step towards finding the classical limit.





# Bibliography

- [1] B. P. Abbott et al. “Observation of Gravitational Waves from a Binary Black Hole Merger”. In: *Phys. Rev. Lett.* 116.6 (2016), p. 061102. doi: [10.1103/PhysRevLett.116.061102](https://doi.org/10.1103/PhysRevLett.116.061102). arXiv: [1602.03837](https://arxiv.org/abs/1602.03837) [gr-qc].
- [2] Ruth Britto, Freddy Cachazo, and Bo Feng. “New recursion relations for tree amplitudes of gluons”. In: *Nucl. Phys. B* 715 (2005), pp. 499–522. doi: [10.1016/j.nuclphysb.2005.02.030](https://doi.org/10.1016/j.nuclphysb.2005.02.030). arXiv: [hep-th/0412308](https://arxiv.org/abs/hep-th/0412308).
- [3] Ruth Britto, Freddy Cachazo, Bo Feng, and Edward Witten. “Direct proof of tree-level recursion relation in Yang-Mills theory”. In: *Phys. Rev. Lett.* 94 (2005), p. 181602. doi: [10.1103/PhysRevLett.94.181602](https://doi.org/10.1103/PhysRevLett.94.181602). arXiv: [hep-th/0501052](https://arxiv.org/abs/hep-th/0501052) [hep-th].
- [4] Zvi Bern, Lance J. Dixon, David C. Dunbar, and David A. Kosower. “One loop  $n$ -point gauge theory amplitudes, unitarity and collinear limits”. In: *Nucl. Phys. B* 425 (1994), pp. 217–260. doi: [10.1016/0550-3213\(94\)90179-1](https://doi.org/10.1016/0550-3213(94)90179-1). arXiv: [hep-ph/9403226](https://arxiv.org/abs/hep-ph/9403226) [hep-ph].
- [5] Ruth Britto, Freddy Cachazo, and Bo Feng. “Generalized unitarity and one-loop amplitudes in  $N = 4$  super-Yang-Mills”. In: *Nucl. Phys. B* 725 (2005), pp. 275–305. doi: [10.1016/j.nuclphysb.2005.07.014](https://doi.org/10.1016/j.nuclphysb.2005.07.014). arXiv: [hep-th/0412103](https://arxiv.org/abs/hep-th/0412103) [hep-th].
- [6] J. M. Drummond, J. Henn, G. P. Korchemsky, and E. Sokatchev. “Dual superconformal symmetry of scattering amplitudes in  $N = 4$  super-Yang-Mills theory”. In: *Nucl. Phys. B* 828 (2010), pp. 317–374. doi: [10.1016/j.nuclphysb.2009.11.022](https://doi.org/10.1016/j.nuclphysb.2009.11.022). arXiv: [0807.1095](https://arxiv.org/abs/0807.1095) [hep-th].
- [7] Z. Bern, J. J. M. Carrasco, and Henrik Johansson. “New Relations for Gauge-Theory Amplitudes”. In: *Phys. Rev. D* 78 (2008), p. 085011. doi: [10.1103/PhysRevD.78.085011](https://doi.org/10.1103/PhysRevD.78.085011). arXiv: [0805.3993](https://arxiv.org/abs/0805.3993) [hep-ph].
- [8] Zvi Bern, John Joseph M. Carrasco, and Henrik Johansson. “Perturbative Quantum Gravity as a Double Copy of Gauge Theory”. In: *Phys. Rev. Lett.* 105 (2010), p. 061602. doi: [10.1103/PhysRevLett.105.061602](https://doi.org/10.1103/PhysRevLett.105.061602). arXiv: [1004.0476](https://arxiv.org/abs/1004.0476) [hep-th].
- [9] Z. Bern, J. J. M. Carrasco, Henrik Johansson, and D. A. Kosower. “Maximally supersymmetric planar Yang-Mills amplitudes at five loops”. In: *Phys. Rev. D* 76 (2007), p. 125020. doi: [10.1103/PhysRevD.76.125020](https://doi.org/10.1103/PhysRevD.76.125020). arXiv: [0705.1864](https://arxiv.org/abs/0705.1864) [hep-th].
- [10] Ryo Saotome and Ratindranath Akhoury. “Relationship between gravity and gauge scattering in the high energy limit”. In: *JHEP* 01 (2013), p. 123. doi: [10.1007/JHEP01\(2013\)123](https://doi.org/10.1007/JHEP01(2013)123). arXiv: [1210.8111](https://arxiv.org/abs/1210.8111) [hep-th].
- [11] Ricardo Monteiro, Donal O’Connell, and Chris D. White. “Black holes and the double copy”. In: *JHEP* 12 (2014), p. 056. doi: [10.1007/JHEP12\(2014\)056](https://doi.org/10.1007/JHEP12(2014)056). arXiv: [1410.0239](https://arxiv.org/abs/1410.0239) [hep-th].

- [12] Andrés Luna, Ricardo Monteiro, Donal O’Connell, and Chris D. White. “The classical double copy for Taub–NUT spacetime”. In: *Phys. Lett.* B750 (2015), pp. 272–277. doi: [10.1016/j.physletb.2015.09.021](https://doi.org/10.1016/j.physletb.2015.09.021). arXiv: [1507.01869](https://arxiv.org/abs/1507.01869) [hep-th].
- [13] Alexander K. Ridgway and Mark B. Wise. “Static spherically symmetric Kerr-Schild metrics and implications for the classical double copy”. In: *Phys. Rev.* D94.4 (2016), p. 044023. doi: [10.1103/PhysRevD.94.044023](https://doi.org/10.1103/PhysRevD.94.044023). arXiv: [1512.02243](https://arxiv.org/abs/1512.02243) [hep-th].
- [14] Andrés Luna, Ricardo Monteiro, Isobel Nicholson, Donal O’Connell, and Chris D. White. “The double copy: Bremsstrahlung and accelerating black holes”. In: *JHEP* 06 (2016), p. 023. doi: [10.1007/JHEP06\(2016\)023](https://doi.org/10.1007/JHEP06(2016)023). arXiv: [1603.05737](https://arxiv.org/abs/1603.05737) [hep-th].
- [15] Chris D. White. “Exact solutions for the biadjoint scalar field”. In: *Phys. Lett.* B763 (2016), pp. 365–369. doi: [10.1016/j.physletb.2016.10.052](https://doi.org/10.1016/j.physletb.2016.10.052). arXiv: [1606.04724](https://arxiv.org/abs/1606.04724) [hep-th].
- [16] Walter D. Goldberger and Alexander K. Ridgway. “Radiation and the classical double copy for color charges”. In: *Phys. Rev.* D95.12 (2017), p. 125010. doi: [10.1103/PhysRevD.95.125010](https://doi.org/10.1103/PhysRevD.95.125010). arXiv: [1611.03493](https://arxiv.org/abs/1611.03493) [hep-th].
- [17] Gabriel Cardoso, Silvia Nagy, and Suresh Nampuri. “Multi-centered  $N = 2$  BPS black holes: a double copy description”. In: *JHEP* 04 (2017), p. 037. doi: [10.1007/JHEP04\(2017\)037](https://doi.org/10.1007/JHEP04(2017)037). arXiv: [1611.04409](https://arxiv.org/abs/1611.04409) [hep-th].
- [18] Andrés Luna, Ricardo Monteiro, Isobel Nicholson, Alexander Ochirov, Donal O’Connell, Niclas Westerberg, and Chris D. White. “Perturbative spacetimes from Yang-Mills theory”. In: *JHEP* 04 (2017), p. 069. doi: [10.1007/JHEP04\(2017\)069](https://doi.org/10.1007/JHEP04(2017)069). arXiv: [1611.07508](https://arxiv.org/abs/1611.07508) [hep-th].
- [19] Walter D. Goldberger, Siddharth G. Prabhu, and Jedidiah O. Thompson. “Classical gluon and graviton radiation from the bi-adjoint scalar double copy”. In: *Phys. Rev.* D96.6 (2017), p. 065009. doi: [10.1103/PhysRevD.96.065009](https://doi.org/10.1103/PhysRevD.96.065009). arXiv: [1705.09263](https://arxiv.org/abs/1705.09263) [hep-th].
- [20] Tim Adamo, Eduardo Casali, Lionel Mason, and Stefan Nekovar. “Scattering on plane waves and the double copy”. In: *Class. Quant. Grav.* 35.1 (2018), p. 015004. doi: [10.1088/1361-6382/aa9961](https://doi.org/10.1088/1361-6382/aa9961). arXiv: [1706.08925](https://arxiv.org/abs/1706.08925) [hep-th].
- [21] Pieter-Jan De Smet and Chris D. White. “Extended solutions for the biadjoint scalar field”. In: *Phys. Lett.* B775 (2017), pp. 163–167. doi: [10.1016/j.physletb.2017.11.007](https://doi.org/10.1016/j.physletb.2017.11.007). arXiv: [1708.01103](https://arxiv.org/abs/1708.01103) [hep-th].
- [22] Nadia Bahjat-Abbas, Andrés Luna, and Chris D. White. “The Kerr-Schild double copy in curved spacetime”. In: *JHEP* 12 (2017), p. 004. doi: [10.1007/JHEP12\(2017\)004](https://doi.org/10.1007/JHEP12(2017)004). arXiv: [1710.01953](https://arxiv.org/abs/1710.01953) [hep-th].
- [23] Mariana Carrillo-González, Riccardo Penco, and Mark Trodden. “The classical double copy in maximally symmetric spacetimes”. In: *JHEP* 04 (2018), p. 028. doi: [10.1007/JHEP04\(2018\)028](https://doi.org/10.1007/JHEP04(2018)028). arXiv: [1711.01296](https://arxiv.org/abs/1711.01296) [hep-th].
- [24] Walter D. Goldberger, Jingping Li, and Siddharth G. Prabhu. “Spinning particles, axion radiation, and the classical double copy”. In: *Phys. Rev.* D97.10 (2018), p. 105018. doi: [10.1103/PhysRevD.97.105018](https://doi.org/10.1103/PhysRevD.97.105018). arXiv: [1712.09250](https://arxiv.org/abs/1712.09250) [hep-th].

- [25] Jingping Li and Siddharth G. Prabhu. “Gravitational radiation from the classical spinning double copy”. In: *Phys. Rev. D* 97.10 (2018), p. 105019. doi: [10.1103/PhysRevD.97.105019](https://doi.org/10.1103/PhysRevD.97.105019). arXiv: [1803.02405 \[hep-th\]](https://arxiv.org/abs/1803.02405).
- [26] A. Ilderton. “Screw-symmetric gravitational waves: a double copy of the vortex”. In: *Phys. Lett. B* 782 (2018), pp. 22–27. doi: [10.1016/j.physletb.2018.04.069](https://doi.org/10.1016/j.physletb.2018.04.069). arXiv: [1804.07290 \[gr-qc\]](https://arxiv.org/abs/1804.07290).
- [27] Chia-Hsien Shen. “Gravitational radiation from color-kinematics duality”. In: *JHEP* 11 (2018), p. 162. doi: [10.1007/JHEP11\(2018\)162](https://doi.org/10.1007/JHEP11(2018)162). arXiv: [1806.07388 \[hep-th\]](https://arxiv.org/abs/1806.07388).
- [28] Kanghoon Lee. “Kerr-Schild double field theory and classical double copy”. In: *JHEP* 10 (2018), p. 027. doi: [10.1007/JHEP10\(2018\)027](https://doi.org/10.1007/JHEP10(2018)027). arXiv: [1807.08443 \[hep-th\]](https://arxiv.org/abs/1807.08443).
- [29] Jan Plefka, Jan Steinhoff, and Wadim Wormsbecher. “Effective action of dilaton gravity as the classical double copy of Yang-Mills theory”. In: *Phys. Rev. D* 99.2 (2019), p. 024021. doi: [10.1103/PhysRevD.99.024021](https://doi.org/10.1103/PhysRevD.99.024021). arXiv: [1807.09859 \[hep-th\]](https://arxiv.org/abs/1807.09859).
- [30] Clifford Cheung, Ira Z. Rothstein, and Mikhail P. Solon. “From scattering amplitudes to classical potentials in the post-Minkowskian expansion”. In: *Phys. Rev. Lett.* 121.25 (2018), p. 251101. doi: [10.1103/PhysRevLett.121.251101](https://doi.org/10.1103/PhysRevLett.121.251101). arXiv: [1808.02489 \[hep-th\]](https://arxiv.org/abs/1808.02489).
- [31] David S. Berman, Erick Chacón, Andrés Luna, and Chris D. White. “The self-dual classical double copy, and the Eguchi-Hanson instanton”. In: *JHEP* 01 (2019), p. 107. doi: [10.1007/JHEP01\(2019\)107](https://doi.org/10.1007/JHEP01(2019)107). arXiv: [1809.04063 \[hep-th\]](https://arxiv.org/abs/1809.04063).
- [32] Metin Gurses and Bayram Tekin. “Classical double copy: Kerr-Schild-Kundt metrics from Yang-Mills theory”. In: *Phys. Rev. D* 98.12 (2018), p. 126017. doi: [10.1103/PhysRevD.98.126017](https://doi.org/10.1103/PhysRevD.98.126017). arXiv: [1810.03411 \[gr-qc\]](https://arxiv.org/abs/1810.03411).
- [33] Tim Adamo, Eduardo Casali, Lionel Mason, and Stefan Nekovar. “Plane wave backgrounds and colour-kinematics duality”. In: *JHEP* 02 (2019), p. 198. doi: [10.1007/JHEP02\(2019\)198](https://doi.org/10.1007/JHEP02(2019)198). arXiv: [1810.05115 \[hep-th\]](https://arxiv.org/abs/1810.05115).
- [34] Nadia Bahjat-Abbas, Ricardo Stark-Muchão, and Chris D. White. “Biadjoint wires”. In: *Phys. Lett. B* 788 (2019), pp. 274–279. doi: [10.1016/j.physletb.2018.11.026](https://doi.org/10.1016/j.physletb.2018.11.026). arXiv: [1810.08118 \[hep-th\]](https://arxiv.org/abs/1810.08118).
- [35] Andrs Luna, Ricardo Monteiro, Isobel Nicholson, and Donal O’Connell. “Type D Spacetimes and the Weyl Double Copy”. In: (2018). arXiv: [1810.08183 \[hep-th\]](https://arxiv.org/abs/1810.08183).
- [36] David A. Kosower, Ben Maybee, and Donal O’Connell. “Amplitudes, Observables, and Classical Scattering”. In: (2018). arXiv: [1811.10950 \[hep-th\]](https://arxiv.org/abs/1811.10950).
- [37] Joseph A. Farrow, Arthur E. Lipstein, and Paul McFadden. “Double copy structure of CFT correlators”. In: *JHEP* 02 (2019), p. 130. doi: [10.1007/JHEP02\(2019\)130](https://doi.org/10.1007/JHEP02(2019)130). arXiv: [1812.11129 \[hep-th\]](https://arxiv.org/abs/1812.11129).
- [38] Zvi Bern, Clifford Cheung, Radu Roiban, Chia-Hsien Shen, Mikhail P. Solon, and Mao Zeng. “Scattering Amplitudes and the Conservative Hamiltonian for Binary Systems at Third Post-Minkowskian Order”. In: (2019). arXiv: [1901.04424 \[hep-th\]](https://arxiv.org/abs/1901.04424).

- [39] Zvi Bern, Clifford Cheung, Radu Roiban, Chia-Hsien Shen, Mikhail P. Solon, and Mao Zeng. “Black Hole Binary Dynamics from the Double Copy and Effective Theory”. In: *JHEP* 10 (2019), p. 206. doi: [10.1007/JHEP10\(2019\)206](https://doi.org/10.1007/JHEP10(2019)206). arXiv: [1908.01493](https://arxiv.org/abs/1908.01493) [hep-th].
- [40] Andrea Antonelli, Alessandra Buonanno, Jan Steinhoff, Maarten van de Meent, and Justin Vines. “Energetics of two-body Hamiltonians in post-Minkowskian gravity”. In: *Phys. Rev. D* 99.10 (2019), p. 104004. doi: [10.1103/PhysRevD.99.104004](https://doi.org/10.1103/PhysRevD.99.104004). arXiv: [1901.07102](https://arxiv.org/abs/1901.07102) [gr-qc].
- [41] Mariana Carrillo González, Brandon Melcher, Kenneth Ratliff, Scott Watson, and Chris D. White. “The classical double copy in three spacetime dimensions”. In: *JHEP* 07 (2019), p. 167. doi: [10.1007/JHEP07\(2019\)167](https://doi.org/10.1007/JHEP07(2019)167). arXiv: [1904.11001](https://arxiv.org/abs/1904.11001) [hep-th].
- [42] Ben Maybee, Donal O’Connell, and Justin Vines. “Observables and amplitudes for spinning particles and black holes”. In: *JHEP* 12 (2019), p. 156. doi: [10.1007/JHEP12\(2019\)156](https://doi.org/10.1007/JHEP12(2019)156). arXiv: [1906.09260](https://arxiv.org/abs/1906.09260) [hep-th].
- [43] Athira PV and A. Manu. “Classical double copy from color kinematics duality: A proof in the soft limit”. In: (2019). arXiv: [1907.10021](https://arxiv.org/abs/1907.10021) [hep-th].
- [44] Yu-Tin Huang, Uri Kol, and Donal O’Connell. “Double copy of electric-magnetic duality”. In: *Phys. Rev. D* 102.4 (2020), p. 046005. doi: [10.1103/PhysRevD.102.046005](https://doi.org/10.1103/PhysRevD.102.046005). arXiv: [1911.06318](https://arxiv.org/abs/1911.06318) [hep-th].
- [45] Rashid Alawadhi, David S. Berman, Bill Spence, and David Peinador Veiga. “S-duality and the double copy”. In: *JHEP* 03 (2020), p. 059. doi: [10.1007/JHEP03\(2020\)059](https://doi.org/10.1007/JHEP03(2020)059). arXiv: [1911.06797](https://arxiv.org/abs/1911.06797) [hep-th].
- [46] William T. Emond, Yu-tin Huang, Uri Kol, Nathan Moynihan, and Donal O’Connell. “Amplitudes from Coulomb to Kerr-Taub-NUT”. In: (Oct. 2020). arXiv: [2010.07861](https://arxiv.org/abs/2010.07861) [hep-th].
- [47] David S. Berman, Kwangeon Kim, and Kanghoon Lee. “The Classical Double Copy for M-theory from a Kerr-Schild Ansatz for Exceptional Field Theory”. In: (Oct. 2020). arXiv: [2010.08255](https://arxiv.org/abs/2010.08255) [hep-th].
- [48] Yilber Fabian Bautista and Alfredo Guevara. “On the Double Copy for Spinning Matter”. In: (Aug. 2019). arXiv: [1908.11349](https://arxiv.org/abs/1908.11349) [hep-th].
- [49] Enrico Herrmann, Julio Parra-Martinez, Michael S. Ruf, and Mao Zeng. “Gravitational Bremsstrahlung from Reverse Unitarity”. In: *Phys. Rev. Lett.* 126.20 (2021), p. 201602. doi: [10.1103/PhysRevLett.126.201602](https://doi.org/10.1103/PhysRevLett.126.201602). arXiv: [2101.07255](https://arxiv.org/abs/2101.07255) [hep-th].
- [50] Stavros Mougiakakos and Pierre Vanhove. “Schwarzschild-Tangherlini metric from scattering amplitudes in various dimensions”. In: *Phys. Rev. D* 103.2 (2021), p. 026001. doi: [10.1103/PhysRevD.103.026001](https://doi.org/10.1103/PhysRevD.103.026001). arXiv: [2010.08882](https://arxiv.org/abs/2010.08882) [hep-th].
- [51] Zvi Bern, Julio Parra-Martinez, Radu Roiban, Michael S. Ruf, Chia-Hsien Shen, Mikhail P. Solon, and Mao Zeng. “Scattering Amplitudes and Conservative Binary Dynamics at  $O(G^4)$ ”. In: *Phys. Rev. Lett.* 126.17 (2021), p. 171601. doi: [10.1103/PhysRevLett.126.171601](https://doi.org/10.1103/PhysRevLett.126.171601). arXiv: [2101.07254](https://arxiv.org/abs/2101.07254) [hep-th].
- [52] Enrico Herrmann, Julio Parra-Martinez, Michael S. Ruf, and Mao Zeng. “Radiative Classical Gravitational Observables at  $O(G^3)$  from Scattering Amplitudes”. In: (Apr. 2021). arXiv: [2104.03957](https://arxiv.org/abs/2104.03957) [hep-th].

- [53] N. Emil J. Bjerrum-Bohr, Poul H. Damgaard, Ludovic Planté, and Pierre Vanhove. “Classical Gravity from Loop Amplitudes”. In: (Apr. 2021). arXiv: [2104.04510 \[hep-th\]](#).
- [54] N. E. J. Bjerrum-Bohr, P. H. Damgaard, L. Planté, and P. Vanhove. “The Amplitude for Classical Gravitational Scattering at Third Post-Minkowskian Order”. In: (May 2021). arXiv: [2105.05218 \[hep-th\]](#).
- [55] Zvi Bern, Andres Luna, Radu Roiban, Chia-Hsien Shen, and Mao Zeng. “Spinning Black Hole Binary Dynamics, Scattering Amplitudes and Effective Field Theory”. In: (May 2020). arXiv: [2005.03071 \[hep-th\]](#).
- [56] Leonardo de la Cruz, Ben Maybee, Donal O’Connell, and Alasdair Ross. “Classical Yang-Mills observables from amplitudes”. In: (Sept. 2020). arXiv: [2009.03842 \[hep-th\]](#).
- [57] John Joseph M. Carrasco and Ingrid A. Vazquez-Holm. “Loop-Level Double-Copy for Massive Quantum Particles”. In: (Oct. 2020). arXiv: [2010.13435 \[hep-th\]](#).
- [58] Henrik Johansson and Alexander Ochirov. “Color-Kinematics Duality for QCD Amplitudes”. In: *JHEP* 01 (2016), p. 170. doi: [10.1007/JHEP01\(2016\)170](#). arXiv: [1507.00332 \[hep-ph\]](#).
- [59] Lance J. Dixon. “A Brief Introduction to Modern Amplitude Methods”. In: *Proceedings, Theoretical Advanced Study Institute in Elementary Particle Physics: Journeys Through the Precision Frontier: Amplitudes for Colliders (TASI2014): Boulder, Colorado, June 2-27, 2014*. 2015, pp. 39–97. doi: [10.1142/9789814678766\\_0002](#).
- [60] Zvi Bern, Lance J. Dixon, David C. Dunbar, and David A. Kosower. “Fusing gauge theory tree amplitudes into loop amplitudes”. In: *Nucl. Phys. B* 435 (1995), pp. 59–101. doi: [10.1016/0550-3213\(94\)00488-Z](#). arXiv: [hep-ph/9409265 \[hep-ph\]](#).
- [61] Z. Bern and A. G. Morgan. “Massive loop amplitudes from unitarity”. In: *Nucl. Phys. B* 467 (1996), pp. 479–509. doi: [10.1016/0550-3213\(96\)00078-8](#). arXiv: [hep-ph/9511336 \[hep-ph\]](#).
- [62] Giovanni Ossola, Costas G. Papadopoulos, and Roberto Pittau. “Reducing full one-loop amplitudes to scalar integrals at the integrand level”. In: *Nucl. Phys. B* 763 (2007), pp. 147–169. doi: [10.1016/j.nuclphysb.2006.11.012](#). arXiv: [hep-ph/0609007](#).
- [63] Darren Forde. “Direct extraction of one-loop integral coefficients”. In: *Phys. Rev. D* 75 (2007), p. 125019. doi: [10.1103/PhysRevD.75.125019](#). arXiv: [0704.1835 \[hep-ph\]](#).
- [64] S. D. Badger, E. W. Nigel Glover, V. V. Khoze, and P. Svrcek. “Recursion relations for gauge theory amplitudes with massive particles”. In: *JHEP* 07 (2005), p. 025. doi: [10.1088/1126-6708/2005/07/025](#). arXiv: [hep-th/0504159 \[hep-th\]](#).
- [65] Nima Arkani-Hamed, Tzu-Chen Huang, and Yu-tin Huang. “Scattering amplitudes for all masses and spins”. In: (2017). arXiv: [1709.04891 \[hep-th\]](#).
- [66] Henriette Elvang and Yu-tin Huang. “Scattering Amplitudes”. In: (Aug. 2013). arXiv: [1308.1697 \[hep-th\]](#).



- [67] Zvi Bern, John Joseph M. Carrasco, Wei-Ming Chen, Henrik Johansson, Radu Roiban, and Mao Zeng. “Five-loop four-point integrand of  $N = 8$  supergravity as a generalized double copy”. In: *Phys. Rev. D* 96.12 (2017), p. 126012. doi: [10.1103/PhysRevD.96.126012](https://doi.org/10.1103/PhysRevD.96.126012). arXiv: [1708.06807](https://arxiv.org/abs/1708.06807) [hep-th].
- [68] H. Kawai, D. C. Lewellen, and S. H. H. Tye. “A relation between tree amplitudes of closed and open strings”. In: *Nucl. Phys. B* 269 (1986), pp. 1–23. doi: [10.1016/0550-3213\(86\)90362-7](https://doi.org/10.1016/0550-3213(86)90362-7).
- [69] Frits A. Berends, W.T. Giele, and H. Kuijf. “On relations between multi-gluon and multigraviton scattering”. In: *Phys. Lett. B* 211 (1988), pp. 91–94. doi: [10.1016/0370-2693\(88\)90813-1](https://doi.org/10.1016/0370-2693(88)90813-1).
- [70] Zvi Bern, John Joseph Carrasco, Marco Chiodaroli, Henrik Johansson, and Radu Roiban. “The Duality Between Color and Kinematics and its Applications”. In: (2019). arXiv: [1909.01358](https://arxiv.org/abs/1909.01358) [hep-th].
- [71] Andrs Luna, Ricardo Monteiro, Isobel Nicholson, Alexander Ochirov, Donal O’Connell, Niclas Westerberg, and Chris D. White. “Perturbative spacetimes from Yang-Mills theory”. In: *JHEP* 04 (2017), p. 069. doi: [10.1007/JHEP04\(2017\)069](https://doi.org/10.1007/JHEP04(2017)069). arXiv: [1611.07508](https://arxiv.org/abs/1611.07508) [hep-th].
- [72] Henrik Johansson and Alexander Ochirov. “Pure Gravities via Color-Kinematics Duality for Fundamental Matter”. In: *JHEP* 11 (2015), p. 046. doi: [10.1007/JHEP11\(2015\)046](https://doi.org/10.1007/JHEP11(2015)046). arXiv: [1407.4772](https://arxiv.org/abs/1407.4772) [hep-th].
- [73] Andrs Luna, Isobel Nicholson, Donal O’Connell, and Chris D. White. “Inelastic Black Hole Scattering from Charged Scalar Amplitudes”. In: *JHEP* 03 (2018), p. 044. doi: [10.1007/JHEP03\(2018\)044](https://doi.org/10.1007/JHEP03(2018)044). arXiv: [1711.03901](https://arxiv.org/abs/1711.03901) [hep-th].
- [74] Z. Bern, J. J. M. Carrasco, L. J. Dixon, H. Johansson, and R. Roiban. “Simplifying multiloop integrands and ultraviolet divergences of gauge theory and gravity amplitudes”. In: *Phys. Rev. D* 85 (2012), p. 105014. doi: [10.1103/PhysRevD.85.105014](https://doi.org/10.1103/PhysRevD.85.105014). arXiv: [1201.5366](https://arxiv.org/abs/1201.5366) [hep-th].
- [75] Z. Bern, C. Boucher-Veronneau, and H. Johansson. “ $N = 4$  supergravity amplitudes from gauge theory at one loop”. In: *Phys. Rev. D* 84 (2011), p. 105035. doi: [10.1103/PhysRevD.84.105035](https://doi.org/10.1103/PhysRevD.84.105035). arXiv: [1107.1935](https://arxiv.org/abs/1107.1935) [hep-th].
- [76] C. Boucher-Veronneau and L. J. Dixon. “ $N \geq 4$  supergravity amplitudes from gauge theory at two Loops”. In: *JHEP* 12 (2011), p. 046. doi: [10.1007/JHEP12\(2011\)046](https://doi.org/10.1007/JHEP12(2011)046). arXiv: [1110.1132](https://arxiv.org/abs/1110.1132) [hep-th].
- [77] Zvi Bern, Scott Davies, Tristan Dennen, and Yu-tin Huang. “Absence of Three-Loop Four-Point Divergences in  $N=4$  Supergravity”. In: *Phys. Rev. Lett.* 108 (2012), p. 201301. doi: [10.1103/PhysRevLett.108.201301](https://doi.org/10.1103/PhysRevLett.108.201301). arXiv: [1202.3423](https://arxiv.org/abs/1202.3423) [hep-th].
- [78] Zvi Bern, Scott Davies, Tristan Dennen, and Yu-tin Huang. “Ultraviolet cancellations in half-maximal supergravity as a consequence of the double-copy structure”. In: *Phys. Rev. D* 86 (2012), p. 105014. doi: [10.1103/PhysRevD.86.105014](https://doi.org/10.1103/PhysRevD.86.105014). arXiv: [1209.2472](https://arxiv.org/abs/1209.2472) [hep-th].
- [79] Rutger H. Boels and Reinke Sven Isermann. “On powercounting in perturbative quantum gravity theories through color-kinematic duality”. In: *JHEP* 06 (2013), p. 017. doi: [10.1007/JHEP06\(2013\)017](https://doi.org/10.1007/JHEP06(2013)017). arXiv: [1212.3473](https://arxiv.org/abs/1212.3473) [hep-th].

- [80] Zvi Bern, Scott Davies, and Tristan Dennen. “The ultraviolet structure of half-maximal supergravity with matter multiplets at two and three loops”. In: *Phys. Rev. D* 88 (2013), p. 065007. doi: [10.1103/PhysRevD.88.065007](https://doi.org/10.1103/PhysRevD.88.065007). arXiv: [1305.4876](https://arxiv.org/abs/1305.4876) [hep-th].
- [81] Zvi Bern, Scott Davies, and Tristan Dennen. “The Ultraviolet Critical Dimension of Half-Maximal Supergravity at Three Loops”. In: (Dec. 2014). arXiv: [1412.2441](https://arxiv.org/abs/1412.2441) [hep-th].
- [82] Zvi Bern, John Joseph Carrasco, Wei-Ming Chen, Alex Edison, Henrik Johansson, Julio Parra-Martinez, Radu Roiban, and Mao Zeng. “Ultraviolet properties of  $N = 8$  supergravity at five loops”. In: *Phys. Rev. D* 98.8 (2018), p. 086021. doi: [10.1103/PhysRevD.98.086021](https://doi.org/10.1103/PhysRevD.98.086021). arXiv: [1804.09311](https://arxiv.org/abs/1804.09311) [hep-th].
- [83] Enrico Herrmann and Jaroslav Trnka. “Gravity On-shell diagrams”. In: *JHEP* 11 (2016), p. 136. doi: [10.1007/JHEP11\(2016\)136](https://doi.org/10.1007/JHEP11(2016)136). arXiv: [1604.03479](https://arxiv.org/abs/1604.03479) [hep-th].
- [84] Enrico Herrmann and Jaroslav Trnka. “UV cancellations in gravity loop integrands”. In: *JHEP* 02 (2019), p. 084. doi: [10.1007/JHEP02\(2019\)084](https://doi.org/10.1007/JHEP02(2019)084). arXiv: [1808.10446](https://arxiv.org/abs/1808.10446) [hep-th].
- [85] Z. Bern, J. J. Carrasco, D. Forde, H. Ita, and Henrik Johansson. “Unexpected Cancellations in Gravity Theories”. In: *Phys. Rev. D* 77 (2008), p. 025010. doi: [10.1103/PhysRevD.77.025010](https://doi.org/10.1103/PhysRevD.77.025010). arXiv: [0707.1035](https://arxiv.org/abs/0707.1035) [hep-th].
- [86] Stephen G. Naculich. “Scattering equations and BCJ relations for gauge and gravitational amplitudes with massive scalar particles”. In: *JHEP* 09 (2014), p. 029. doi: [10.1007/JHEP09\(2014\)029](https://doi.org/10.1007/JHEP09(2014)029). arXiv: [1407.7836](https://arxiv.org/abs/1407.7836) [hep-th].
- [87] Jan Plefka, Canxin Shi, and Tianheng Wang. “Double copy of massive scalar QCD”. In: *Phys. Rev. D* 101.6 (2020), p. 066004. doi: [10.1103/PhysRevD.101.066004](https://doi.org/10.1103/PhysRevD.101.066004). arXiv: [1911.06785](https://arxiv.org/abs/1911.06785) [hep-th].
- [88] Dimitrios Kosmopoulos. “Simplifying  $D$ -Dimensional Physical-State Sums in Gauge Theory and Gravity”. In: (Aug. 2020). arXiv: [2009.00141](https://arxiv.org/abs/2009.00141) [hep-th].
- [89] Andrés Luna, Isobel Nicholson, Donal O’Connell, and Chris D. White. “Inelastic black hole scattering from charged scalar amplitudes”. In: *JHEP* 03 (2018), p. 044. doi: [10.1007/JHEP03\(2018\)044](https://doi.org/10.1007/JHEP03(2018)044). arXiv: [1711.03901](https://arxiv.org/abs/1711.03901) [hep-th].
- [90] John Joseph M. Carrasco and Henrik Johansson. “Generic multiloop methods and application to  $N=4$  super-Yang-Mills”. In: *J. Phys.* A44 (2011), p. 454004. doi: [10.1088/1751-8113/44/45/454004](https://doi.org/10.1088/1751-8113/44/45/454004). arXiv: [1103.3298](https://arxiv.org/abs/1103.3298) [hep-th].
- [91] Barry R. Holstein and Andreas Ross. “Spin Effects in Long Range Gravitational Scattering”. In: (Feb. 2008). arXiv: [0802.0716](https://arxiv.org/abs/0802.0716) [hep-ph].
- [92] Varun Vaidya. “Gravitational spin Hamiltonians from the S matrix”. In: *Phys. Rev. D* 91.2 (2015), p. 024017. doi: [10.1103/PhysRevD.91.024017](https://doi.org/10.1103/PhysRevD.91.024017). arXiv: [1410.5348](https://arxiv.org/abs/1410.5348) [hep-th].
- [93] Alfredo Guevara. “Holomorphic classical limit for spin effects in gravitational and electromagnetic scattering”. In: *JHEP* 04 (2019), p. 033. doi: [10.1007/JHEP04\(2019\)033](https://doi.org/10.1007/JHEP04(2019)033). arXiv: [1706.02314](https://arxiv.org/abs/1706.02314) [hep-th].
- [94] Donato Bini and Thibault Damour. “Gravitational spin-orbit coupling in binary systems, post-Minkowskian approximation and effective one-body theory”. In: *Phys. Rev. D* 96.10 (2017), p. 104038. doi: [10.1103/PhysRevD.96.104038](https://doi.org/10.1103/PhysRevD.96.104038). arXiv: [1709.00590](https://arxiv.org/abs/1709.00590) [gr-qc].



- [95] Justin Vines, Jan Steinhoff, and Alessandra Buonanno. “Spinning-black-hole scattering and the test-black-hole limit at second post-Minkowskian order”. In: (2018). arXiv: [1812.00956 \[gr-qc\]](#).
- [96] Alfredo Guevara, Alexander Ochirov, and Justin Vines. “Scattering of spinning black holes from exponentiated soft factors”. In: (2018). arXiv: [1812.06895 \[hep-th\]](#).
- [97] Ming-Zhi Chung, Yu-Tin Huang, Jung-Wook Kim, and Sangmin Lee. “The simplest massive S-matrix: from minimal coupling to Black Holes”. In: *JHEP* 04 (2019), p. 156. doi: [10.1007/JHEP04\(2019\)156](#). arXiv: [1812.08752 \[hep-th\]](#).
- [98] Alfredo Guevara, Alexander Ochirov, and Justin Vines. “Black-hole scattering with general spin directions from minimal-coupling amplitudes”. In: (2019). arXiv: [1906.10071 \[hep-th\]](#).
- [99] Henrik Johansson and Alexander Ochirov. “Double copy for massive quantum particles with spin”. In: (2019). arXiv: [1906.12292 \[hep-th\]](#).
- [100] Ming-Zhi Chung, Yu-Tin Huang, and Jung-Wook Kim. “Classical potential for general spinning bodies”. In: *JHEP* 09 (2020), p. 074. doi: [10.1007/JHEP09\(2020\)074](#). arXiv: [1908.08463 \[hep-th\]](#).
- [101] Poul H. Damgaard, Kays Haddad, and Andreas Helset. “Heavy Black Hole Effective Theory”. In: *JHEP* 11 (2019), p. 070. doi: [10.1007/JHEP11\(2019\)070](#). arXiv: [1908.10308 \[hep-ph\]](#).
- [102] Rafael Aoude, Kays Haddad, and Andreas Helset. “On-shell heavy particle effective theories”. In: *JHEP* 05 (2020), p. 051. doi: [10.1007/JHEP05\(2020\)051](#). arXiv: [2001.09164 \[hep-th\]](#).
- [103] Zvi Bern, John Joseph M. Carrasco, and Henrik Johansson. “Perturbative quantum gravity as a double copy of gauge theory”. In: *Phys. Rev. Lett.* 105 (2010), p. 061602. doi: [10.1103/PhysRevLett.105.061602](#). arXiv: [1004.0476 \[hep-th\]](#).
- [104] Zvi Bern, John Joseph Carrasco, Marco Chiodaroli, Henrik Johansson, and Radu Roiban. “The Duality Between Color and Kinematics and its Applications”. In: (2019). arXiv: [1909.01358 \[hep-th\]](#).
- [105] Zvi Bern, John Joseph Carrasco, Wei-Ming Chen, Henrik Johansson, and Radu Roiban. “Gravity amplitudes as generalized double copies of gauge-theory amplitudes”. In: *Phys. Rev. Lett.* 118.18 (2017), p. 181602. doi: [10.1103/PhysRevLett.118.181602](#). arXiv: [1701.02519 \[hep-th\]](#).
- [106] Zvi Bern, Clifford Cheung, Radu Roiban, Chia-Hsien Shen, Mikhail P. Solon, and Mao Zeng. “Black hole binary dynamics from the double copy and effective theory”. In: (2019). arXiv: [1908.01493 \[hep-th\]](#).
- [107] Z. Bern, Lance J. Dixon, D. C. Dunbar, M. Perelstein, and J. S. Rozowsky. “On the relationship between Yang-Mills theory and gravity and its implication for ultraviolet divergences”. In: *Nucl. Phys.* B530 (1998), pp. 401–456. doi: [10.1016/S0550-3213\(98\)00420-9](#). arXiv: [hep-th/9802162 \[hep-th\]](#).
- [108] Zvi Bern, David C. Dunbar, and Tokuzo Shimada. “String based methods in perturbative gravity”. In: *Phys. Lett. B* 312 (1993), pp. 277–284. doi: [10.1016/0370-2693\(93\)91081-W](#). arXiv: [hep-th/9307001](#).

- [109] David C. Dunbar and Paul S. Norridge. “Calculation of graviton scattering amplitudes using string based methods”. In: *Nucl. Phys. B* 433 (1995), pp. 181–208. doi: [10.1016/0550-3213\(94\)00385-R](https://doi.org/10.1016/0550-3213(94)00385-R). arXiv: [hep-th/9408014](https://arxiv.org/abs/hep-th/9408014).
- [110] Henrik Johansson and Alexander Ochirov. “Pure gravities via color-kinematics duality for fundamental matter”. In: *JHEP* 11 (2015), p. 046. doi: [10.1007/JHEP11\(2015\)046](https://doi.org/10.1007/JHEP11(2015)046). arXiv: [1407.4772 \[hep-th\]](https://arxiv.org/abs/1407.4772).
- [111] Dong-pei Zhu. “Zeros in scattering amplitudes and the structure of nonabelian gauge theories”. In: *Phys. Rev. D* 22 (1980), p. 2266. doi: [10.1103/PhysRevD.22.2266](https://doi.org/10.1103/PhysRevD.22.2266).
- [112] C. J. Goebel, F. Halzen, and J. P. Leveille. “Angular zeros of Brown, Mikaelian, Sahdev, and Samuel and the factorization of tree amplitudes in gauge theories”. In: *Phys. Rev. D* 23 (1981), pp. 2682–2685. doi: [10.1103/PhysRevD.23.2682](https://doi.org/10.1103/PhysRevD.23.2682).
- [113] Paolo Benincasa, Camille Boucher-Veronneau, and Freddy Cachazo. “Taming Tree Amplitudes In General Relativity”. In: *JHEP* 11 (2007), p. 057. doi: [10.1088/1126-6708/2007/11/057](https://doi.org/10.1088/1126-6708/2007/11/057). arXiv: [hep-th/0702032](https://arxiv.org/abs/hep-th/0702032).
- [114] Kazunori Akiyama et al. “First M87 Event Horizon Telescope Results. I. The Shadow of the Supermassive Black Hole”. In: *Astrophys. J. Lett.* 875 (2019), p. L1. doi: [10.3847/2041-8213/ab0ec7](https://doi.org/10.3847/2041-8213/ab0ec7). arXiv: [1906.11238 \[astro-ph.GA\]](https://arxiv.org/abs/1906.11238).
- [115] N. E. J. Bjerrum-Bohr, John F. Donoghue, and Pierre Vanhove. “On-shell techniques and universal results in quantum gravity”. In: *JHEP* 02 (2014), p. 111. doi: [10.1007/JHEP02\(2014\)111](https://doi.org/10.1007/JHEP02(2014)111). arXiv: [1309.0804 \[hep-th\]](https://arxiv.org/abs/1309.0804).
- [116] Duff Neill and Ira Z. Rothstein. “Classical Space-Times from the S Matrix”. In: *Nucl. Phys. B* 877 (2013), pp. 177–189. doi: [10.1016/j.nuclphysb.2013.09.007](https://doi.org/10.1016/j.nuclphysb.2013.09.007). arXiv: [1304.7263 \[hep-th\]](https://arxiv.org/abs/1304.7263).
- [117] Walter D. Goldberger and Ira Z. Rothstein. “An effective field theory of gravity for extended objects”. In: *Phys. Rev. D* 73 (2006), p. 104029. doi: [10.1103/PhysRevD.73.104029](https://doi.org/10.1103/PhysRevD.73.104029). arXiv: [hep-th/0409156 \[hep-th\]](https://arxiv.org/abs/hep-th/0409156).
- [118] Thibault Damour. “Radiative contribution to classical gravitational scattering at the third order in  $G$ ”. In: *Phys. Rev. D* 102.12 (2020), p. 124008. doi: [10.1103/PhysRevD.102.124008](https://doi.org/10.1103/PhysRevD.102.124008). arXiv: [2010.01641 \[gr-qc\]](https://arxiv.org/abs/2010.01641).
- [119] Gregor Kälin and Rafael A. Porto. “From Boundary Data to Bound States”. In: *JHEP* 01 (2020), p. 072. doi: [10.1007/JHEP01\(2020\)072](https://doi.org/10.1007/JHEP01(2020)072). arXiv: [1910.03008 \[hep-th\]](https://arxiv.org/abs/1910.03008).
- [120] Gregor Kälin and Rafael A. Porto. “From boundary data to bound states. Part II. Scattering angle to dynamical invariants (with twist)”. In: *JHEP* 02 (2020), p. 120. doi: [10.1007/JHEP02\(2020\)120](https://doi.org/10.1007/JHEP02(2020)120). arXiv: [1911.09130 \[hep-th\]](https://arxiv.org/abs/1911.09130).
- [121] N. E. J. Bjerrum-Bohr, Andrea Cristofoli, and Poul H. Damgaard. “Post-Minkowskian Scattering Angle in Einstein Gravity”. In: *JHEP* 08 (2020), p. 038. doi: [10.1007/JHEP08\(2020\)038](https://doi.org/10.1007/JHEP08(2020)038). arXiv: [1910.09366 \[hep-th\]](https://arxiv.org/abs/1910.09366).
- [122] N. Emil J. Bjerrum-Bohr, Barry R. Holstein, John F. Donoghue, Ludovic Planté, and Pierre Vanhove. “Illuminating Light Bending”. In: *PoS CORFU2016* (2017), p. 077. doi: [10.22323/1.292.0077](https://doi.org/10.22323/1.292.0077). arXiv: [1704.01624 \[gr-qc\]](https://arxiv.org/abs/1704.01624).



# Resumé

L'avènement de l'observation des ondes gravitationnelles au LIGO et à VIRGO [1] et les expériences de haute précision pour les théories de jauge fondamentales au LHC sont une forte motivation pour repousser les limites des calculs analytiques. Dans les théories de jauge non abéliennes et la gravité, les amplitudes de diffusion ont toujours été difficiles à calculer car le nombre de graphes de Feynman contributeurs augmente de façon exponentielle avec la multiplicité et le niveau de boucle, et les expressions intermédiaires deviennent grandes et lourdes. En particulier, parce que la gravité a des termes de contact à toutes les multiplicités, écrire les graphes de Feynman d'une amplitude peut rapidement devenir une tâche impossible. Au cours des dernières décennies, le domaine des amplitudes de diffusion a évolué pour décrire la physique des hautes énergies d'une manière moins dépendante des choix temporels effectués en cours de route dans les calculs, tels que la dépendance de jauge - en exploitant et parfois en découvrant de nouvelles symétries des quantités observables de la nature. Un certain nombre de techniques puissantes ont été développées, telles que les méthodes récursives pour les amplitudes au niveau de l'arbre [2, 3], les méthodes d'unitarité généralisée [4–6] et la dualité Bern-Carrasco-Johansson (BCJ) entre couleur et cinématique [7] et sa construction en double copie associée pour les amplitudes gravitationnelles [8].

La dualité Bern-Carrasco-Johansson (BCJ) entre la couleur et les ingrédients cinématiques des amplitudes est un bel aperçu de la structure des amplitudes de la théorie de jauge. Dans une théorie de jauge où cette dualité est manifeste, les amplitudes peuvent être agencées de telle sorte que les poids de couleur et les poids cinématiques des diagrammes contributeurs obéissent aux mêmes identités algébriques. Pour le cas des scalaires massifs couplés à la théorie de jauge, ces identités sont représentées sur la Figure 5.3. Cela signifie que les numérateurs cinématiques des graphiques d'amplitude ne sont pas indépendants, mais peuvent en fait être exprimés en termes d'un plus petit ensemble de numérateurs de base. Cela nous permet de recycler les informations entre les diagrammes et en pratique réduit considérablement le nombre de calculs nécessaires pour une amplitude à  $n$ -points.

Une avancée cruciale dans les prévisions de jauge et de gravité est d'inclure les effets des particules avec une masse intrinsèque. Cependant, l'introduction de masses pour les amplitudes au niveau de la boucle apporte une complexité plus élevée. On peut comparer, par exemple, l'amplitude à une boucle dans  $N = 4$  sYM, où les coefficients des intégrales de triangle et de bulle disparaissent, avec l'amplitude à une boucle pour les quarks massifs en QCD, où il faut prendre en compte non seulement les triangles et les bulles, mais inclure des diagrammes de têtards massifs dont l'accessibilité via les méthodes d'unitarité est subtile. La dualité entre la couleur et la cinématique a ici un réel potentiel : propager les informations de coupe à partir de graphiques maîtres accessibles vers des contributions plus délicates.

Dans cette thèse, je développe une représentation graphique des amplitudes au niveau des arbres et des boucles avec des scalaires massifs couplés à des bosons de Yang-Mills qui obéissent à la dualité BCJ. Les diagrammes relatifs à une amplitude sont générés simultanément avec les relations BCJ entre eux, ce qui nous permet de

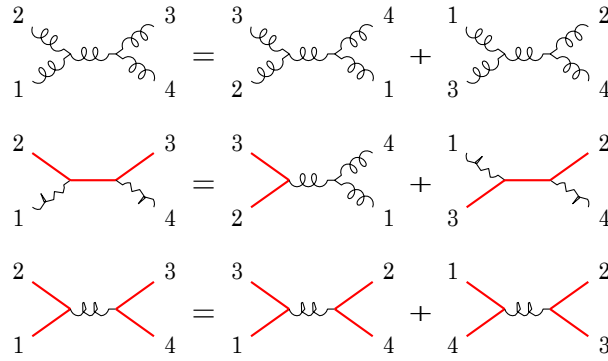


Figure 5.3: Représentation schématique des relations possibles entre les poids de couleurs et les poids cinématiques des diagrammes. Les lignes pleines (rouges) représentent des particules scalaires de même masse.

réduire les numérateurs de diagrammes cinématiques à des ensembles de diagrammes de base plus petits. Je choisis des ansätze pour les fonctions du numérateur des diagrammes de base dont les coefficients sont fixés par les relations BCJ entre les diagrammes, les propriétés de symétrie et les coupes unitaires généralisées. Par exemple, l'amplitude à quatre points au niveau de l'arbre avec un scalaire massif a deux topologies de diagrammes cubiques qui reçoivent des fonctions de numérateur distinctes

$$\begin{array}{c} c \\ \diagdown \\ b \end{array} \begin{array}{c} \text{---} M \text{---} \\ \diagup \\ a \end{array} \begin{array}{c} d \\ \diagup \\ a \end{array} = n_{4,1}^M(a, b, c, d), \quad \begin{array}{c} d \\ \diagdown \\ c \end{array} \begin{array}{c} \text{---} \bar{M} \text{---} \\ \diagup \\ b \end{array} \begin{array}{c} a \\ \diagup \\ b \end{array} = n_{4,1}^{\bar{M}}(a, b, c, d), \quad (5.81)$$

où les fonctions du numérateur sont liées par la relation BCJ suivante

$$n_{4,1}^{\bar{M}}(a, b, c, d) = n_{4,1}^M(a, b, c, d) - n_{4,1}^M(b, a, c, d). \quad (5.82)$$

Un ansatz cinématique est donc donné au diagramme de base  $n_{4,1}^M$  et est complètement déterminée par les propriétés de symétrie et de factorisation des diagrammes individuels et des amplitudes ordonnées. Au niveau de la boucle, les coefficients sont déterminés en se fixant sur des coupes unitaires généralisées.

Nous constatons que des représentations satisfaisantes BCJ existent à la fois au niveau de l'arbre et de la boucle, et les numérateurs cinématiques résultants ont une caractéristique intéressante : ils peuvent être utilisés pour décrire des scalaires massifs à la fois dans la représentation fondamentale et adjointe du groupe de jauge. Nous trouvons des représentations satisfaisantes BCJ pour les amplitudes au niveau de l'arbre à quatre et cinq points avec un et deux scalaires massifs respectivement. Nous trouvons également des représentations pour l'amplitude à quatre points à une boucle avec deux scalaires massifs, qui a six topologies cubiques distinctes<sup>4</sup>. Les coefficients physiquement pertinents de cette amplitude sont fixés sur trois coupes unitaires. Nous trouvons également une représentation satisfaisante BCJ pour l'amplitude à cinq points à une boucle avec deux scalaires massifs et un gluon externe, qui a 33

<sup>4</sup>Ne pas inclure les topologies de têtards.

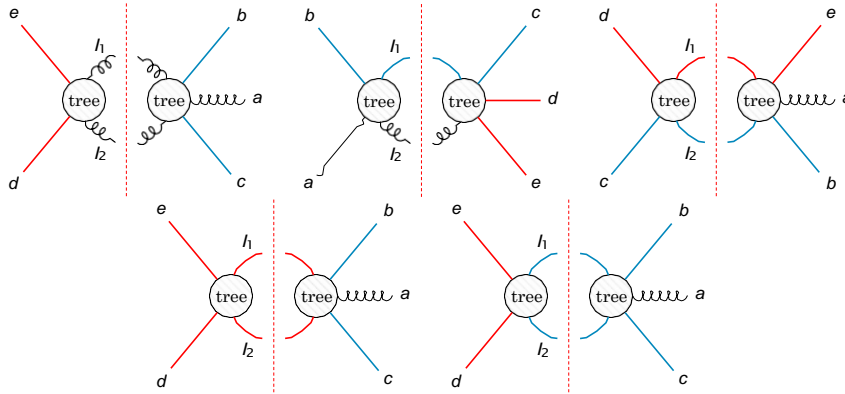


Figure 5.4: Coupes unitaires généralisées pour l'amplitude à une boucle à cinq points avec deux scalaires massifs de masse distincte.

topologies cubiques distinctes, et est fixée sur les cinq coupes unitaires illustrées à la Figure 5.4.

Les numérateurs cinématiques qui obéissent aux relations BCJ manifestent également un autre ensemble de relations profondes liant les théories physiques et qui doivent encore être complètement comprises : la structure en double copie des prédictions. Pour les numérateurs BCJ, nous pouvons, graphique par graphique, échanger les facteurs de couleur par un autre ensemble de numérateurs cinématiques, ce qui donne l'amplitude correspondante dans une théorie gravitationnelle. La construction en double copie a remplacé l'énorme complexité des calculs gravitationnels par la relative simplicité des prédictions de la théorie de jauge. Cela a été important pour les explorations formelles des propriétés UV des théories de la supergravité, et a maintenant un réel impact phénoménologique à l'ère de l'observation précise des ondes gravitationnelles. Dans cette thèse, la double copie de scalaires massifs couplée à la théorie de Yang-Mills donne la théorie des scalaires massifs en supergravité  $N = 0$ .

Comme les numérateurs cinématiques que nous générons obéissent aux relations BCJ par construction, nous pouvons facilement prendre la double copie pour obtenir les amplitudes de supergravité  $N = 0$ . Cependant, les amplitudes de cette théorie ont - en plus des gravitons souhaités - d'autres particules sans masse qui circulent comme états internes. Nous présentons donc une approche basée sur des diagrammes, que nous appelons double copie projective, qui combine des idées de la méthode des coupes maximales [9] et de la construction en double copie pour obtenir des numérateurs de gravité d'Einstein-Hilbert. Premièrement, les numérateurs  $N = 0$  sont trouvés en mettant au carré les numérateurs de la théorie de jauge. Ceux-ci sont ensuite modifiés en effectuant les coupes maximales de toutes les topologies pertinentes, et en les comparant avec les expressions obtenues avec un projecteur d'état physique qui permet uniquement aux gravitons de traverser la coupe. Tout écart entre les deux est ensuite attribué à des états supplémentaires, puis soustrait des numérateurs. Ensuite, une procédure similaire est effectuée pour les coupes presque-maximales, les coupes presque-presque-maximales, et ainsi de suite, jusqu'à ce qu'aucune autre condition de coupe ne puisse être retirée. À titre d'exemple, considérons l'amplitude d'une boucle à quatre points avec deux scalaires massifs. Le numérateur de supergravité  $N = 0$  de la topologie boîte est le carré du numérateur QCD, et avec des conditions de coupe maximale imposées, nous trouvons

$$M_4^{1\text{-loop}\uparrow\text{cut}}_{\text{MC1}} = n_{N=0} \left( \begin{array}{c} 2 \\ 1 \end{array} \begin{array}{|c|} \hline \text{---} \\ \hline \end{array} \begin{array}{c} 3 \\ 4 \end{array} \right) \uparrow\text{cut}_{\text{MC1}} = (k_1 \cdot k_4)^4. \quad (5.83)$$



Nous comparons cela avec la somme des états du projecteur d'états physiques sur le produit des amplitudes de l'arbre à trois points,

$$\begin{aligned} \mathcal{M}_{MC1}^{\text{trees}\uparrow} &= \mathcal{M}_{\text{states}}^{\text{tree}}(k_3^{m_1}, l_1^{m_1}, l_1^{s_1}) \mathcal{M}_3^{\text{tree}}(-l_3^{m_1}, k_1^{m_1}, l_2^{s_2}) \\ &\quad \times \mathcal{M}_3^{\text{tree}}(-l_2^{s_2}, k_3^{m_2}, -l_4^{m_2}) \mathcal{M}_3^{\text{tree}}(l_4^{m_2}, k_4^{m_2}, -l_3^{s_3}) \\ &= \frac{m_1^2 m_2^2}{D_s - 2} - (k_1 \cdot k_4)^2. \end{aligned} \quad (5.84)$$

La contribution des états non gravitationnels est alors donnée par la différence entre l'expression complète de la supergravité  $N = 0$  et l'expression médiée par le graviton

$$\begin{aligned} \Delta_{MC1} &= \mathcal{M}_4^{\text{loop cut}} - \frac{\mathcal{M}_{MC1}^{\text{trees}\uparrow}}{\mathcal{M}_{MC1}} \\ &= 2 \frac{m_1 m_2 (k_1 \cdot k_4)^2}{D_s - 2} - \frac{(m_1^2 m_2^2)^2}{(D_s - 2)^2}, \end{aligned} \quad (5.85)$$

et la contribution d'Einstein-Hilbert est alors obtenue en soustrayant le terme d'états supplémentaires du numérateur  $N = 0$ . Nous continuons ainsi, en corrigeant les numérateurs à l'aide des coupes proches du maximum *etc.* La procédure projective de double copie est complètement systématique, et nous trouvons un ensemble de numérateurs de gravité d'Einstein-Hilbert pour des amplitudes au niveau de l'arbre à quatre et cinq points avec un et deux scalaires massifs, et pour des intégrandes d'amplitude à une boucle à quatre et cinq- points avec deux scalaires massifs.

Les avantages du calcul des amplitudes de diffusion ont incité les physiciens à utiliser les connaissances obtenues des théories quantiques dans la recherche d'observables en physique classique (voir *eg* [10–54]). Les modèles d'ondes gravitationnelles qui peuvent être comparés aux données d'expériences nécessitent que nous combinions la relativité numérique avec une entrée analytique. Cela peut être sous la forme d'hamiltoniens gravitationnels et des équations de mouvement ultérieures, ou directement sous forme d'observables, tels que le changement d'impulsion de deux corps gravitationnels en collision. Il y a déjà eu d'énormes progrès dans ce domaine – le potentiel du problème binaire du trou noir a été déterminé jusqu'au troisième et quatrième ordre dans l'expansion post-minkowskienne [51, 55], ainsi que le rayonnement effets de réaction [49, 52, 54]. Une méthode d'extraction directe d'observables classiques à partir d'amplitudes de diffusion, le formalisme de Kosower-Maybee-O'Connell (KMOC), a été introduite dans [36] où le changement d'impulsion et de rayonnement dans la limite classique de l'électrodynamique quantique est donné. De manière analogue, le formalisme KMOC a été utilisé pour trouver l'impulsion de couleur et la couleur totale rayonnée dans la limite classique de QCD [56], et nous constatons que les numérateurs développés dans cette thèse reproduisent avec succès certains des résultats de cet article.

Nous reproduisons l'impulsion de couleur à l'ordre dominant (au niveau de l'arbre) et à l'ordre sub-dominant (au niveau d'une boucle), qui est décrit dans [56] et donné par

$$\Delta c_1^a \rightarrow \Delta c_1^a = i \int d^4 \hat{q} \delta(2m_2 t \hat{q}) \delta(2p_2 \cdot \hat{q}) e^{-ib \cdot \hat{q}} G, \quad (5.86)$$

où le noyau de couleur  $G$  est défini comme

$$\begin{aligned}
 G^a &= n^2 [C^a, C(D)] A_D(p_1, p_2 \rightarrow p_1 + q, p_2 - q) \\
 &- in^4 \prod_{i=1,2}^D r \hat{d}^4 \bar{\omega}_i \hat{\delta}(2p_1 \cdot \bar{\omega}_i + n\bar{\omega}_i^2) \hat{\delta}^{(4)}(\bar{\omega}_1 + \bar{\omega}_2 - \bar{r}_X) C_{D,D'}^t [C^a, C(D)] \\
 &\times A_{D'}^\dagger(p_1 + q, p_2 - q \rightarrow p_1 + \omega_1, p_2 + \omega_2, r_X) A_D(p_1, p_2 \rightarrow p_1 + \omega_1, p_2 - \omega_2, r_X).
 \end{aligned}
 \tag{5.87}$$

Le calcul de l'impulsion de couleur d'ordre suivant dans la représentation BCJ des amplitudes développée dans cette thèse diffère de l'article original car toutes les topologies sont cubiques

$$\begin{aligned}
 A^{(1)} &= C \left[ \begin{array}{c} b \\ \text{---} \\ a \end{array} \right] \left[ \begin{array}{c} c \\ \text{---} \\ d \end{array} \right] I_{b1} + C \left[ \begin{array}{c} a \\ \text{---} \\ b \end{array} \right] \left[ \begin{array}{c} c \\ \text{---} \\ d \end{array} \right] I_{b2} + C \left[ \begin{array}{c} b \\ \text{---} \\ a \end{array} \right] \left[ \begin{array}{c} c \\ \text{---} \\ d \end{array} \right] I_{t1} \\
 &+ C \left[ \begin{array}{c} b \\ \text{---} \\ a \end{array} \right] \left[ \begin{array}{c} c \\ \text{---} \\ d \end{array} \right] I_{t2} + C \left[ \begin{array}{c} b \\ \text{---} \\ a \end{array} \right] \left[ \begin{array}{c} c \\ \text{---} \\ d \end{array} \right] I_{t1} + C \left[ \begin{array}{c} b \\ \text{---} \\ a \end{array} \right] \left[ \begin{array}{c} c \\ \text{---} \\ d \end{array} \right] I_{t2} \\
 &+ C \left[ \begin{array}{c} b \\ \text{---} \\ a \end{array} \right] \left[ \begin{array}{c} c \\ \text{---} \\ d \end{array} \right] I_o^{(1)} + C \left[ \begin{array}{c} b \\ \text{---} \\ a \end{array} \right] \left[ \begin{array}{c} c \\ \text{---} \\ d \end{array} \right] I_{\hat{o}1}^{(1)} + C \left[ \begin{array}{c} b \\ \text{---} \\ a \end{array} \right] \left[ \begin{array}{c} c \\ \text{---} \\ d \end{array} \right] I_{\hat{o}2}^{(1)} \\
 &+ C \left[ \begin{array}{c} b \\ \text{---} \\ a \end{array} \right] \left[ \begin{array}{c} c \\ \text{---} \\ d \end{array} \right] I_{s1}^{(1)} + C \left[ \begin{array}{c} b \\ \text{---} \\ a \end{array} \right] \left[ \begin{array}{c} c \\ \text{---} \\ d \end{array} \right] I_{s2}^{(1)} + C \left[ \begin{array}{c} b \\ \text{---} \\ a \end{array} \right] \left[ \begin{array}{c} c \\ \text{---} \\ d \end{array} \right] I_{s3}^{(1)} \\
 &+ C \left[ \begin{array}{c} b \\ \text{---} \\ a \end{array} \right] \left[ \begin{array}{c} c \\ \text{---} \\ d \end{array} \right] I_{s4}^{(1)}.
 \end{aligned}
 \tag{5.88}$$

Dans le formalisme présenté dans [56] les facteurs de couleur avec des constantes de structure,  $f^{abc}$ , obtiennent une puissance supplémentaire de  $n$  par rapport aux générateurs,  $T_{ij}^a$ , supprimant ainsi ces termes dans la limite classique. On retrouve donc une base de couleur cubique qui privilégie les topologies avec des sommets composés uniquement de gluons, qui diffère de la base présentée dans l'article

$$C \left[ \begin{array}{c} b \\ \text{---} \\ a \end{array} \right] \left[ \begin{array}{c} c \\ \text{---} \\ d \end{array} \right], C \left[ \begin{array}{c} a \\ \text{---} \\ b \end{array} \right] \left[ \begin{array}{c} c \\ \text{---} \\ d \end{array} \right], C \left[ \begin{array}{c} b \\ \text{---} \\ a \end{array} \right] \left[ \begin{array}{c} c \\ \text{---} \\ d \end{array} \right], C \left[ \begin{array}{c} b \\ \text{---} \\ a \end{array} \right] \left[ \begin{array}{c} c \\ \text{---} \\ d \end{array} \right].
 \tag{5.89}$$

L'impulsion de couleur calculée à l'aide des représentations satisfaisantes BCJ à l'ordre dominant et à l'ordre sub-dominant correspond aux résultats dans [56], tout comme le rayonnement de couleur à l'ordre dominant.



**Titre :** La matière massive et la double copie: Bootstrap des amplitudes dans les théories de jauge et de gravité

**Mots clés :** Amplitudes, Gravité quantique, Particules, Haute énergies, QCD

**Résumé :** Le LHC et l'avènement de l'observation des ondes gravitationnelles ont motivé des progrès considérables dans le développement d'approches des prédictions de précision dans les théories de jauge fondamentales et la relativité générale classique, et les deux peuvent être intimement liés. La dualité couleur-cinématique de Bern, Carrasco et Johansson (BCJ) pour les théories de jauge est une dualité où en amplitudes, graphique par graphique, les poids cinématiques obéissent aux mêmes contraintes algébriques générales que les poids de couleur. Lorsqu'ils sont disposés dans une telle représentation, les poids de couleur peuvent être remplacés par une autre copie des poids cinématiques, générant des amplitudes de diffusion invariantes difféomorphes pour les théories gravitationnelles dans une procédure connue sous le nom de construction en double copie. Ces amplitudes gravitationnelles peuvent à leur tour être appliquées à la prédiction d'observables classiques.

La forme bicolore pour les prédictions de la théorie de jauge signifie que nous n'avons besoin de fixer les informations physiques que dans un petit nombre de graphes de base, et les relations algébriques propagent cela à la prédiction complète, à la fois au niveau de l'arbre et surtout au niveau de la boucle pour l'intégrande la description. Cette thèse développe une dualité BCJ satisfaisant la représentation des amplitudes au niveau de l'arbre et de la boucle dans la QCD massive couplée scalaire. Les amplitudes en double copie sont alors pertinentes pour la diffusion des trous noirs non rotatifs. Nous utilisons la dualité BCJ pour réduire l'ensemble de graphes d'amplitudes jusqu'à une boucle à cinq points à un ensemble plus petit de graphes de base, auxquels nous donnons des ansätze qui sont contraints par des coupes unitaires et des relations couleur-cinématique.

Nos représentations à double couleur ont une caractéristique importante. Les mêmes poids cinématiques, graphe par graphe, sont applicables aux scalaires qu'ils soient chargés dans le fondamental ou dans l'adjoint. En effet, on peut utiliser des coupes ordonnées de type adjoint pour contraindre ces

poids cinématiques à utiliser pour les prédictions dans une multitude de théories, en fonction des graphiques que vous autorisez à contribuer et de la façon dont vous pondérez leur couleur.

La construction en double copie va de la diffusion des gluons à la diffusion des gravitons en supergravité  $N=0$ , avec des états sans masse supplémentaires au-delà du couplage du graviton aux scalaires massifs. Au niveau de l'arbre et de la boucle, nous montrons qu'une double copie projective, combinant une double copie naïve avec une application de la méthode des coupes maximales, peut être facilement exploitée pour projeter des états non gravitationnels à partir de la double copie naïve, en amorçant les prédictions associée à des interactions gravitationnelles pures entre scalaires massifs.

Nous nous attendons à ce que les intégrandes trouvés dans cette thèse puissent être utilisés pour trouver des prédictions à une boucle en cinq points vers des corrections radiatives aux observables classiques. Dans cet esprit, nous nous réchauffons en utilisant les amplitudes trouvées dans cette thèse pour reproduire les résultats connus pour l'impulsion de couleur à l'ordre dominant et sub-dominant, et le rayonnement à l'ordre dominant.

**Title :** Massive matter and the double copy: Bootstrapping amplitudes in gauge and gravity theories

**Keywords :** Amplitudes, Quantum gravity, Particles, High energy, QCD

**Abstract :** The LHC and the advent of gravitational wave observation have motivated tremendous progress in developing approaches to precision predictions in fundamental gauge theories and classical general relativity, and the two can be intimately connected. The color-kinematics duality of Bern, Carrasco, and Johansson (BCJ) for gauge theories is a duality where in amplitudes, graph-by-graph, kinematic weights obey the same general algebraic constraints as color weights. When arranged in such a representation the color-weights can be replaced by another copy of kinematic weights, generating diffeomorphic invariant scattering amplitudes for gravitational theories in a procedure known as double-copy construction. These gravitational amplitudes can then in turn be applied to predicting classical observables.

The color-dual form for gauge theory predictions means we only need to fix the physical information in a small number of basis graphs, and algebraic relations propagate this to the full prediction—both at tree-level and importantly at loop-level for the integrand description. This thesis develops a BCJ duality satisfying representation of tree- and loop-level amplitudes in massive scalar coupled QCD. The double-copy amplitudes are then relevant to non-rotating black hole scattering. We use the BCJ duality to reduce the set of graphs of amplitudes up to one-loop five-point to a smaller set of basis graphs, to which we give ansätze that are constrained by unitarity cuts and color-kinematics relations.

Our color-dual representations have an important feature. The same kinematic weights, graph by graph, are applicable to scalars regardless of whether they are charged in the fundamental or the adjoint. Indeed one can use adjoint-type ordered cuts to constrain these kinematic weights to be used for predictions in a multitude of theories, depending on which graphs you allow to contribute and how you weight their color.

The double copy construction maps from the scattering of gluons to the scattering of gravitons in  $N=0$  supergravity, with additional massless states beyond the graviton coupling to the massive scalars. At tree- and loop-level we show that a projective double copy, combining naive double-copy with an application of the method of maximal cuts, can be easily exploited to project out non-gravitational states from the naive double copy, bootstrapping the predictions associated with pure-gravitational interactions between massive scalars.

We expect that the integrands found in this thesis can be used to find one-loop five-point predictions towards radiative corrections to classical observables. With that in mind, we warm up by using the amplitudes found in this thesis to reproduce known results for the color-impulse at leading and next-to-leading order, and radiation at leading order.